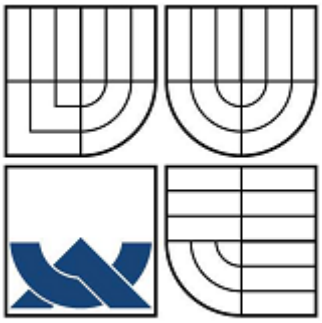

BRNO UNIVERSITY OF TECHNOLOGY
VYSOKÉ UČENÍ TECHNICKÉ V BRNĚ

FACULTY OF MECHANICAL ENGINEERING
INSTITUTE OF AEROSPACE ENGINEERING

FAKULTA STROJNÍHO INŽENÝRSTVÍ
LETECKÝ ÚSTAV

EFFECTS OF DEFECTS ON COMPOSITE STRUCTURES LOAD CARRYING CAPACITY: DELAMINATIONS AT BI-MATERIAL INTERFACES

VLIV VAD NA ÚNOSNOST KOMPOZITNÍCH KONSTRUKCÍ:
DELAMINACE NA ROZHRANÍ DVOU MATERIÁLŮ

DOCTORAL THESIS
DIZERTAČNÍ PRÁCE

AUTHOR — Ing. VLADIMÍR MATĚJÁK
AUTOR PRÁCE

SUPERVISOR — doc. Ing. JAROSLAV JURAČKA, Ph.D.
VEDOUCÍ PRÁCE

BRNO 2016

Abstract

Composite materials exhibit a complex failure behaviour, which may be further affected by various defects that arise either during the manufacturing process or during the service life of the component. A detailed understanding of the failure behaviour, and the factors affecting it, is essential for designing composite structures that are safer, more durable and economical.

First part of this thesis gives an overview of typical failure mechanisms in composite materials and describes mathematical theories, currently being used in analysing and predicting the failure. Different types of defects are reviewed and their effects on composite materials performance briefly discussed. Delaminations are described in more detail together with basic fracture mechanics principles and their application in the analysis and experimental testing of composite materials.

The second part focuses on delamination at an interface of two different materials. An experimental measurement of fracture toughness was performed under three types of loading conditions in order to determine a delamination failure criterion based on a ratio of mode I and mode II. As a part of the experiment, a novel method of measuring the crack length based on digital image processing was developed and also a new type of delamination initiation point definition proposed. Analytical equations for calculating the energy release rate from experimentally measured data were reviewed and extended to account for different elastic moduli of the two materials at the interface. Analytical and finite element investigation revealed that the mode I and mode II contributions are dependent on the distance from the crack tip and therefore a failure criterion based on the mixed mode ratio cannot be used.

Key words

Delamination, Interface, Fracture, Strength, Failure, Composite, Mixed mode, Delamination testing, Energy release rate, Digital image processing, Crack length

Abstrakt

Kompozitní materiály se projevují komplexním způsobem porušování, které může být dále ovlivněno přítomností různých poruch plynoucích z výrobních processů nebo se vyskytujících v průběhu života součásti. Důkladné porozmění procesů porušování a jejich okolností je nezbytné pro navrhování kompozitních konstrukcí, jenž budou bezpečnější, trvanlivější a ekonomičtější.

V první části disertační práce jsou popsány způsoby porušování kompozitů a uvedeny současné matematické metody pro analýzu a výpočet únosnosti. Dále jsou zde vyjmenovány hlavní druhy vad a stručně diskutován jejich vliv na vlastnosti kompozitních materiálů. Zvláštní důraz je kladen na delaminace, společně se základními principy lomové mechaniky a jejich uplatnění při výpočtech a zkoušení kompozitů.

Druhá část je zaměřena na delaminace na rozhranní dvou různých materialů. Lomová houževnatost byla experimantálně měřena ve třech typech zatížení za účelem stanovení poruchového kritéria založeného na podílu módu I a módu II. Během tohoto experimentu byla vyvinuta nová metoda měření délky trhliny pomocí digitáního zpracování obrazu a rovněž byla navržena nová definice počátku šíření trhliny. Analytické vztahy pro výpočet míry uvolnění deformační energie z naměřených dat byly rozšířeny o vliv rozdílných elastické parametrů materiálů na rozhranní. Podrobnější prozkoumání analytických vztahů a výpočet metodou konečných prvků odhalil, že podíl módu I a módu II je závislý na vzdálenosti od čela trhliny a poruchové kritérium založené na podílu smíšenosti tak nemůže být použito.

Klíčová slova

Delaminace, Rozhranní, Lom, Porucha, Pevnost, Kompozit, Smíšený mód, Zkoušení delaminací, Rychlost uvolenění energie, Digitální zpracování obrazu, Délka trhliny

MATĚJÁK, V. Effects of Defects on Composite Structures Load Carrying Capacity: Delaminations at a Bi-Material Interface. Brno: Brno University of Technology, Faculty of Mechanical Engineering, 2016. 120 p. Supervised by doc. Ing. Jaroslav Juračka, Ph.D..

Declaration

This thesis is a presentation of my original research work. Wherever contributions of others are involved, every effort is made to indicate this clearly, with due reference to the literature, and acknowledgement of collaborative research and discussions.

V Brně dne .....

.....
Vladimír Matěják

Acknowledgement

I would like to express my deepest gratitude to everyone who have supported me in writing this thesis. Firstly, I would like to thank my supervisor doc. Ing. Jaroslav Juračka, Ph.D. for his guidance. Special thanks belong to Salim Mirza, Ph.D. and Stefanos Giannis, Ph.D. from Element Materials Technolgy for their numerous and valuable advice and inspiration. Last but not least, I want to thank my family and friends for their support.

Contents

1 Introduction

In material science, an ability of a material to withstand an applied load without failure is commonly called the strength. Sometimes also the term load-carrying capacity is also used. Even for a simple example such as uniaxially loaded member from isotropic material, several failure points can be defined, depending on the purpose of the structure and whether the material response is ductile or brittle. The most often used limit states of the material are yield strength and ultimate strength. Besides this, structures can also fail by a loss of stiffness in compression, i.e. buckling, also by shear, fatigue, creep, corrosion and wear. Nevertheless, when we talk about the strength and load-carrying capacity of structures, the term failure is most often connected with a fracture and breakage of the component which is the most unambiguous sign that the structure is not able to withstand more loading.

Understanding how materials fail is essential for designing safer and more reliable structures. Many failure theories have been developed in the past for homogeneous materials with various level of success. The advances of new composite materials during the last several decades has brought many advantages but also many challenges for the engineers. The non-homogeneous and complex structure of composite materials leads into many more failure modes, both on microscopic and macroscopic scale. The number of constituent materials and their possible arrangements makes it almost impossible to define a unified failure theory.

Modern composite materials are finding increasing application in aerospace, transportation, energy, and many other industries due to the advantages in performance, structural efficiency and cost they provide. Manufacturing process of composite components may result in the presence or introduction of unwanted defects such as voids, resin-rich areas, and inclusions. Although many of these so called defects may be difficult to detect, their effects on the overall structural integrity may be very dangerous. Damage and general material degradation can also occur during the in-service operation of composite components. Typical causes of such damage are continuous cyclic loading, rapid changes in local temperature, and impact loading. Often, damage develops over a period of months or years, and is not immediately visible to even the trained eye. However, once the size of defect or stress-raiser reaches a critical value, failure can be catastrophic and consequences severe. Clearly, there is a strong need to identify the various types of damage and defects that occur in composite materials during manufacture and operational service and assess their effects on the performance and safety of the structure.

One of the most commonly observed failure modes in composite materials is delamination. The most common sources of delamination are the material and structural discontinuities that give rise to interlaminar stresses. Delaminations occur at stress-free edges due to a mismatch in properties of the individual layers, at ply drops (both internal and external) where thickness must be reduced,

and at regions subjected to out-of-plane loading, such as bending of curved beams. Debonding is another commonly observed failure, which is closely related to delamination. Both, delamination and debonding are often considered as one phenomenon, which can be analysed with identical assumptions and methods. Fracture mechanics is a useful tool for approaching composite delamination and debonding, due to the crack-like type of discontinuity accompanying these defects. The harmful effects of delamination and debonding have made these defects the subject of particularly extensive research. This includes extension of the fundamental principles of fracture mechanics to include anisotropy typically present in composite materials, development of standard test procedures for delamination resistance testing, and including numerical computational methods into FE codes.

Delamination at bi-material interfaces needs to be investigated with special attention. A stress-singularity is present at the vertex of the bi-material interface due to mismatch in elastic parameters. Also state-of-art of the standardised test methods for delamination resistance doesn't include the effect of crack propagating between two dissimilar materials. In reality the delamination occurrence is highly probable at the interface of two different materials; therefore the analysis and testing methods must be established to include these facts.

This thesis is divided into two main parts. First part, the literature review, gives an overview of typical failure mechanisms in composite materials and describes mathematical theories, currently being used in analysing and predicting the failure. Delaminations are described in more detail together with basic fracture mechanics principles and their application in the analysis and experimental testing of composite materials. Next, main type of defects that may occur in a composite structure, either during the manufacture or during the service life, are described and the possible effects of defects on the structural performance and material strength are discussed. First part of the thesis is concluded with a summary of composite materials testing methods, which is an important part in understanding the failure. Special attention is given to a delamination and fracture toughness testing.

Second part of the thesis describes the author's experimental work on the delamination at bi-material interfaces. The test methods and analysis are adopted from fracture toughness testing of composite materials and extended to account for materials with different moduli in the beam test specimen. In this work, a combination of glass and carbon composite is tested over a range of mixed mode conditions; however the methods can be used in any other combination of any two materials. A crack length measurement is an important part of the experimental procedure. A new method of automated crack length measurement by digital image processing has been developed which improves the currently used procedures, where the measurement accuracy is dependent on the test operator. This method works best for the mode I testing and can also be used for traditional single material fracture toughness measurements.

2 Literature review

2.1 Composite materials

Composite structures have become a widespread engineering concept during past decades. Cars, trains, marine structures, wind turbines, spacecraft, medical tools, sporting goods and many others are often made from modern composite materials now. In a broad sense, composite material is a material made from two or more constituent materials, which include steel reinforced concrete, ceramic composites, metal and plastic composites. In a more narrow sense, the term composite materials is often used for fibre reinforced plastic materials, as is the case throughout this thesis. In fibre reinforce plastic, usually some sort of reinforcing fibre with high strength and stiffness is combined with plastic matrix, which provides continuous bonding between the fibres. The most common types of fibres are glass, carbon and aramid. The matrix material usually consists of a thermoset or thermoplastic polymer. Depending on a fibre arrangement and orientation, composites can be unidirectional or multidirectional. Very often, several layers with different fibre orientations are stacked in multi-layered composites, generally referred to as laminates.

The history of composite materials in general dates as back as prehistoric times, when mud and straw were used for simple building constructions. Also, the wood, a natural composite material, has been used for many structures in the past as well as today. The fibre reinforce composites have started to emerge at the beginning of the 20th century. Originally, the fibreglass has found its use in car and boat manufacture. Later, during the second half of the 20th century, composite became wide spread material, mainly because their high specific stiffness and strength. The aviation industry has been the main contributor in this area but composite materials are very important also in other applications, where low weight and high stiffness is an advantage, such as wind turbines and sporting equipment.

The main reason for composite's material growing success is the weight-saving factor. Compared to the conventional metallic materials, they offer higher strength-to-weight and stiffness-to-weight ratios. Another advantage is that the material can be tailored for a specific application by altering the fibre directions. Also corrosion resistance and fatigue properties are generally better compared to the metals. On the other hand, composite materials have complicated manufacturing process, poor through-thickness characteristics, great sensitivity to environmental heat and moisture and poor energy absorption and impact damage resistance. Also, composite materials are often associated with higher cost.

The demand for composite materials across all sectors is only expected to grow during next years. This extensive usage also brings many research and engineering topics. Many details of the composite materials mechanics, both on micro- and macro-scale need to be understood in more detail, so the new

composite structures can be designed safer, more durable and economic. The understanding of composite failure mechanisms and effects of manufacturing and in-service defects is an essential part of this.

2.2 Failure of laminated composites

There is no clear definition of what 'failure' in composite laminates actually means. In general, a structure is considered as failed, when it ceases to fulfil its function. For example, someone designing a composite pipe might consider a liquid leaking through the pipe wall as a failure, for others it might be a certain loss of stiffness or even total structural disintegration. So, from this point of view, it is a clearly a matter of purpose how the failure is understood and it is likely to be different for various applications.

Certainly, the failure of composite materials is a complex process, consisting mainly of matrix cracking, interface debonding, fibre breakage and interaction of these. The evolution of the damage depends on many factors such as orientation of the fibres, matrix content, general state of stress in the material and other environmental effects. One might expect that after more than 50 years of development and successful usage of composite materials in numerous applications, in many of them as a primary load bearing structures, the design procedures and strength prediction methods are fully mature. On the contrary, the design practices place little or no reliance on the ability to predict the ultimate strength of the structure with any great accuracy. Failure theories are often used in the initial sizing of a component, beyond that point experimental tests on coupons and structural elements are used to determine the global design allowables. A 'make and test' approach combined with generous safety factors is a commonplace, which simply is too costly and slow. It is clear that improved design methods and modelling techniques and better understanding of the failure processes can significantly improve this. One of the latest efforts in this area is the World-Wide Failure Exercise (WWFE). [1]

A common approach to predict the failure of a composite laminate is to calculate stresses or strains at a lamina level, where the onset of the damage is then called 'first ply failure'. Different failure criteria can be used at the lamina level, as further described in Section 2.3.2. Often laminates have substantial strength remaining after the first ply failure and further analysis needs to be done to calculate the laminate ultimate strength. A conservative approach is to assume that the contribution of the failed ply is reduced to zero. However, this might be far from the truth, especially when the failure is dominated by matrix, where the fibres might still be able to transfer loads to some extent. Another weak point of this approach is that it neglects any interaction of failures, while in reality the cracks might grow from one ply to another and local stress concentrations are likely to have influence on the damage progression.

Another important mode of failure is a delamination, which can have various effects on the strength of the whole laminate, depending on it location, extent and loading type. Also, composite laminate parts are usually thin walled structures and thus a buckling, either global or local, needs to be considered for the prediction of the structural strength. Fatigue is the next important type of failure potentially affecting composite materials structures. All of these are described in more detail in following chapters.

2.2.1 Lamina failure

Several failure mechanisms can be identified in a composite ply, both macroscopic and microscopic. These include matrix cracking, plastic flow, fibre-matrix debonding, fibre pull-out and fibre fracture. The relative contribution of each during the fracture will depend upon many parameters, mainly on the loading type, fibre and matrix properties, stacking sequence, part geometry.

Matrix cracking is usually the first failure to occur. It starts at regions of higher stresses or stress concentrations, also around manufacturing imperfections, in areas of high porosity or fibre waviness. Originally small isolated micro-cracks grow and coalesce together to form larger macroscopic cracks. This can lead to decrease in stiffness and to locally overloading fibres, which then break.

Fibres can fail mainly in tension and in compression. When a single fibre fails in tension, the load concentration in the adjacent fibres increases the probability that a second fibre will break. This again increases a probability of additional fibre breaks and so on. In compression, the situation is different. Fibres in compression do not fail by simple compression but rather by local buckling. The actual behaviour is very complex and depends on the stiffness of the two components, residual stresses and fibre volume fraction.

The internal fibre structure of a lamina is an important factor in the failure process. Damage will propagate differently in unidirectional lamina or in woven lamina. Many mathematical theories have been developed as an extension or modification of failure theories of homogeneous materials. The most important ones are described in more detail in Chapter 2.3.2. It is important to note, that many of these theories were developed mainly for unidirectional composite materials and their application to woven fabric laminates is not always appropriate.

2.2.2 Delaminations

A separation of the layers of material in a laminate is called delamination. Sometimes, also the term debonding is used. This may be local or may cover a large area of the laminate. It may occur at any time in the cure or subsequent life of the laminate and may arise from a wide variety of causes. One of the main causes is geometric or material discontinuity, such as free edges, ply drops, sharp corners and transitions (see Figure 2.1). Impact damage is another important source of delamination. The delamination itself, depending on the scale, may not cause a catastrophic failure, but it is often a precursor to such an event. Small delaminations from several sources can grow and accumulate, eventually leading to a fatigue failure. The composite delamination represents the most commonly observed macroscopic damage mechanism in laminated composite structures. Many efforts have been made to analyse this failure mode as is described in more detail in Chapter 2.3.3.

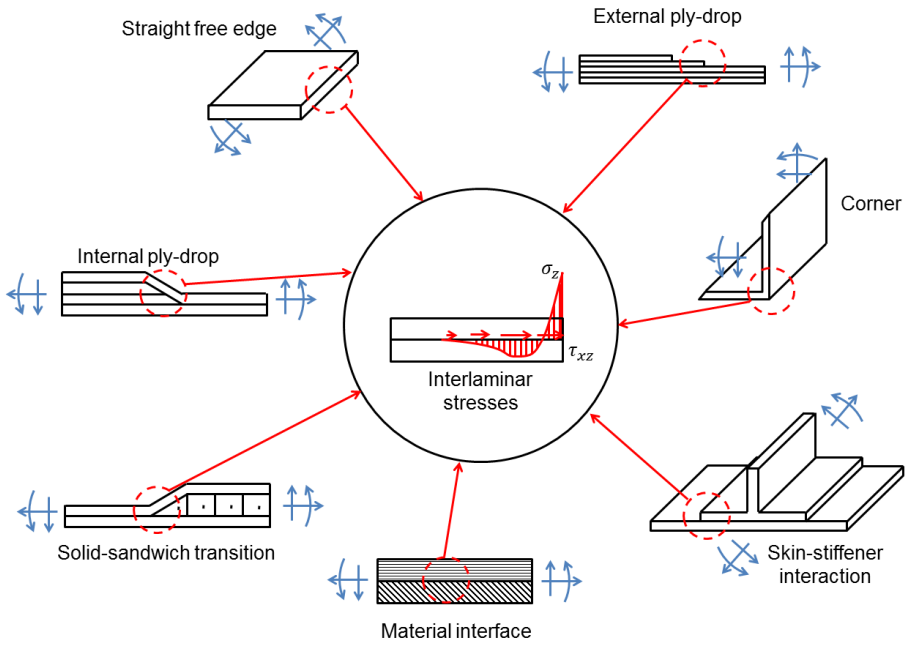

Figure 2.1: Sources of delamination [2]

2.2.3 Buckling

Buckling is a failure mode that can happen usually under compressive stresses, characterized by geometrical instability under which the structure will fail earlier than the theoretical compressive strength of the component is reached. It is mainly a concern for thin walls and plates. Also with regard to the composite materials, buckling can be a dangerous failure mode. We can distinguish between two types of buckling. First is a macro-buckling, associated with out-of plane displacements of the whole component. Buckling load is determined by the stiffness of the laminate, together with the geometry and boundary conditions. The buckling load can be calculated by the same equations as traditionally used for structures from isotropic materials. Second form is a micro-buckling of individual fibres, which is associated with the compressive strength of the composite material. Local buckling of fibres can take two forms as shown in Figure 2.2; shear mode and transverse extension mode. The most likely mode is that producing the lowest energy in the system. Micro-buckling load depends on elastic properties of the fibres and matrix and also on the fibre volume fraction. When delaminations are present in the laminate under compressive load, the sub-laminate buckling is another failure mechanism occurring in composites. The delamination breaks the laminate into sub-laminates, each having associated stiffness, stability and strength characteristic. The stability of sub-laminate plates is strongly tied with ultimate compressive failure of the whole laminate.

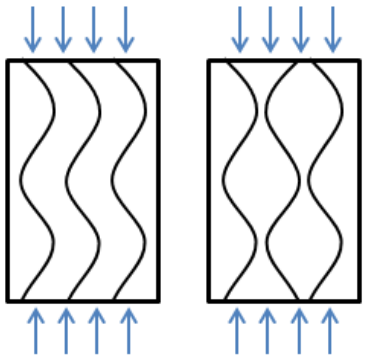

Figure 2.2: Fibre local buckling modes

2.2.4 Fatigue

Fatigue in metals occurs by the initiation of a single crack and its intermittent propagation until catastrophic failure occurs with little warning and no sign of gross distortion, even in highly ductile metals, except at the final tensile region of fracture. In contrast to homogeneous materials, composites accumulate damage in a general rather than a localised fashion, and fracture does not always occur by propagation of a single macroscopic crack. The microstructural mechanisms of damage accumulation, including fibre/matrix debonding, matrix cracking, delamination and fibre fracture, occur sometimes independently and sometimes interactively, and the predominance of one or other of them may be strongly affected by both material' variables and testing conditions. [3] The difference between fatigue behaviour of a composite and of a metal structure is schematically showed in Figure 2.3. The damage in composites propagates in a less regular manner and damage modes can change. Also the quantitative difference usually seen in metals, where the long and slow rate initiation is followed by more rapid propagation, appears to be less apparent with composites.

Although high volume-fraction carbon/epoxy and other carbon fibre-based laminates exhibit extremely good fatigue resistance, this is not the case for lower stiffness laminates such as glass/epoxy. [5]

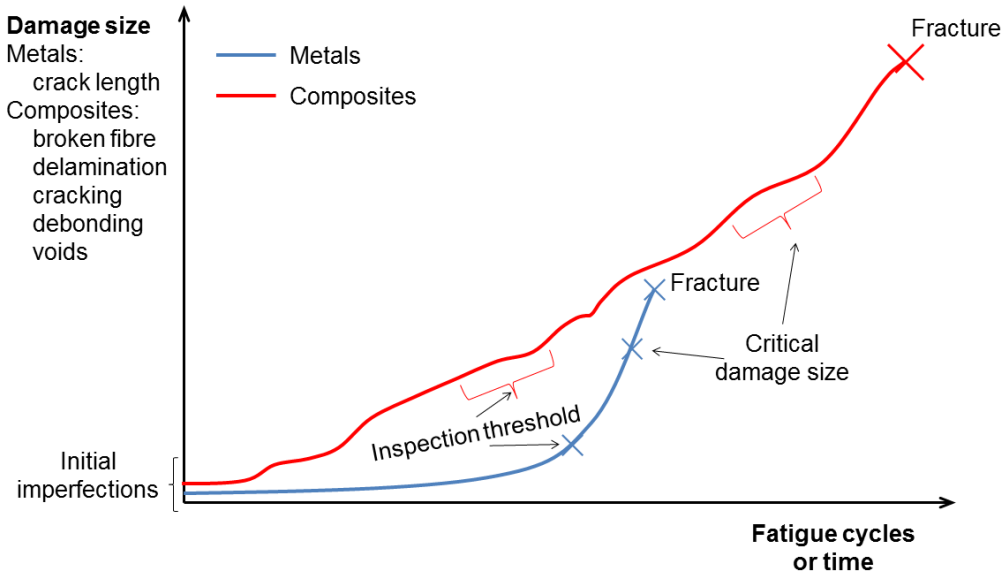

Figure 2.3: Comparison of fatigue behaviour in metals and composites [4]

2.3 Failure theories

The mechanical behaviour of isotropic materials (metals, ceramics and polymers) had been a fairly mature field when in the early 1960s composite materials such as glass/polyester and carbon/epoxy began emerging as promising materials of the future. It was natural for the scientific community then to apply and extend concepts and analyses developed for the monolithic materials to composites. In the decades that followed, great success was achieved in micromechanics estimates of effective elastic properties, homogenization, laminate plate theory, etc. However, theories for treating failure of composite materials did not succeed to the same extent. In fact after numerous efforts extending over approximately five decades many uncertainties and controversies still remain in predicting composite failure. [6] The majority of the developed methods or theories are based on a phenomenological approach to a UD lamina. In general, extensive experiments on the composite lamina are necessary in order to determine the critical strength parameters involved in the phenomenological or macro-mechanical strength theory. Such experiments may be difficult or expensive, and even impossible in some circumstances. [7]

2.3.1 Isotropic materials failure

Most of these phenomenological failure theories for composite materials can be considered more or less as a generalization from failure theories of isotropic materials. These theories are usually applied in the form of material principal stresses ($\sigma_1, \sigma_2, \sigma_3$, where $\sigma_1 \geq \sigma_2 \geq \sigma_3$). The most widely used strength theories for isotropic materials are expressed below.

Maximum normal stress theory
The theory of failure due to the maximum normal stress is generally attributed to W. J. M. Rankine [8]. The theory states that a brittle material will fail when the maximum principal stress, σ_1, exceeds the ultimate value from uniaxial test, σ_u, independent of whether other components of the stress tensor are present.

$$\sigma_1 \geq \sigma_u \tag{2.1}$$

Maximum distortional energy theory (von Mises)[9]
This theory was proposed for yield failure of ductile materials. According to this theory, a ductile solid will yield when the distortion energy reaches a critical value for the material. The equivalent stress to characterize the distorted energy can be expressed in the terms of principal stresses as

$$\sigma_{eq} = \sqrt{\frac{(\sigma_1 - \sigma_2)^2 + (\sigma_2 - \sigma_3)^2 + (\sigma_3 - \sigma_1)^2}{2}} \tag{2.2}$$

The maximum distorted energy theory postulates that no matter whether a ductile material is under a uniaxial or multi-axial state of stress, the yield

failure of the material occurs if its equivalent stress, defined by 2.2 , attains a limit value σ_y. The failure criterion is thus

$$\sigma_{eq} \geq \sigma_y \tag{2.3}$$

where σ_y is the yield strength of the material corresponding to a uniaxial loading test.

Maximum shear stress theory (Tresca)
The maximum shearing stress theory comes from the experimental observation that a ductile material yields as a result of slip or shear along crystalline planes. According to the maximum shear stress theory, the material yields when the maximum shear stress at a point equals the critical shear stress value for that material.

$$\tau_{max} = max\left(\frac{\sigma_1 - \sigma_2}{2}, \frac{\sigma_2 - \sigma_3}{2}, \frac{\sigma_1 - \sigma_3}{2}\right) \geq \tau_y = \frac{\sigma_y}{2} \tag{2.4}$$

2.3.2 Lamina failure

The most common lamina failure theories are developed phenomenologically and are to some extent a generalization from corresponding failure theories of isotropic materials. In general, these theories are directly applied to the stress components of the composite laminae, but in their local (or material) coordinate system. [1] Usually they are defined for a thin orthotropic lamina in a plane stress condition. Lamina failure criteria can be categorized into three main groups:

- Limit criteria - these criteria predict failure only by comparing lamina stresses with corresponding strengths. The interaction between stresses is not considered. Among these criteria belong Maximum stress criterion and Maximum strain criterion.
- Interactive criteria - these criteria predict the failure load by using a single polynomial equation involving all stress (or strain) components. Many such criteria were proposed. The most notable are: Tsai-Hill and Tsai-Wu criterion
- Separate mode criteria - there is a separate failure criterion for different failure modes, with accounting for some interaction between them. Most used criteria from this group are Hashin failure criterion and Puck failure criterion

[1] Often the term 'principal stress' is used for failure theories in general. However it is important to distinguish between:

(a) Principal stress, which is used often for isotropic material failure theories. Here the principal stress is defined as component of the stress tensor when the basis is changed in such a way that the shear stress components become zero.

(b) Material principal stress, which is used for composite materials. Here it means the stress in main material coordinate system, i.e. along the fibres etc.

Maximum stress and strain criteria
These two theories are based on the assumption that there can exist three possible modes of failure caused by stresses σ_{11}, σ_{22}, and τ_{12} or strains ε_{11}, ε_{22}, and γ_{12}, when they reach the corresponding ultimate values. Mathematically, the maximum stress failure criteria can be expressed as

$$\sigma_{11} \geq \begin{cases} X_T & \text{if } \sigma_{11} > 0 \\ X_C & \text{if } \sigma_{11} < 0 \end{cases} \tag{2.5}$$

$$\sigma_{22} \geq \begin{cases} Y_T & \text{if } \sigma_{22} > 0 \\ Y_C & \text{if } \sigma_{22} < 0 \end{cases} \tag{2.6}$$

$$\tau_{12} \geq S \tag{2.7}$$

where

X_T, X_C are tensile and compressive strength in longitudinal (fiber) direction

Y_T, Y_C are tensile and compressive strength in transverse direction

S is maximum shear strength.

Maximum strain failure criterion is similar to the maximum stress failure criterion, but it is formulated in terms of strain in material principal axes. The maximum stress and strain failure theories generally yield different results and are not extremely accurate. The main inaccuracy in this theory comes from the assumption that there is no interaction between the failure modes and they are completely separate. Despite this fact, they are often used because of their simplicity.

Tsai-Hill failure criterion
The Tsai-Hill failure criterion is considered and extension of the von Mises yield failure criterion. The original isotropic material yield criterion by von Mises was generalized by Hill in 1948 [10] for anisotropic materials. Later in 1965, Azzi and Tsai [11] applied Hill's theory to a thin orthotropic lamina. The Tsai-Hill failure criterion takes form

$$\frac{\sigma_{11}^2}{X^2} + \frac{\sigma_{22}^2}{Y^2} - \frac{\sigma_{11}\sigma_{22}}{X^2} + \frac{\tau_{12}^2}{S^2} \geq 1 \tag{2.8}$$

where

$$X = \begin{cases} X_T & \text{if } \sigma_{11} > 0 \\ X_C & \text{if } \sigma_{11} < 0 \end{cases} \tag{2.9}$$

$$Y = \begin{cases} Y_T & \text{if } \sigma_{22} > 0 \\ Y_C & \text{if } \sigma_{22} < 0 \end{cases} \tag{2.10}$$

This criterion was the first attempt to account for an interaction of failure modes in multi-axial stress state, which is closer to the reality than the maximum stress criterion. Nevertheless, it is rooted in the mechanism of yielding, and therefore is appropriate for orthotropic metal sheets, its adaptation to failure of a unidirectional composite raises severe doubts about its validity because of the diverse failure mechanisms that operate under different imposed stress states as described by Telreja [6].

Tsai-Wu failure criterion
Tsai-Wu [12] theory is a simplification of a general anisotropic failure theory by Gol'denblat and Kopnov. The most compact form for expressing the Tsai-Wu failure criterion is through tensor notation:

$$F_i\sigma_i + F_{ij}\sigma_i\sigma_j \geq 1 \qquad i,j = 1,2,...,6 \tag{2.11}$$

where F_i and F_{ij} are strength tensors. For an orthotropic lamina it can be expressed in a form

$$\frac{\sigma_{11}^2}{X_T X_C} + \frac{\sigma_{22}^2}{Y_T Y_C} - \frac{\sigma_{11}\sigma_{22}}{\sqrt{X_T X_C Y_T Y_C}} + \frac{\tau_{12}^2}{S^2} + \frac{X_C - X_T}{X_T X_C}\sigma_{11} + \frac{Y_C - Y_T}{Y_T Y_C}\sigma_{22} \geq 1 \tag{2.12}$$

The graphically this is a single failure surface in the form of ellipsoid. This failure criterion show much better correlation with experimental results. The only region which it does not work very well is for fibre compression failure. However, the fact remains that the ellipsoidal representation of the strength of thin sheets of unidirectional composites in the in-plane stress components is only a postulate that is not motivated or supported by any physical consideration of the failure mechanisms. [6]

Puck failure criterion
Puck [13] followed the failure theory framework of Hashin. A lot of new symbols and terminology have been introduced in Puck's theory. It also recognizes fibre failure and matrix failure modes as Hashin, however the later one was renamed as inter fibre failure mode. An elaborate procedure is proposed for evaluating the inclination of the failure plane and the critical tractions on the failure plane, resulting in very adaptable 7-parameter model. The Puck criterion recognizes three different inter-fibre failure modes, referred to as modes A, B, and C. These inter-fibre failure modes are distinguished by the orientation of the fracture planes relative to the reinforcing fibres. A comprehensive description of Puck's theory and its mathematical details can be found in the German guideline VDI 2014 Part 3 [14]

With a large number of empirical constants in Puck's failure theory, its ability to describe failure data is better than all previous failure theories. However, some of the seven constants associated with failure in the matrix are difficult to determine, even for a UD composite layer. [15]

Failure theories limitations
Over the years, many composite laminates failure theories have been proposed.

However, there was a very little evidence of their accuracy and general usability. An extensive research program, called the World Wide Failure Exercise [1] (WWFE) has been conducted between the 1996 and 2004, when 19 theories for predicting failure in composite laminates have been tested against experimental evidence. The comparison has been made through 14 carefully selected test cases, which include biaxial strength envelopes for a range of unidirectional and multi-directional laminates, and stress-strain curves for a range of multi-directional laminates, loaded under uniaxial or biaxial conditions. The predictions were provided by the originators of the theories, not by third parties, and were made without access to the experimental results beforehand. The predictions and experimental data have been compared in a systematic and detailed manner, to identify the strengths and weaknesses of each theory, together with a ranking of the overall effectiveness of each theory. [16]

Results of the WWFE are summarized in [1], together with a recommendations for designers. Basically, none of the theories give satisfactory results for all cases, but the most promising theories were identified. Also, there are number of topics, which have not been assessed by WWFE, such as delamination initiations, buckling, and effect of fibre reinforcement such as woven and non-woven cloth.

One of the problems identified by WWFE is the lack of implementation of the most successful theories in user friendly computer codes and state of the art finite element packages. There are many ways to implement a failure theory into a code and this can influence the predictions made. Thus, there is no guarantee that, for instance, a theory used within an FE idealisation and the same theory employed in an analytical model by the originator of that theory, will produce equivalent predictions. One of those, who decline participating in WWFE was professor Hashin, who is very well known by the composite community and his letter to the organizers is worth noting [1]:

> "My only work in this subject relates to failure criteria of unidirectional fibre composites, not to laminates. I do not believe that even the most complete information about failure of single plies is sufficient to predict the failure of a laminate, consisting of such plies. A laminate is a structure which undergoes a complex damage process (mostly of cracking) until it finally fails. The analysis of such a process is a prerequisite for failure analysis. While significant advances have been made in this direction we have not yet arrived at the practical goal of failure prediction. I must say to you that I personally do not know how to predict the failure of a laminate (and furthermore, that I do not believe that anybody else does."

The organizers of WWFE initiated a two more competitions, which attempted to analyse these theories against a number of tri-axial test cases (WWFE-II), and gain more insight into the prediction of evolving composite damage (WWFE-III). The results of WWFE-II have been published in special issue of Journal of Composite Materials [17]. WWFE-III is still being conducted.

Another limitation of the phenomenological failure theories lies in their inability to account for manufacturing defects that are inevitable in practical composite structures. In recent years, the composite structural applications have increased in non-aerospace fields such as wind turbine blades and automotive structures, where cost requirements do not allow high levels of quality control of manufacturing processes and limit in-service inspection. The importance of accounting for manufacturing defects in the design phase has therefore become vital. [15]

2.3.3 Delamination

A complete understanding of composite delamination requires an appreciation for the fundamental principles of fracture mechanics and how these principles have been extended from the original concepts developed for isotropic materials. There are two alternative approaches to fracture analysis: the energy criterion and the stress intensity approach. These two approaches are equivalent in certain circumstances. Both are discussed briefly below. [18]

Stress intensity factor
Figure 2.4 schematically shows an element near the tip of crack in an elastic material, together with the in-plane stresses on this element. The stresses for the isotropic case at a point near the crack tip defined by polar coordinates r, θ can be expressed as

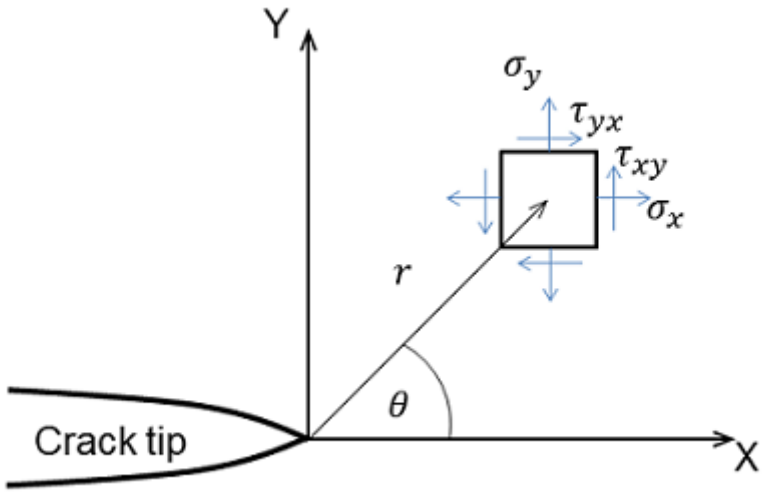

Figure 2.4: Stresses near the crack tip of a crack in an elastic material

$$\sigma_x = \frac{K_I}{\sqrt{2\pi r}} f_1(\theta) \tag{2.13}$$

$$\sigma_y = \frac{K_I}{\sqrt{2\pi r}} f_2(\theta) \tag{2.14}$$

$$\tau_x y = \frac{K_I}{\sqrt{2\pi r}} f_3(\theta) \tag{2.15}$$

where $f_i(\theta)$ are trigonometric function of the angle. [19] Note that each stress component is proportional to a single constant, K_I. If this constant is known, the entire stress distribution at the crack tip can be computed. This constant, which is called stress intensity factor, completely characterizes the crack tip conditions in a linear material. For the plate illustrated in Figure 2.5, the stress intensity factor is given by

$$K_I = \sigma\sqrt{\pi a} \tag{2.16}$$

If one assumes that the material fails locally at some critical combination of stress and strain, then it follows that fracture must occur at critical stress intensity, K_{Ic}. Thus K_{Ic} is a measure of fracture toughness. One of the major drawbacks of the stress intensity approach is that a stress analysis of the crack tip region is required. While such analyses have been done for variety of loading conditions and crack geometries for isotropic materials, the corresponding analyses for anisotropic materials have only been done for relatively few cases because of mathematical difficulties. [19]

Strain energy release rate

The energy approach states that crack extension occurs when the energy available for crack growth is sufficient to overcome the resistance of material. The material resistance may include the surface energy, plastic work, or other type of energy dissipation associated with a propagating crack. Present version of this approach is based on the work of Griffith [20] and Irwin [21]. The energy release rate, G, is defined as the rate of change in potential energy with crack area for a linear elastic material. At the moment of fracture, $G = G_c$, the critical energy release rate which is a measure of fracture toughness. For a crack of length $2a$ in an infinite plate subject to a remote tensile stress (Figure 2.5), the energy release rate is given by

$$G = \frac{\pi\sigma^2 a}{E} \tag{2.17}$$

where E is Young's modulus, σ is the remotely applied stress, and a is the half crack length. At fracture, $G = G_c$, and Equation (2.17) describes the critical combination of stress an crack size for failure:

$$G_c = \frac{\pi\sigma_f^2 a_c}{E} \tag{2.18}$$

Comparing equations (2.17) and (2.16) results in a relationship between K_I and G:

$$G = \frac{K_I^2}{E} \tag{2.19}$$

Thus, the energy and stress intensity approaches to fracture mechanics are essentially equivalent for linear elastic materials.

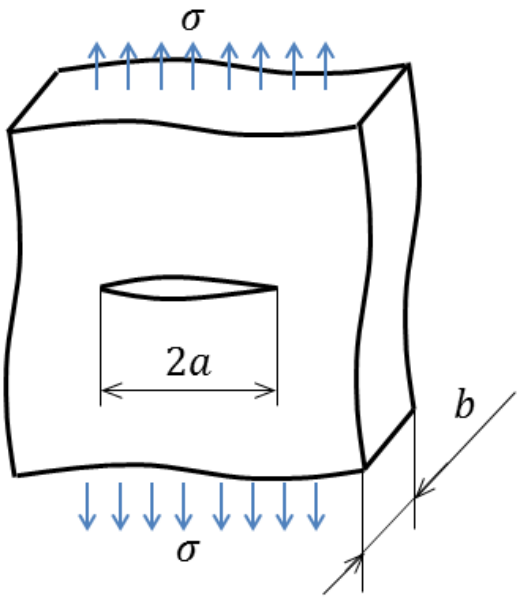

Figure 2.5: Through-thickness crack in an infinite plate subject to a remote tensile stress

The strain energy release rate approach has an easily understood physical interpretation that is equally valid for either isotropic or anisotropic materials, and it turns out that this rate is also related to the stress intensity factor. The strain energy release rate approach has proved to be a powerful tool in both experimental and computational studies of crack growth.[12]

Loading modes

There are three types of loading that crack can experience, as Figure 2.6 illustrates. Mode I loading, where the principal load is applied normal to the crack plane, tends to open the crack. Mode II corresponds to in-plane shear loading and tends to slide one crack face with respect to the other. Mode III refers to out-of-plane shear. A cracked body can be loaded in any one of these modes, or a combination of two or three modes.

The most usual fracture mode to be considered is the opening mode I which results from stresses normal to crack. In homogeneous isotropic materials, even if other type of loading is present, a propagating crack seeks the path of least resistance and need not be confined to its initial plane, so the crack usually kinks and propagates under mode I conditions. However, this is not a case for material interfaces, where mode II, mode III and their combination with mode I are more important.

Delamination analysis

The growth of a crack between two solids with different elastic behaviour is a difficult problem to deal with. Using the linear elasticity theory, the obtained results show unusual complex singularities in the neighbourhood of the crack

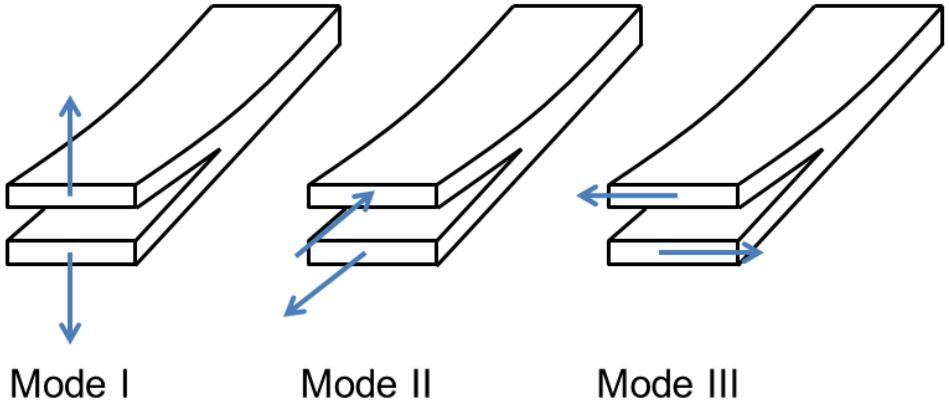

Figure 2.6: Loading modes

tip. In addition, the three stress intensity factors at the crack tip, K_I, K_{II} and K_{III}, are coupled to each other and achieve complex values. Although the many proposals to avoid the stress singularity at the crack tip, the stress intensity factor is governed by the local crack-tip field and is extremely sensitive. Thus, most of the studies about composite delaminations are based on the critical energy release rate, G_c, instead of the critical stress intensity factor K_c, to predict the onset of interlaminar cracks. [22]

For laminated composites, interlaminar fracture mechanics has proven useful for characterizing the onset and growth of delaminations. To fully understand this failure mechanism, the total strain energy release rate, G_T, the mode I component due to interlaminar tension, G_I, the mode II component due to interlaminar sliding shear, G_{II}, and the mode III component, G_{III}, due to interlaminar scissoring shear, need to be calculated. In order to accurately predict delamination onset or growth for two dimensional problems, these calculated G components are compared to interlaminar fracture toughness properties experimentally measured over a range from pure mode I loading to pure mode II loading. [23]

There are many forms of delamination onset criteria. The one used by Benzeggagh and Kenanane [25] determines the quasi-static mixed-mode fracture criterion by plotting the interlaminar fracture toughness, G_c , versus the mixed-mode ratio, G_{II}/G_T , obtained from data generated using pure mode I Double Cantilever Beam (DCB), pure mode II End Notched Flexure (ENF) and Mixed Mode Bending (MMB) tests of varying ratios. For a detailed description of these methods see Chapter 2.5.2. A curve fit of these data is performed to determine a mathematical relationship between G_c and G_{II}/G_T , as shown in Figure 2.7. Failure is expected when, for a given mixed mode ratio, G_{II}/G_T , the calculated total energy release rate, G_T, exceeds the interlaminar fracture

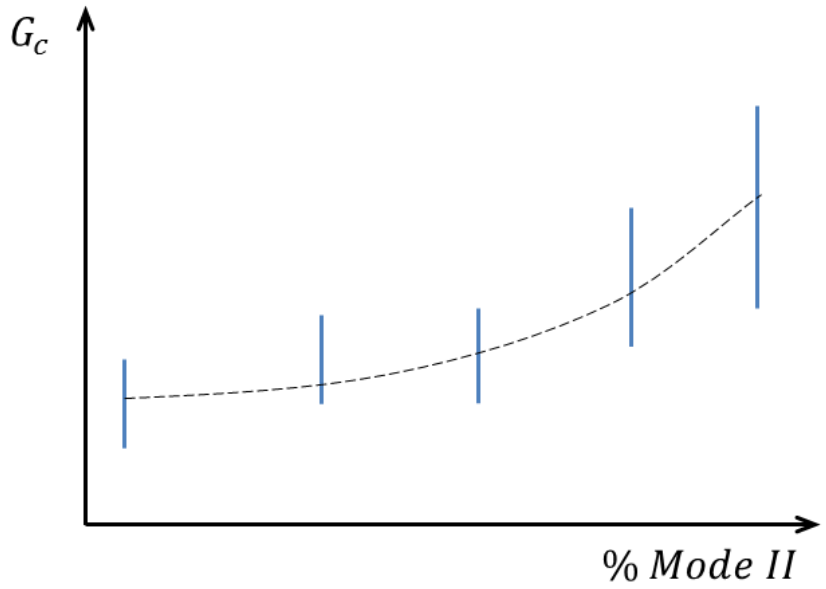

Figure 2.7: Mixed mode fracture envelope (schematic presentation) [24]

toughness, G_c. Mathematically, this criterion can be expressed

$$G_{Tc} = G_{Ic} + (G_{IIc} - G_{Ic}) \left(\frac{G_{II}}{G_T} \right)^m \tag{2.20}$$

where m is a fitting coefficient.

Another frequently used mixed mode failure criterion is the power law described by Wu [26] and has a form

$$\left(\frac{G_I}{G_{Ic}} \right)^\alpha + \left(\frac{G_{II}}{G_{IIc}} \right)^\beta = 1 \tag{2.21}$$

Although several different types of test specimens have also been suggested for the measurement of the mode III interlaminar fracture toughness property, an interaction criterion incorporating the scissoring shear, however, has not yet been established and remains a challenge.

Delamination fatigue

The methodology described above has been extended to predict fatigue delamination onset and fatigue life but to date a standard only exists for the mode I DCB test. In analogy with metals, delamination growth rate can therefore be expressed as a power law function (i.e. Paris Law). [23]

$$\frac{da}{dN} = B(G_{max})^n \tag{2.22}$$

Based on the modified Paris' law, a total fatigue life model was suggested by Shivakumar et al. [27]. The crack growth rate is characterized experimentally

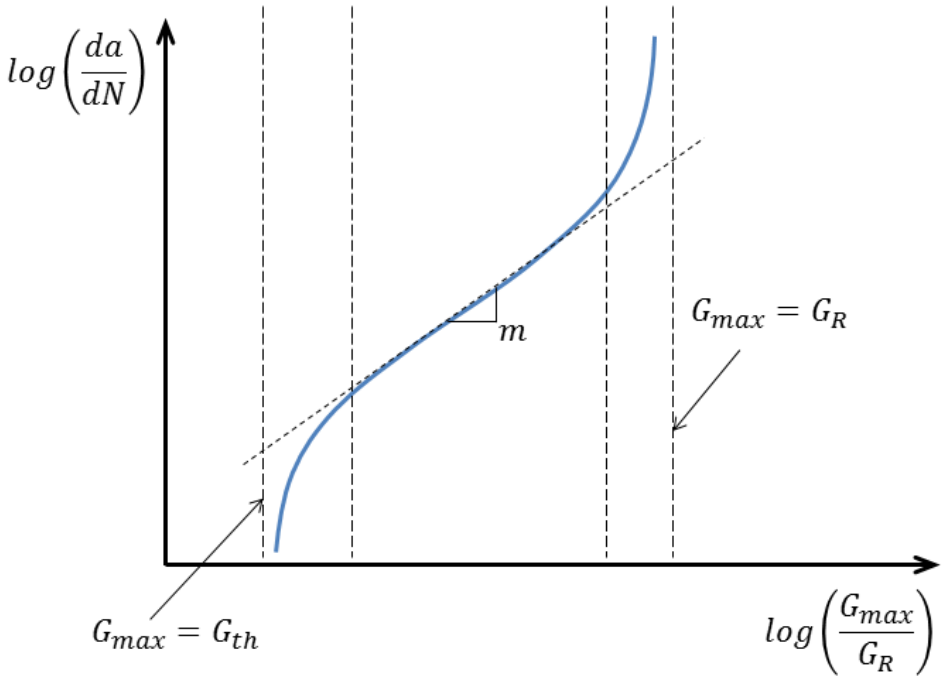

Figure 2.8: Fatigue delamination life model [27]

in terms of the applied strain energy release rate and visualised in log-log plat as shown in Figure 2.8. The delamination growth region is bounded by threshold strain energy release rate, G_{th}, on the left and by maximum cyclic strain energy release rate, G_{max}, on the right. The delamination growth rate for mode I can be expressed as

$$\frac{da}{dN} = Am\left(\frac{G_{Imax}}{G_{IR}}\right)^m \frac{\left(1-\left(\frac{G_{Ith}}{G_{Imax}}\right)^{D_1}\right)}{\left(1-\left(\frac{G_{Imax}}{G_{IR}}\right)^{D_2}\right)} \tag{2.23}$$

where A, m, D_1 and D_2 are material constraints.

Strain energy release rate based on specimen compliance

Irwin [21] defined an energy release rate, G, which is a measure of the energy available for an increment of crack extension

$$G = -\frac{d\Pi}{dA} \tag{2.24}$$

The potential energy of an elastic body, Π, is defined as

$$\Pi = U - F \tag{2.25}$$

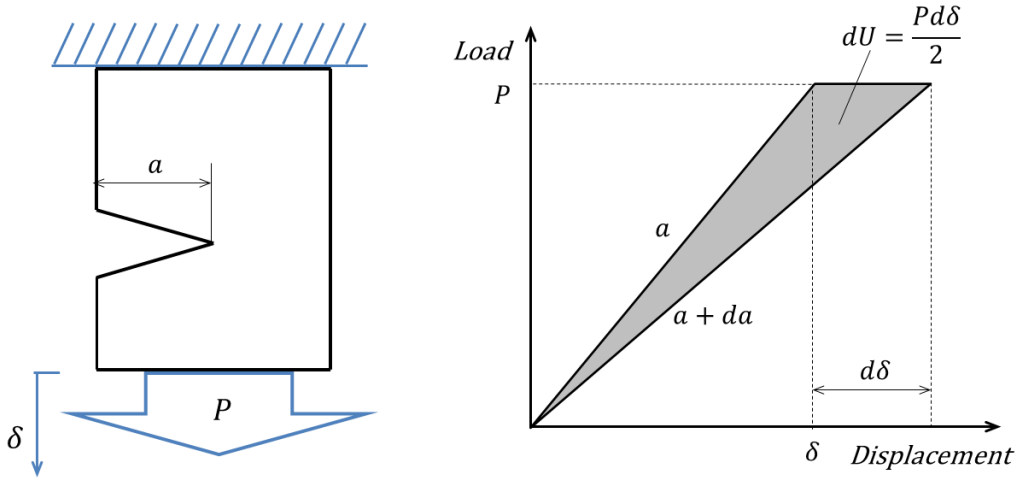

Figure 2.9: Cracked plate at fixed load P [18]

where U is the strain energy stored in the body and F is the work done by external forces. If we consider a load controlled cracked plate, as illustrated in Figure 2.9, the work done by the external force is

$$F = P\delta \tag{2.26}$$

and strain energy is

$$U = \int_0^{\delta} P d\delta = \frac{P\delta}{2} \tag{2.27}$$

Therefore

$$\Pi = -U \tag{2.28}$$

and if b is the width of the body, the energy release rate becomes

$$G = \frac{1}{b}\left(\frac{dU}{da}\right)_P = \frac{P}{2b}\left(\frac{d\delta}{da}\right)_P \tag{2.29}$$

For a displacement controlled cracked plate, as shown in Figure 2.10, $F = 0$ and $\Pi = U$, so the energy release rete may be written as

$$G = -\frac{1}{b}\left(\frac{dU}{da}\right)_\delta = -\frac{\delta}{2b}\left(\frac{dP}{da}\right)_\delta \tag{2.30}$$

We can introduce compliance as an inverse of the plate stiffness

$$C = \frac{\delta}{P} \tag{2.31}$$

By substituting equation 2.31 into 2.29 and 2.30, it can be shown that

$$G = \frac{P^2}{2b}\left(\frac{dC}{da}\right) \tag{2.32}$$

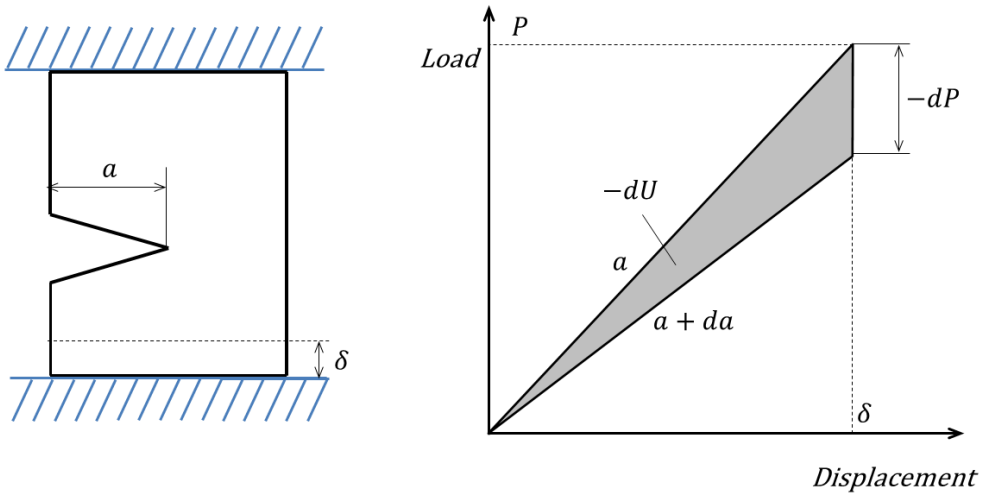

Figure 2.10: Cracked plate at fixed displacement [18]

Equation 2.32 is a frequently used form of calculating energy release rate from specimen compliance.

Strain energy release rate based on beam theory

Simple beam theory as used by [28] has been found to be effective for calculating the energy release rate from the local value of bending moments, shear and axial loads in cracked laminate. This method considers a delamination with a uniform width b in a thin sheet of thickness $2h$, as shown in Figure 2.11. The bending moments M_1 and M_2 are applied to the upper and lower sections respectively.

Energy release rate, G, may be defined as

$$G = \frac{1}{b}\left(\frac{\Delta U_E}{\Delta a} - \frac{\Delta U_s}{\Delta a}\right) \tag{2.33}$$

where U_E is the external work performed and $U_S$is the strain energy. When the crack moves from O to O' then the change in angle in the upper beam is

$$\left(\frac{d\varphi_1}{da} - \frac{d\varphi_0}{da}\right)\Delta a \tag{2.34}$$

and in the lower beam

$$\left(\frac{d\varphi_2}{da} - \frac{d\varphi_0}{da}\right)\Delta a \tag{2.35}$$

External work can then be expressed as

$$\Delta U_E = M_1\left(\frac{d\varphi_1}{da} - \frac{d\varphi_0}{da}\right)\Delta a + M_2\left(\frac{d\varphi_2}{da} - \frac{d\varphi_0}{da}\right)\Delta a \tag{2.36}$$

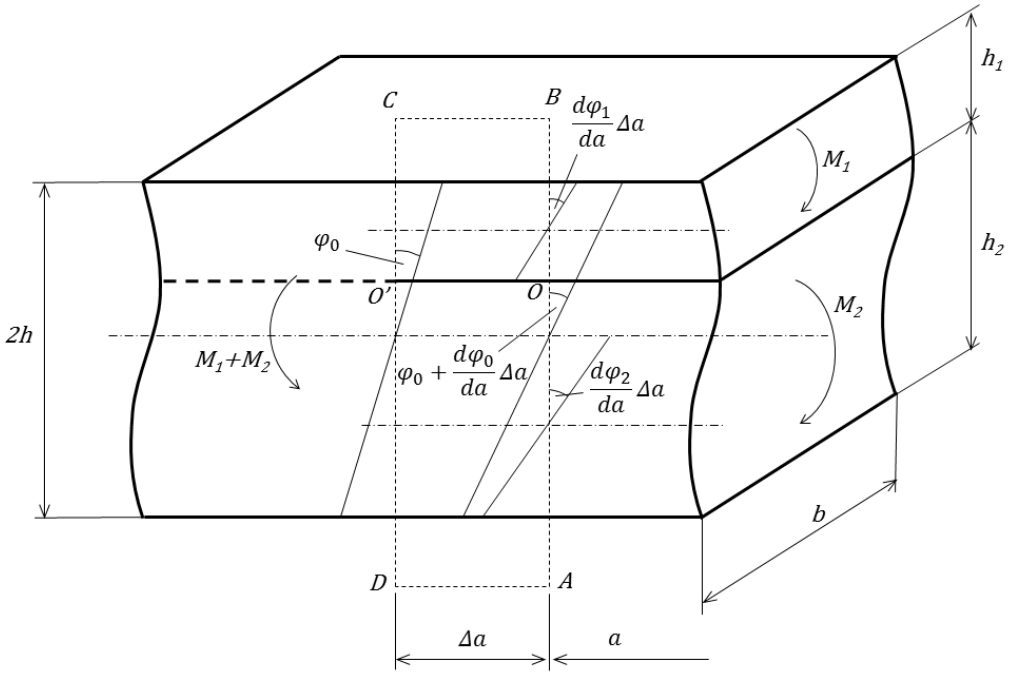

Figure 2.11: Crack tip contour with rotations

where

$$\frac{d\varphi_1}{da} = \frac{M_1}{EI_1} \tag{2.37}$$

$$\frac{d\varphi_2}{da} = \frac{M_2}{EI_2} \tag{2.38}$$

$$\frac{d\varphi_0}{da} = \frac{M_1 + M_2}{EI} \tag{2.39}$$

if we consider a thickness parameter

$$\xi = \frac{h_1}{2h} \tag{2.40}$$

second moment of area for each section can be writen as

$$I = \frac{2bh^3}{3} \tag{2.41}$$

$$I_1 = \frac{bh_1^3}{12} = \xi^3 I \tag{2.42}$$

$$I_2 = \frac{bh_2^3}{12} = (1-\xi)^3 I \tag{2.43}$$

Then external work is

$$\Delta U_E = \frac{\Delta a}{EI_0}\left[\frac{M_1^2}{\xi^3} + \frac{M_2^2}{(1-\xi)^3} - (M_1+M_2)^2\right] \tag{2.44}$$

The strain energy in a beam is given by

$$\frac{\Delta U_S}{\Delta a} = \frac{1}{2}\frac{M^2}{EI} \tag{2.45}$$

so the change within the contour is

$$\Delta U_S = \frac{1}{2}\frac{M_1^2}{EI_1}\Delta a + \frac{1}{2}\frac{M_2^2}{EI_2}\Delta a - \frac{1}{2}\frac{(M_1+M_2)^2}{EI}\Delta a \tag{2.46}$$

i.e.,

$$\Delta U_S = \frac{\Delta a}{2EI}\left[\frac{M_1^2}{\xi^3} + \frac{M_2^2}{(1-\xi)^3} - (M_1+M_2)^2\right] \tag{2.47}$$

and on substituing 2.47 and 2.44 into 2.33 we have

$$G = \frac{1}{2bEI}\left[\frac{M_1^2}{\xi^3} + \frac{M_2^2}{(1-\xi)^3} - (M_1+M_2)^2\right] \tag{2.48}$$

This is a very powerful result since it enables to calculate G only from local values of bending moments and no energies are required. Other type of loads such as shear and axial forces may be included by superposition.

Mode partitioning

As the contribution of mode III is not considered, the total energy release rate in equation (2.48) the sum of mode I and mode II. To obtain the contribution of each individual mode, equation (2.48) must be partitioned.

Pure mode II propagation occurs when the curvature of both arms is the same and therefore

$$\frac{d\varphi_1}{da} = \frac{d\varphi_2}{da} \tag{2.49}$$

and if we have M_{II} on the upper arm and ψM_{II} on the lower then

$$\frac{M_{II}}{EI_1} = \frac{\psi M_{II}}{EI_2} \tag{2.50}$$

i.e.,

$$\psi = \left(\frac{1-\xi}{\xi}\right)^3 \tag{2.51}$$

The opening mode only requires moments in opposite senses so we have $-M_I$ on the upper arm and M_I on the lower arm so that applied moments may be resolved as

$$M_1 = M_{II} - M_I \tag{2.52}$$

$$M_2 = \psi M_{II} + M_I \tag{2.53}$$

i.e.,

$$M_I = \frac{M_2 - \psi M_1}{1+\psi} \tag{2.54}$$

$$M_{II} = \frac{M_2 + M_1}{1+\psi} \tag{2.55}$$

Substituing these expressions in (2.48) we have

$$G = \frac{M_I^2}{2bEI}\frac{(1+\psi)}{(1-\xi)^3} + \frac{3M_{II}^2}{2bEI}\frac{(1-\xi)}{\xi^2}\ (1+\psi) \tag{2.56}$$

Note that ther is no cross product term, as required by partitioning.

The general utility of this method is best illustrated on a simple common test geometry such as double cantilever beam test (DCB) for mode I and end load split test (ELS) for mode II, as shown in Figure 2.12.

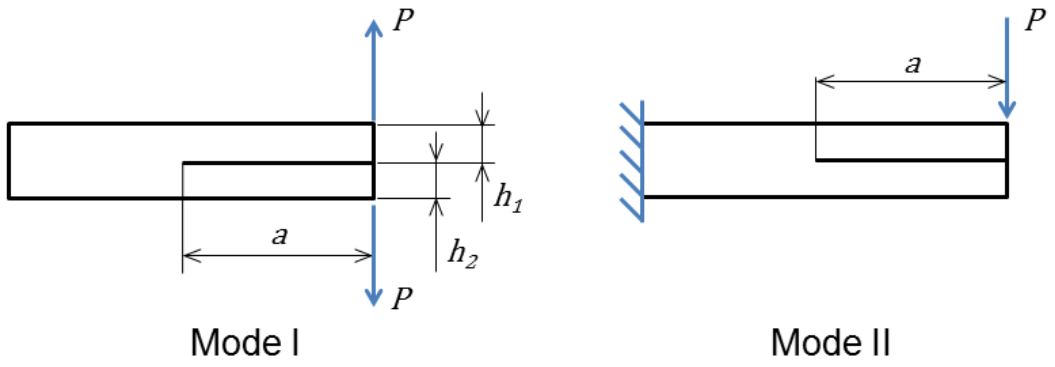

Figure 2.12: Mode I (DCB) and mode II (ELS) test

For a centrally cracked section $\xi = 1/2$ and $\psi = 1$. For symmetrical loading in Figure 2.12 we have $M_2 = -M_1 = Pa$. Therefore $M_{II} = 0$ and $M_I = Pa$ resulting in

$$G_I = \frac{8P^2a^2}{bEI} \tag{2.57}$$

For mode II shown in Figure 2.12, we have $M_2 = M_1 = Pa/2$, giving $M_{II} = Pa/2$ with $M_I = 0$ and final results

$$G_{II} = \frac{9}{4}\frac{P^2a^2}{b^2Eh^3} \tag{2.58}$$

2.4 Defects in composite materials

2.4.1 Type of defects

Defects in composite materials can be grouped into specific categories according to when they arise during their life, their relative size, their location or origin within the structure:

1. Defect occurrence - defects may occur during different stages of the component life:
   (a) Manufacturing process
      i. Materials processing - the processes of advanced composite manufacture are predisposed to errors, especially human errors, that can lead to the formation of defects in structure. Such material processing defects occur because of improper storage of materials, or inadequate quality control and batch certification procedures. Both can lead to material property variations and in some cases can lower the properties below the design allowables.
      ii. Component Manufacture - component manufacture induced defects occur during either lay-up or cure (component fabrication), or machining and assembly of the components.
   (b) In-Service Use - during service, composite structures are prone to many mechanical and environmental conditions such as impact and handling damage, local overloading, local heating, chemical attack, ultraviolet radiation, battle damage, lightning strikes, acoustic vibration, fatigue or inappropriate repair action.
2. Defect size - the size of a defect has significant bearing on its criticality. Therefore, defects are listed under two sizes:
   (a) Microscopic - these defects occur at the level of micromechanics of composites, i.e. at the level of the individual constituents.
   (b) Macroscopic - macroscopic defects can be found at the level of individual plies or the whole structure.
3. Defect location - defects may be present in isolation, originating from structural features such as cut-outs, ply drops and joints, or a random accumulation resulting from their interaction. However, they tend to concentrate at discontinuities, either geometrical or material.

The most common defects occurring in composite material, either in manufacturing process or during service, are:

Delamination refers to situations in which defect occurs on a plane between adjacent layers within a laminate. This type of defect is dominated by the properties of the matrix and since matrix strengths and toughness tend to be

relatively low, laminated composites are prone to the development of delaminations. In many types of composite structure (e.g. aircraft, marine, etc.) delaminations are the most common form of defect. Delaminations are very dangerous defects as they lead to more severe damage or even catastrophic failure. Even small areas of delamination are capable for reducing the compression strength of composite materials by over 50 percent. Delaminations may be formed during manufacture under residual stresses or as a result of the lay-up process or in-service. Impact damage or environmental degradation are common methods for formation of sub-surface delaminations. Edge delaminations are quite common due to environmental effects.

Disbond refers to the situation in composite structures where decohesion of a bonded layer has occurred. This may be the consequence of poor adhesion, service loading or impact damage. The term disbond is defined as a separation of the composite material from another material to which it has been adhesively bonded.

Cracking is a common form of damage in composites and other materials arising in manufacture or under service conditions. Cracking is defined as a discrete single crack type defect in the composite usually through thickness and normally affecting both matrix and fibres. A crack is distinct from a delaminations or disbond which refer to inter-laminar separation of material or decohesion of a bond, matrix cracking or transverse cracking which refer to finer scale types of multiple cracking normally occurring in the central ply of composites under service loading, and fibre cracking or breakage. Cracking has a significant effect on the integrity of the composite, allowing environment ingress and damage to extend under service loading. Cracking is often associated with the final stages of in-service failure.

Voids and porosity can occur in manufacture due to volatile resin components or air not properly controlled during cure. Single or isolated large air bubbles are referred to as voids or. The distinction between discrete voids and porosity is a matter of convenience but for practical purposes, porosity may be thought of as sub-millimetre voids whereas voids of several millimetres dimension would be considered as discrete defects and voids. Voids can act as stress concentrations and will have an effect on some of the mechanical properties, for example giving lower transverse and through-thickness tensile, flexural, shear and compression strengths. Void content is generally considered negligible if less than 3%, but individual voids may have structural significance and assist initiation of other defects particularly if present at interfaces. Void and porosity are the most important manufacturing defects that are likely to occur in practice. 1% porosity reduces strength by 5% and fatigue life by 50% Voids are usually produced during the curing cycle from entrapped air, moisture or volatile pro ducts. Voids and porosity are most likely following manufacturing by hand lay-up.

Inclusion can occur in the manufacture of composites due to foreign matter accidentally included in material. Examples include backing paper, peel ply etc. Inclusions can have degrading effect on mechanical properties and may act as sites for initiation of delaminations and are a common cause of disbonds in composites. Inclusions are more likely in hand lay-up processes than in modern processing methods such as resin transfer moulding.

Erosion of the composite surface can o cur in service, particularly in composite process vessels or pipework from the effects of material flow or impact of particulates. A precursor is the localised breakdown of the gel coat or chemical liner in the case of process vessels. This mechanism may give rise to broad defects or to finer scale pin-hole damage. Erosion can facilitate further environment ingress and damage to the composite material. The localised loss of wall thickness will impact on the integrity of the material.

Matrix micro-cracking refers to intralaminar or ply cracks that traverse the thickness of the ply and run parallel to the fibres in that ply. Their existence does not necessarily mean catastrophic failure of the composite as they can be present only in certain plies (usually those transverse to the main loading direction) and while the fibres (which carry most of the load) remain intact. Matrix micro cracks can develop under tensile loading, fatigue loading, thermal loading and impact conditions. They sometimes arise in composites during manufacture but are more commonly associated with in-service effects. Matrix micro cracking is one of the most common forms of damage encountered in composite materials and is often a precursor to overall failure.

Fibre defects the presence of defects in the fibres themselves is one of the ultimate limiting factors in determining strength of composite materials, and sometimes faulty fibres can be identified as the sites from which damage growth has been initiated.

Fibre wrinkling or waviness refers to the in-plane kinking of the fibres in a ply. Waviness or wrinkling of the fibres can seriously affect laminate strength. This type of defect is particularly of concern in high integrity aerospace and defence components. Fibre misalignment refers to local or more extensive misalignment of fibres in the composite material. This causes local changes in volume fraction by preventing ideal packing of fibres. Ply misalignment refers to the situation where a whole or part of a ply or layer of the composite is misaligned. This is produced as a result of mistakes made in lay-up of the component plies. This alters the overall stiffness and strength of the laminate and may cause bending during cure. The properties of the resulting component will be affected. Fibre and ply misalignment are potentially disastrous defects but are rarely encountered due to high standards of quality control. In a composite laminate, alignment can typically vary by $\pm 2^\circ$ in either direction without noticeable effect on overall strength. One problem that occurs occasionally is that plies are totally out of specified alignment, e.g., 45° or 90° is used where 0° is called for.

Incomplete cure refers to the situation where the matrix has been incompletely cured due to incorrect curing cycle or faulty resin material. This may be localised or affect the whole component. The result will be reduced strength and toughness. Incomplete cure is also an issue in adhesive processes using resin based adhesives affecting the integrity of end-fittings and adhesive joints.

Resin variations Fabrication methods for composites are designed to provide a uniform distribution of fibres in a resin matrix. Properties depend on the fibre volume fraction. Load transfer across the fibre matrix interfaces are a key feature giving rise to the good strength and toughness characteristics of composites. It is a natural consequence of manufacturing methods that local variations in fibre or resin content will occur. Where the resin content is above design limits this is referred to as excess resin. Where the fibre content is outside design limits this is referred to as excess fibre.

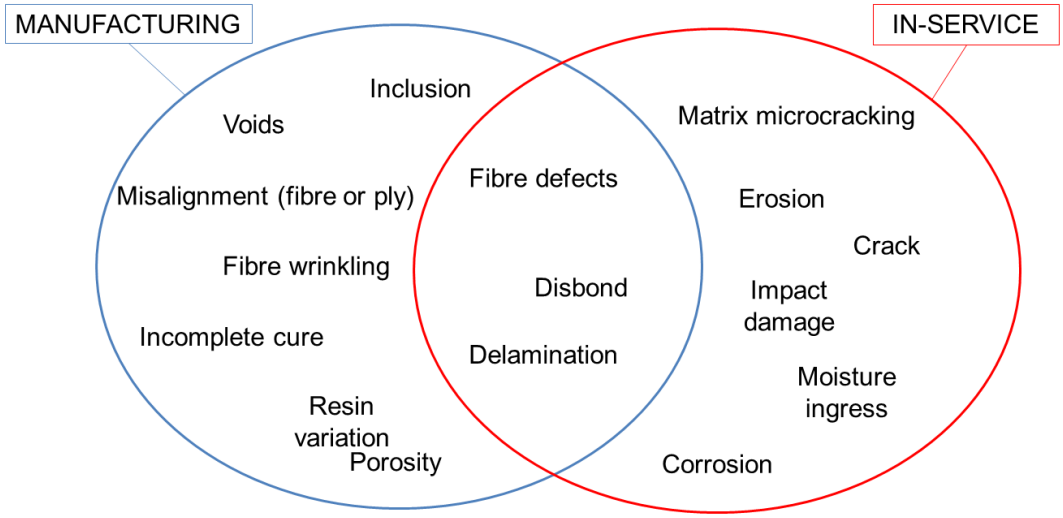

Figure 2.13: Classification of defects by their occurrence

2.4.2 Effects of defects in composites

In general, all types of defects, both manufacturing and in-service, might affect stiffness, strength, stability and fatigue life of the composite structure mainly because they act as the stress concentrators and failure initiation points. Profound understanding of how these defects influence the performance of composites is essential for making the structures safer, more durable, and economic. An example of how porosity and delaminations might affect a compressive strength is shown in Figure 2.14.

Because of the wide range of possible defects and many failure mechanisms occurring in composite materials, the studies on effects of defects are usually performed separately for particular defects. The most common types of defects investigated by various researchers include ply waviness, porosity, impact damage and delaminations.

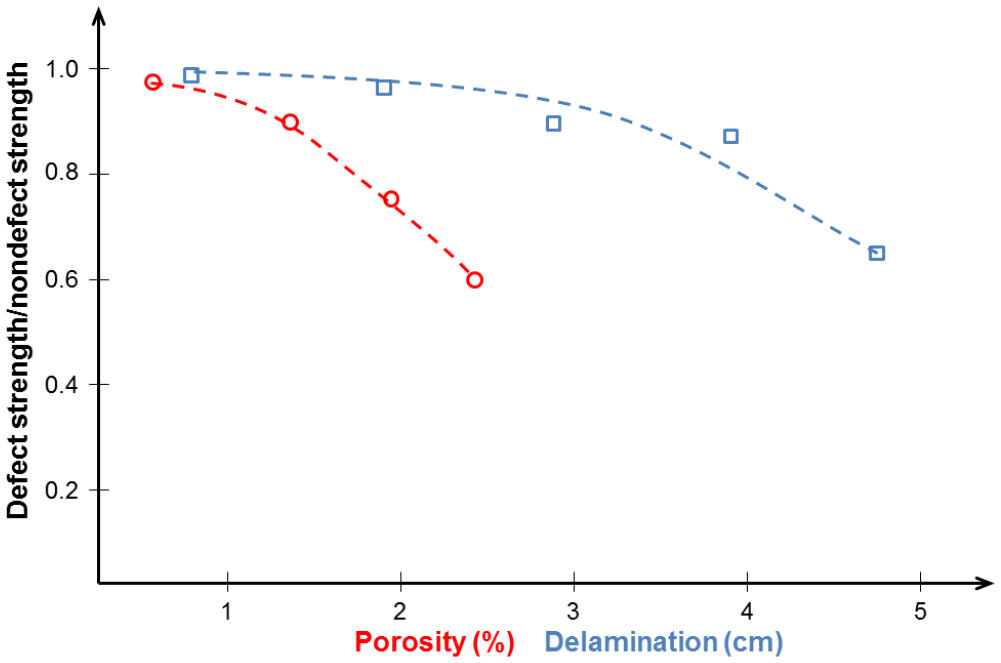

Figure 2.14: Compressive strength versus defect size [29]

2.5 Composite materials testing and characterization

Composites properties can are very complex and depend on fibres, matrix, layup, volume fraction, environmental conditions, manufacturing methods, cure conditions, etc. Thus, mechanical testing methods and requirements are more demanding than is the case for metals. Mechanical testing is mainly for establishing the design allowables, qualification of materials for certain application and quality control. Many of the testing methods have their origin in testing of metals and other homogeneous isotropic materials. However, when a testing method of isotropic materials is adapted for composites, special attention is needed because of the composites anisotropic nature.

2.5.1 Building block approach

Ideally, if structural analysis tools are fully developed and the failure criteria fully established, the structural behaviour would be predictable from constituent properties. Unfortunately, the capability of the state-of-the-art analysis tools is limited. Thus, lower level test data cannot always be used to accurately predict the behaviour of structural elements and components with higher level of complexity. The accuracy of the analytical results is further complicated by the material property variability, the inclusions of defects and the structural scale-up effects. [30] A common approach used in development of aircrafts but also adopted by many other industries is so called "Building Block Approach".

The Building Block Approach is frequently referred to as the Testing Pyramid, as shown in Figure 2.15. On the first two levels, large number of coupons and structural elements are tested in different loading modes, such as tension, compression, flexure and shear in order to generate material design allowables under static and fatigue conditions. Then, a combination of testing and analysis is used at various levels of complexity through structural elements and details, sub-components, components and finally full scale product. Each level builds on knowledge gained at previous, less complex levels. The main purpose of this approach is cost efficiency, which is achieved by testing greater number of less expensive small specimens and fewer of the more expensive component and full scale articles.

The details of applying the Building Block Approach are not standardised. There are number of standards for specimen testing at lowest level, whereas the combination of testing and analysis at higher levels of complexity are based mainly on historical experience, structural criticality, economics and engineering judgement. A good overview of the whole process is given in [30].

The multiplicity of potential failure modes is perhaps the main reason that the Building Block Approach is essential in the development of composite structures. The many failure modes in composites are mainly due to the defect, environmental and out-of-plane sensitivities of the materials. It is important to carefully select the correct test specimens that will simulate the desired failure modes. Special attention should be given to matrix sensitive failure modes. [30]

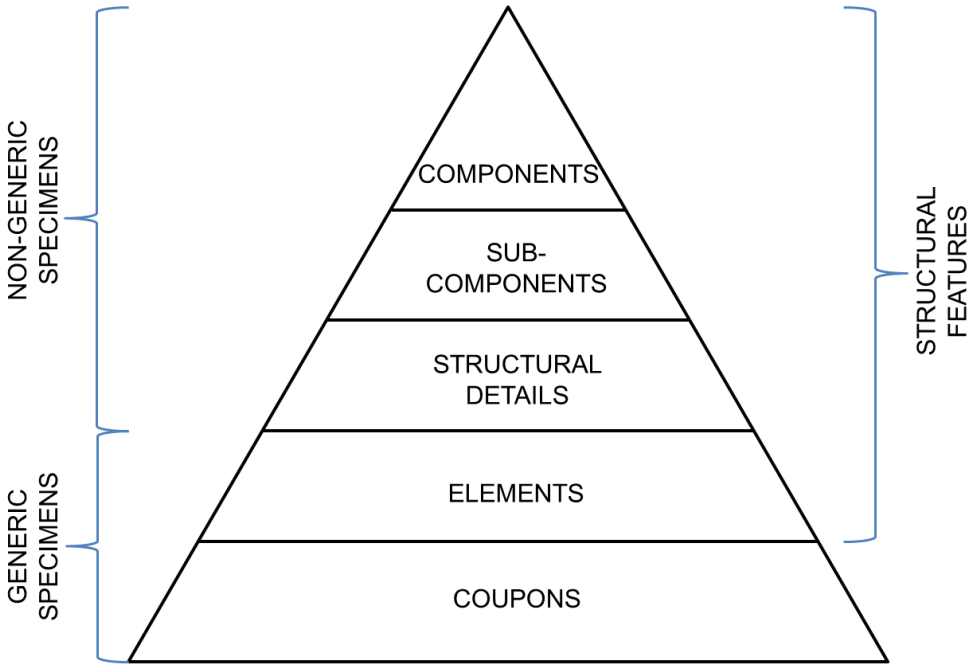

Figure 2.15: Building block approach

2.5.2 Delamination testing

Resistance to interlaminar fracture is a major interest for safe application of composites. This concern is also related to bonded composite joints, as the two phenomena are very closely relate. As described in Section 2.3.3, the fracture mechanics principles are the most used method for analysing delaminations. However, it is not always straightforward to apply the theory in experimental testing. Several methods for measuring interlaminar fracture toughness have been developed. Davies et al. [24] give a basic overview of the test methods, which have been more recently reviewed by Brunner et al [31]. Several standards exist for mode I, mode II and mixed mode loading scenarios. Some of these methods have been standardised either by ISO [32, 33], or ASTM [34, 35, 36].

Mode I

Double Cantilever Beam (DCB) specimen is the most widely used mode I specimen type. Figure 2.16 illustrates The DCB specimen geometry together with two common fixtures for loading the specimen. Blocks or hinges are normally adhesively bonded to the specimen with a starter crack made of very thin insert foil at mid-thickness. The fixtures must allow free rotation of the specimen ends with a minimum of stiffening. The opening load is produced by a test machine cross-head displacement at constant speed.

The load, P, cross-head displacement (i.e. crack opening), δ, and delamination length, a, are recorded continuously during the test. The delamination

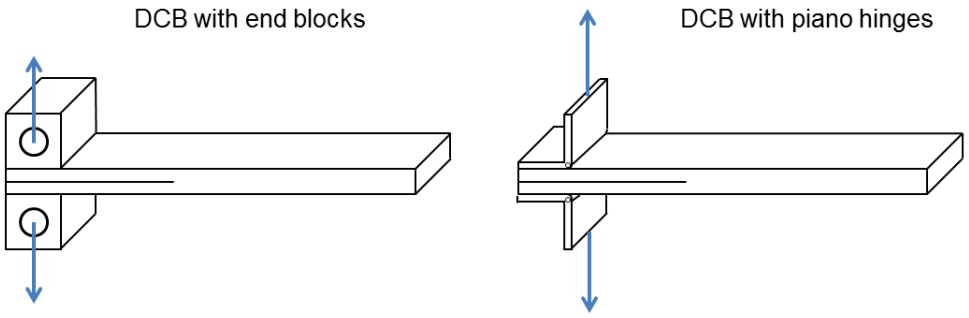

Figure 2.16: DCB specimen

length is determined as the distance from the loading line to the front of delamination as shown in Figure 2.17. Delamination lengths are determined visually during the test, the use of a travelling microscope for more accurate delamination length readings is optional, but recommended. Fracture toughness values, G_Ic, are then calculated either by using the beam theory or compliance calibration methods.

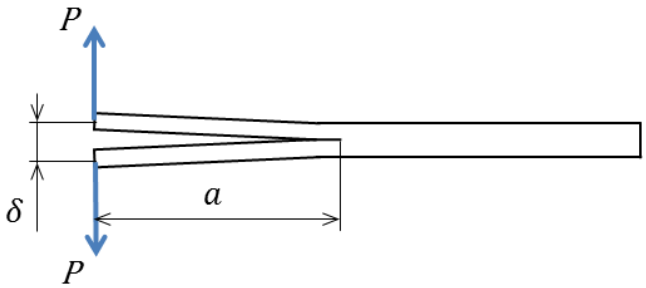

Figure 2.17: Delamination length definition

The basis of all methods of data analysis is equation (2.59) that relates the energy release rate G_C with the change in compliance due to a change in delamination length. The data analysis methods all use different approaches to evaluate dC/da.

$$G_C = \frac{P^2}{2b}\left(\frac{dC}{da}\right) \tag{2.59}$$

"Simple beam theory" takes the compliance to be the compliance of two cantilever beams perfectly clamped at delamination front. For one half of the specimen, the deflection is given by the beam theory as

$$\frac{\delta}{2} = \frac{Pa^3}{3EI} \tag{2.60}$$

and the compliance of the DCB specimen can be then written as

$$C = \frac{\delta}{P} = \frac{2a^3}{3EI} \tag{2.61}$$

Differentiating the compliance by the crack length gives

$$\frac{dC}{da} = \frac{2a^2}{EI} \tag{2.62}$$

Substituting equation (2.62) in (2.59) results in

$$G_{IC} = \frac{P^2 a^2}{bEI} \tag{2.63}$$

EI can be expressed from the beam theory equation (2.60)

$$EI = \frac{2Pa^3}{3\delta} \tag{2.64}$$

And substituting (5.5) in (2.63) leads to a final equation used to calculate fracture toughness by the simple beam theory

$$G_{IC} = \frac{3P\delta}{2ba} \tag{2.65}$$

In practice, this expression will overestimate G_{IC} because the beam is not perfectly built-in and rotation may occur at the delamination front. One way of correcting for this rotation is to treat the DCB as if it contained a slightly longer delamination, $a + |\Delta|$, as shown in Figure 2.18. The correction length, Δ, may be determined experimentally by plotting the cube root of compliance, $C^{1/3}$, as a function of delamination length, a, as in Figure 2.18. According to equation (2.61), for the two beams ideally clamped at delamination front the plot should produce a straight line that passes through the origin. However, the real tests on DCB specimens usually produce a negative intercept, Δ, and the fracture toughness can be calculated by the "modified beam theory" expression

$$G_{IC} = \frac{3P\delta}{2b\,(a + |\Delta|\,)} \tag{2.66}$$

The "compliance calibration" method is based on assumption of a certain type of functional dependence of the compliance on the delamination length. For DCB it is assumed that the compliance is proportional to a^n in the form of equation (2.67)

$$C = Ka^n \tag{2.67}$$

Therefore, the energy release rate from equation (2.59) becomes

$$G_{IC} = \frac{P^2}{2b}\left(\frac{dC}{da}\right) = \frac{P^2 nKa^n}{2ba} \tag{2.68}$$

From equation (2.67) the factor K can be written as

$$K = \frac{C}{a^n} = \frac{\delta}{Pa^n} \tag{2.69}$$

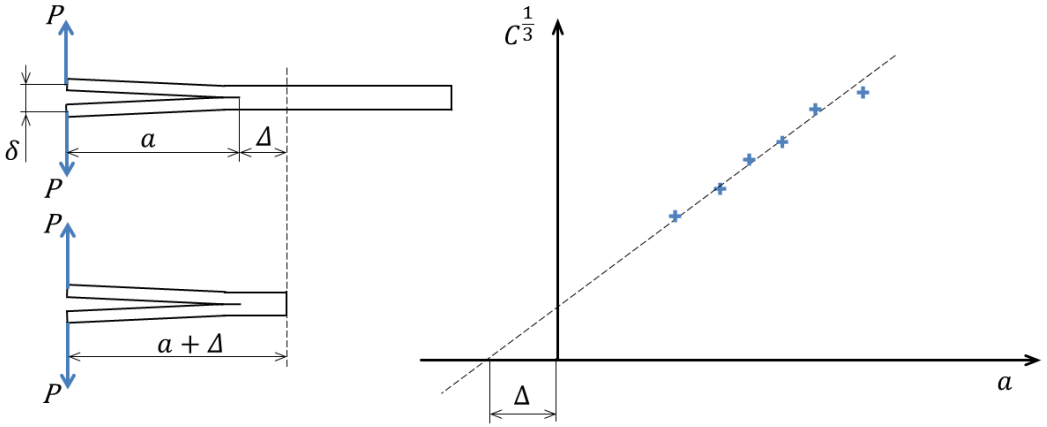

Figure 2.18: Modified beam theory

And after substituting (2.69) into (2.68), the final equation used in compliance calibration data reduction method is

$$G_{IC} = \frac{nP\delta}{2ba} \tag{2.70}$$

The experimental parameter, n, can be determined as a slope of the line fitted to the $log\,(C) - log\,(a)$ plot as shown in Figure 2.19

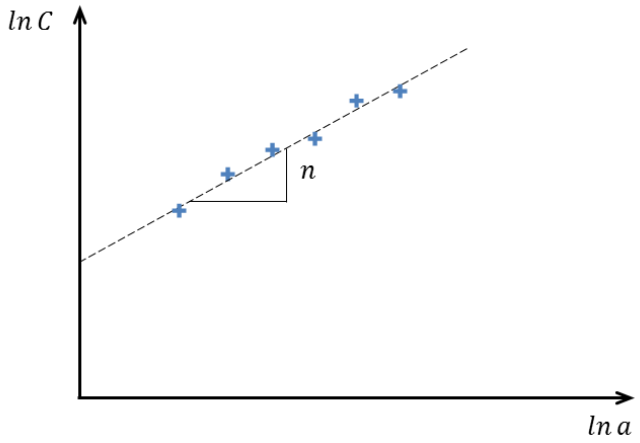

Figure 2.19: Compliance calibration method

The definition of when the crack starts to grow is not straightforward and several methods are used to determine initiation values of fracture toughness. The ASTM standard [34] defines three main points of interest: (a) deviation from nonlinearity, (b) visual observation and (c) 5% offset or maximum load.

The lowest most conservative values are obtained by deviation from linearity (NL) point in the load-displacement plot as shown in Figure 2.20. However, in reality it is often very difficult to establish such a point and this definition

itself allows for some variability. Additionally, nonlinear behaviour may occur due to other reasons, such as material yielding at the crack tip or local crack growth. Less scatter can be obtained by 5% offset method, where the initiation point is determined as an intersection of the load-displacement curve with a line drawn from origin and offset by a 5% increase in compliance from original linear region of the load-displacement curve. If the intersection occurs after the maximum load point, the maximum load should be used to calculate this value. The visual observation point is the point where the crack is observed visually. However, even this method can lead to large scatter in results because it is very much dependent on the operator's eyesight and judgement.

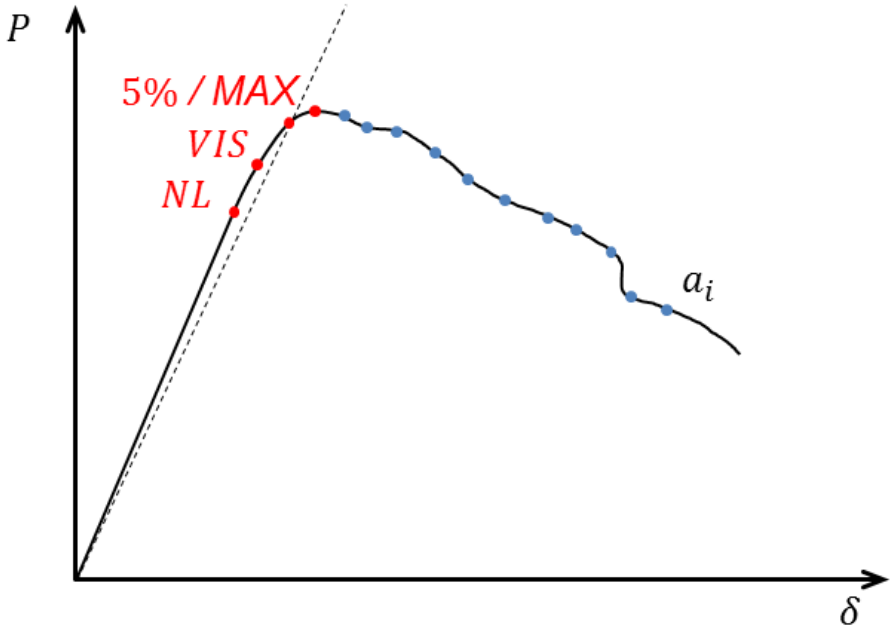

Figure 2.20: Initiation point definition

Mode II

The specimen geometry for testing delamination fracture toughness in mode II is usually the same as in the DCB configuration. There are several loading configuration proposed, three of them can be seen on Figure 2.21. Currently, two standard methods are: ASTM D7905 [36], which uses end notch flexure specimen (ENF); and ISO 15114 [33] which is based on the end load split specimen (ELS). Other methods include stabilized end notched flexure [37] and four point end notch flexure [38].

In the ENF test, the specimen is place in a three point bending fixture which consists of two supports and one loading point in the middle. The load is applied in a displacement controlled mode and the load, displacement and crack length are measured during the test. Several analysis methods can be applied to an ENF test, including classical plate theory, beam theory and compliance calibration method. The main disadvantage with this test is that the

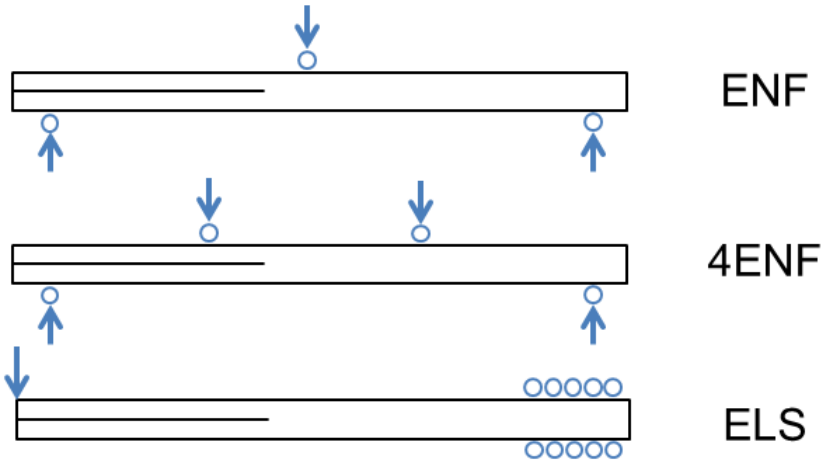

Figure 2.21: Mode II specimens

propagation is unstable except for very long crack lengths (a/L 0.7). On the other hand unstable crack propagation results in much clearer initiation point than in mode I DCB test. Also, effects of friction and initial defect type are not very well understood.

The four point end notch flexure (4ENF) test was proposed by Martin and Davidson in 1997 [38] and appeared to resolve many of the mode II testing problems. It offered three significant advantages, stable crack propagation, a simple test fixture and a straightforward data analysis [31]. Nevertheless, this test yields significantly larger values of G_{IIc} compared to the other methods and many studies have been performed to understand these differences [31]. In SENF test, stable crack propagation is achieved by measuring the crack length or compliance and directly controlling the test machine displacement by a loop circuit. A servo-controlled machine is required.

In ELS configuration, the specimen is clamped at one end and load is applied at the other end by loading blocks or piano hinge, similarly to the DCB test. This method offers more stable crack growth compared to the ENF and also the friction effects appear to be less significant [33]. The crack lengths can be calculated experimentally without complicated and not very reliable optical measurements. The methods for determining the fracture toughness are: simple beam theory, experimental compliance calibration and corrected beam theory.

As for the mode I, the fracture toughness values are determined from equation

$$G_{IIC} = \frac{P^2}{2b}\left(\frac{dC}{da}\right) \tag{2.71}$$

Experimental compliance method predicts that the compliance will take form

$$C = C_0 + ma^3 \tag{2.72}$$

Equation (2.72) can be differentiated with respect to crack length and after substitution into (2.71), the fracture toughness is

$$G_{IIC} = \frac{3P^2a^2m}{2b} \tag{2.73}$$

If values C for crack propagation points are plotted with the cube of the measure crack length, a^3, linear regression of these data will yield a slope m. The main problem with experimental compliance method is that the stable propagation is required. But sometimes, this is difficult to achieve during the test, even if the theoretical condition for stable propagation ($a/L > 0.55$) is met. Another difficulty is to accurately measure the crack length visually.

From simple beam theory, the ELS specimen compliance is

$$C = \frac{\delta}{P} = \frac{3a^3 + L^3}{2bh^3E} \tag{2.74}$$

After differentiation equation (2.74) and substituting in (2.71), the mode II energy release rate resulting from the simple beam theory is

$$G_{IIC} = \frac{9P^2a^2}{4b^2h^3E} \tag{2.75}$$

In equation (2.74) a perfectly clamped boundary condition is assumed. In reality, some amount of beam root deflection and rotation is present. This can be corrected by clamp correction factor in a similar way as delamination length is corrected in modified beam theory for DCB specimen. The specimen compliance including the correction factors is then

$$C = \frac{\delta}{P} = \frac{3a_e^3 + (L + \Delta_{clamp})^3}{2bh^3E} \tag{2.76}$$

where a_e is effective (calculated) crack length and Δ_{clamp} is the clamp correction factor. Effective crack length can be calculated by rearranging equation (2.76)

$$a_e = \sqrt[3]{\frac{2bCh^3E - (L + \Delta_{clamp})^3}{3}} \tag{2.77}$$

And the fracture toughness can be evaluated only by using this calculated "effective" crack length

$$G_{IIC} = \frac{9P^2a_e^2}{4b^2h^3E} \tag{2.78}$$

The clamp correction factor, which is needed to calculate the effective crack length in equation (2.77) can be measured experimentally. The specimen is placed in to the clamp, so there is no crack present within the free length of the specimen as shown in Figure2.22. The specimen is loaded at several different lengths, L.

Compliance is calculated for each length from a linear part of force-displacement curve. The data are plotted in a graph with length, L, on the horizontal axis

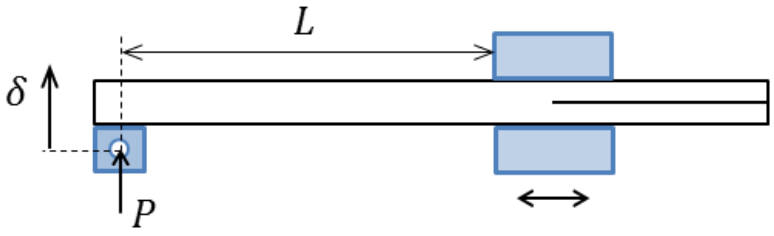

Figure 2.22: Clamp correction factor setup

and cube root of compliance, $C^(1/3)$on the vertical axis. Clamp correction factor is obtained as a negative intercept of linear fit to these data with horizontal axis as shown in Figure 2.23.

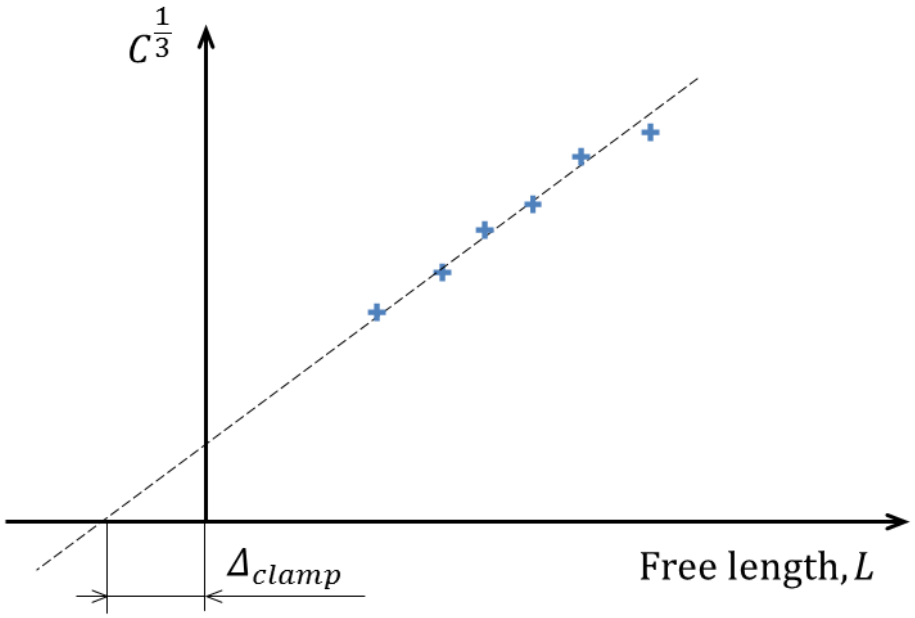

Figure 2.23: Clamp correction factor

Several initiation points can be defined from the shape of load displacement curve as in the DCB test as shown in Figure 2.20. ISO 15114 [33] recommends the 5% or maximum load criteria for definition of the initiation point. Round-robin testing has shown that the nonlinear (NL) initiation point definition is prone to significant scatter. In addition, the visually determined definition of crack initiation is not consistent with the effective crack length approach recommended in the standard.

Mixed mode

Mixed loading conditions can be achieved by unequal tensile loading of the upper and lower portions of the specimen. Common configurations are MMB (mixed mode bending), MMF (mixed mode flexure), CLS (crack lap shear) and ADCB (asymmetric DCB). Figure 2.24 shows schematically these configurations. Mixed mode bending (MMB) configuration allows for many different mode ratios to be tested and has been widely used and ASTM standard exists [35].

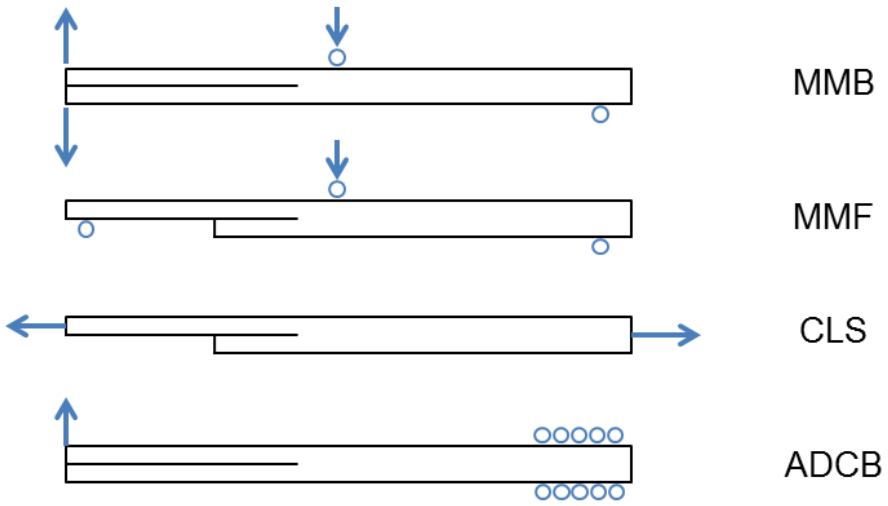

Figure 2.24: Mixed mode loading configurations

One of the rare criticisms of the MMB test has been the cost of relatively complicated fixture, which is schematically shown in Figure 2.25 On the other hand, a great advantage of this method is that the length of the lever arm, c, can be changed and wide range of mixed mode ratios tested with one specimen configuration.

Fixed ratio mixed mode ADCB has only limited mixed mode ratio of 4:3 of mode I to mode II component, but the same fixture as for mode II ELS configuration can be used. The test procedure and data analysis are essentially similar ELS, except that the load is applied in the opposite direction, where one arm of the cantilever beam is lifted up at the free edge, which causes crack to propagate in combination of opening and shearing mode. The beam theory yields following equations for fracture toughness

$$G_{IC} = \frac{3P^2a^2}{b^2Eh^3} \tag{2.79}$$

$$G_{IIC} = \frac{9P^2a^2}{4b^2Eh^3} \tag{2.80}$$

Experimental compliance method has the same form as equation (2.73) in

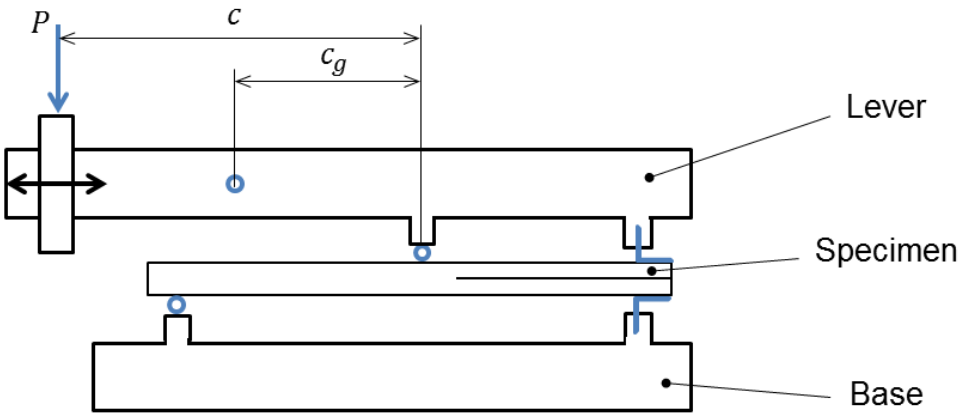

Figure 2.25: Mixed mode bending apparatus

ELS configuration

$$G_{IIC} = \frac{3P^2a^2m}{2b} \tag{2.81}$$

Mode III

The most commonly investigated mode III fracture test method is the edge crack torsion (ECT) test. Schematically, this configuration is shown in Figure 2.26. Load is applied as two opposite moments to the corners of a rectangular specimen.

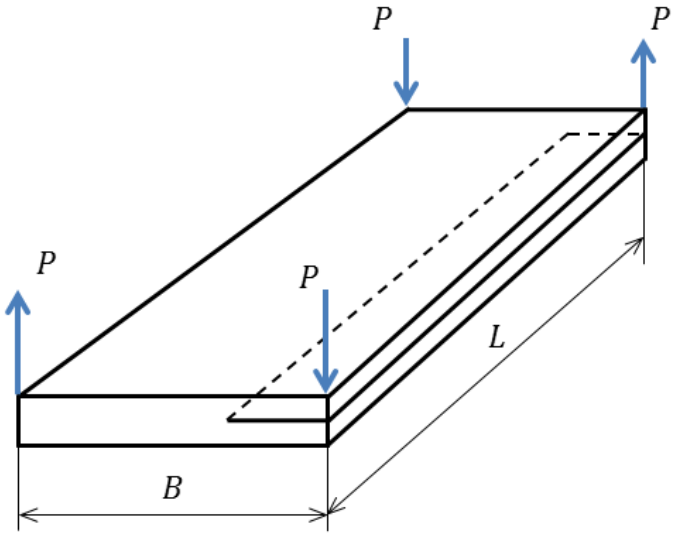

Figure 2.26: Edge crack torsion (ECT)

An ASTM D30 round robin was organized to evaluate this test on car-

bon/epoxy samples but the results reported in 1997 indicated large scatter and considerable non-linearity. The test frame was then modified so that load could be applied symmetrically by two pins, and a second round robin was organized. Results presented in 1999 indicated that delaminations did not always grow at the 90°/90° interface and a significant mode II component was indicated near the loading pins. Longer test specimens were recommended to reduce the latter. Further standardization work on mode III testing has not been reported, but some more recent publications have shown results from this specimen geometry. [31]

Experimental aspects of delamination testing

Depending on the specimen rigidity, large displacement and nonlinearity may arise during mode I, mode II and mixed mode I/mode II testing. Williams [39] suggests that correction factors based on large displacement analysis can be used and the standard methods include equations, which can be used to approximately calculate the correction factors. Round-robin studies have shown that these correction factors represent only relatively small corrections and ELS standard procedure [33] suggests that these correction factors can be excluded from the analysis for the simplicity.

Fibres bridging between specimen arms close to the crack tip and multiple cracking can occur during the crack propagation. In such case, the R-curves determined from the test are not intrinsic material properties and frequently depend on specimen geometry [24]. The multiple cracks and dense fibre bridging can complicate visual location of the crack tip. For this reason, the initiation values are often considered to be the only relevant fracture toughness value obtained by delamination tests.

The crack initiation point is not easy to determine either. Several methods are recommended, such as onset of nonlinearity, 5% offset in compliance and visual onset. Usually, before the crack becomes apparent at the specimen edges (visual onset), micro-scale cracking is present at the centre of the specimen. This leads to nonlinear force-displacement behaviour. Deviation from linearity often yields in the most conservative values of fracture toughness. However, the nonlinear behaviour before the delamination growth can be also attributed to local material plasticity near the crack tip and not always is connected with the material fracture. The initiation offset defined by 5% increase of initial compliance is arbitrary and might not be represent the real crack growth initiation. However, this definition is often very close to the visual onset values and gives the least scatter in the results for most test configurations.

An important aspect of fracture resistance is that it may vary as the crack grows such that G_C is a function of the crack growth Δa. Thus we may have a curve of G_C versus Δa, as shown in Figure 2.27, which usually rises and is termed the resistance or 'R' curve. This curve is a complete description of the fracture toughness of a material and many composites delamination test procedures have its determination as the goal. Initiation value, i.e. when $\Delta a = 0$ is usually the lowest and considered to be the most critical. This however leads to many practical problems such as the definition of an initiation point during the test. As a visual observation is many times difficult to achieve,

other non-direct methods were developed, such as the onset of non-linearity or 5% reduction in the slope of the load-deflection line. Many times the resistance curves have a plateau value which can be used as an upper limit of G_C. However, this is not a rule for every material and sometimes the plateau is not reached during the test or the 'R' curve can have decreasing tendency.

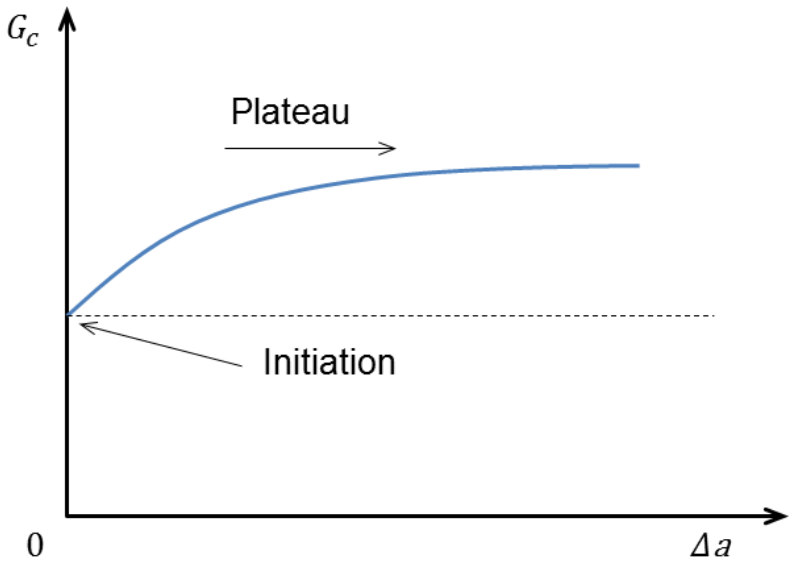

Figure 2.27: Resistance or 'R' curve

2.6 FEA methods for delamination

2.6.1 Virtual Crack Closure Technique (VCCT)

The virtual crack closure technique [40] is widely used for computing energy release rates based on results from continuum two-dimensional (2D) and solid three-dimensional (3D) finite element (FE) analyses. [41] The mode I and mode II components of the strain energy release rate, G_I and G_{II} respectively are computed using VCCT as shown in Figure 2.28 for a 2D four-node element. For geometrically nonlinear analysis where large deformations may occur, both forces and displacements obtained in the global coordinate system need to be transformed into a local coordinate system (x', y') which originates at the crack tip as shown in Figure 2.28. The local crack tip system defines the tangential (x' or mode II) and normal (y' or mode I) coordinate directions at the crack tip in the deformed configuration. The terms F'_{xi}, F'_{yi} are the forces at the crack tip at nodal point i in the local x and y directions respectively. The terms u'_l,v'_l and u'_{l*},v'_{l*} are the displacements at the corresponding nodal points l and $l*$ behind the crack tip. [41]

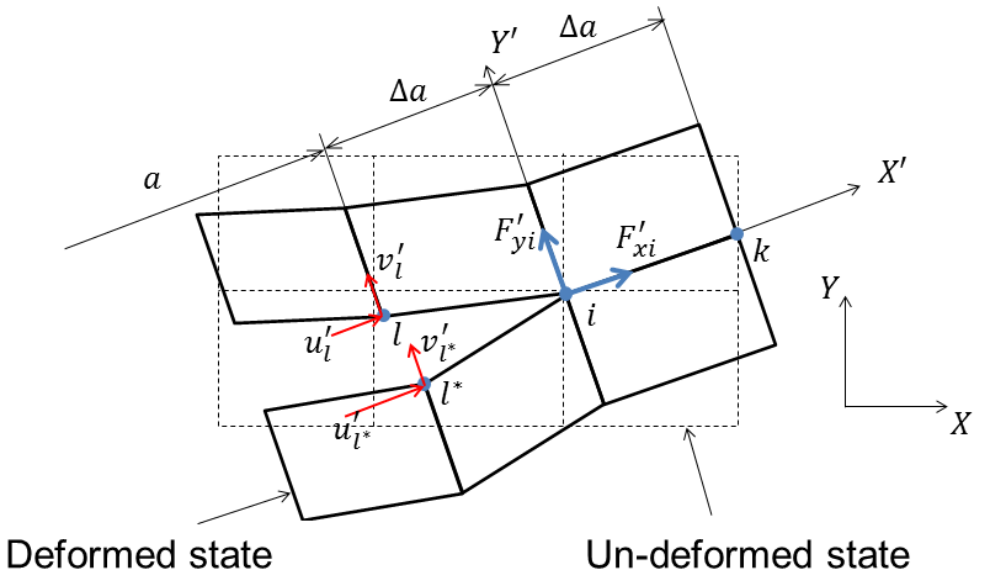

Figure 2.28: VCCT local crack tip system for 2D elements

The equation for mode I and mode II energy release rate are

$$G_I = -\frac{1}{2\Delta a} F'_{yi}(v'_l - v'_{l*}) \tag{2.82}$$

$$G_{II} = -\frac{1}{2\Delta a} F'_{xi}(u'_l - u'_{l*}) \tag{2.83}$$

2.6.2 Cohesive zone

The cohesive zone modelling approach has become a widely used tool for simulating delaminations due to the computational convenience and ease of implementation. In this approach it is assumed that a narrow zone of vanishing thickness called the cohesive zone exists ahead of a crack tip or delamination front. The cohesive zone represents the fracture process zone. The upper and lower surfaces of the narrow zone are held together by forces called cohesive tractions. These tractions follow a cohesive constitutive law (traction-separation law) that relates the cohesive tractions to the separation displacements of the cohesive surfaces. Delamination onset or crack growth occurs when the separation at the end of the cohesive zone, which represents the physical crack tip, reaches a critical value at which the tractions vanish. The failure process is controlled by displacements and stresses, which are consistent with the usual strength of materials theory. Thus the problem of crack tip stress singularity found in the classical linear elastic fracture mechanics is avoided and the singularity is effectively buried in the element since the crack tip is not explicitly modelled. Special finite elements, called decohesion elements, with initially zero thickness, containing the traction-separation law can be formulated. [41]

2.7 Summary

Defects in composite materials can have a significant effect on the structural strength and load-carrying capacity. Moreover, the composite materials have very complex failure behaviour and the presence of defects certainly makes the analysis of failure even more complicated. The material testing is an essential tool in understanding the failure mechanisms and in developing material allowables to be used in analytical calculations and design methods.

The composite material failure theories have been reviewed together with the defects types that can occur in composite material either during the manufacture or during the service life. The review of the testing methods has focused on the fracture toughness testing of delaminations which is one of the most commonly discussed types of defects in composite materials and which has attracted a huge attention within the scientific community in recent years.

3 Thesis aims and objectives

3.1 Delamination at a bi-material interface

Very few studies were done so far, which would include the effect of delamination between two dissimilar materials. In real life constructions made of composite materials, for example small aircrafts, the combination of glass and carbon reinforced plastics is a common design practice. This enables the utilization of carbon composite materials superior mechanical properties and glass composites lower cost. This approach is very effective; however the interface between two materials may cause the delamination initiation. Fatigue and static experiments of small aircraft wing root section conducted in the past at the Institute of Aerospace Engineering, Brno University of Technology, confirms this dangerous effect. Figure 3.1 shows an example of the de boned CFRP flange from GFRP web that occurred during fatigue test of a wing root section.

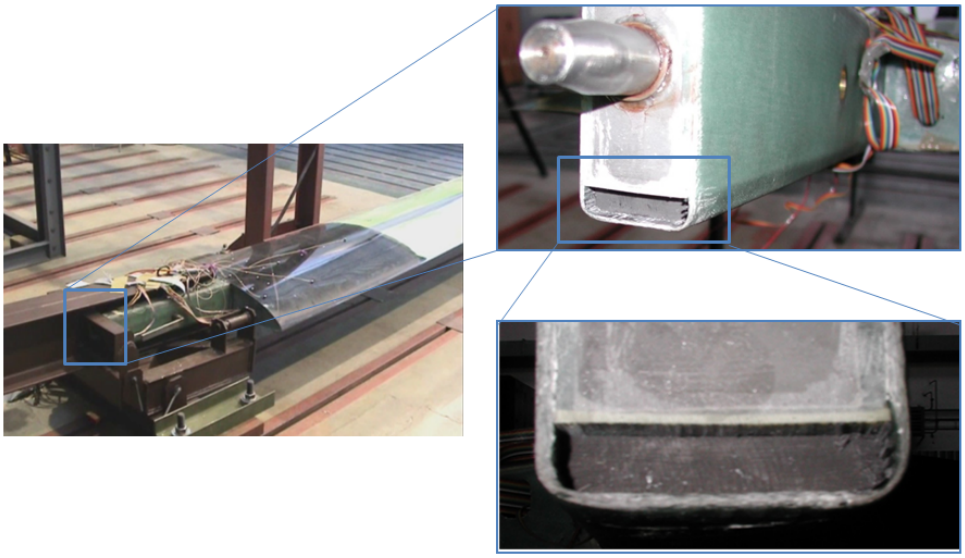

Figure 3.1: Example of delamination on GFRP – CRFP interface

Methods for analysing delamination in composites are well established and widely used as described in Chapter 2.3.3. However, delaminations at bi-material interface needs to be investigated with special attention because of a stress singularity due to mismatch in elastic parameters. Also state-of-art of the standardised test methods for delamination resistance doesn't include the effect of crack propagating between two dissimilar materials. In reality the delamination occurrence is highly probable at the interface of two different

materials; therefore the analysis and testing methods must be established to include these facts.

Test methods presented in 2.5.2 were developed and used extensively to measure fracture toughness in unidirectional fibre composites and the data reduction methods and beam theory equations are only based on single material elastic modulus. If these methods are to be applied to specimens with different elastic moduli in cantilever specimen arms, fracture toughness calculation methods need to be reviewed and modified to account for different elastic moduli.

A common problem in composite materials fracture testing is the accurate crack length measurement. The crack length is needed to calculate propagation values and R-curve, but can also be used for calculating initiation values by compliance calibration methods. Current standard procedures recommend optical measurements with optional use of travelling microscope, which is a test operator dependent method prone to a human error. With modern high resolution digital cameras and computer programming this method can be automated.

3.2 Research aims

With respect to the previous findings, the thesis has following aims:

1. Investigate the influence of different material characteristics on delamination fracture toughness
2. Examine the analytical methods used to calculating fracture toughness in different mixed mode conditions
3. Develop a mixed mode failure criteria that can be used for delaminations at bi-material interface.
4. Automate crack length measurement methods.

3.3 Objectives

Objectives to achieve the aims above can be split into two main categories:

1. Experimental investigation
   (a) Perform a series of fracture toughness measurements at a bi-material interface of a glass-carbon composite in DCB, ADCB and ELS test configuration as shown in Figure 3.2
   (b) Record each test with a high resolution digital camera
   (c) Create a computer program to process the acquired images and automate the crack length measurement
2. Analytical investigation

(a) Modify the analytical methods used to calculate fracture toughness from experimentally measured data (data reduction methods) in order to account for two different material in the specimen arms and non-centrally positioned crack

(b) Calculate a ratio of mode I and mode II in each configuration tested in the experimental investigation

(c) Apply new equations to the data obtained in experimental investigation and construct a mixed mode delamination failure envelope

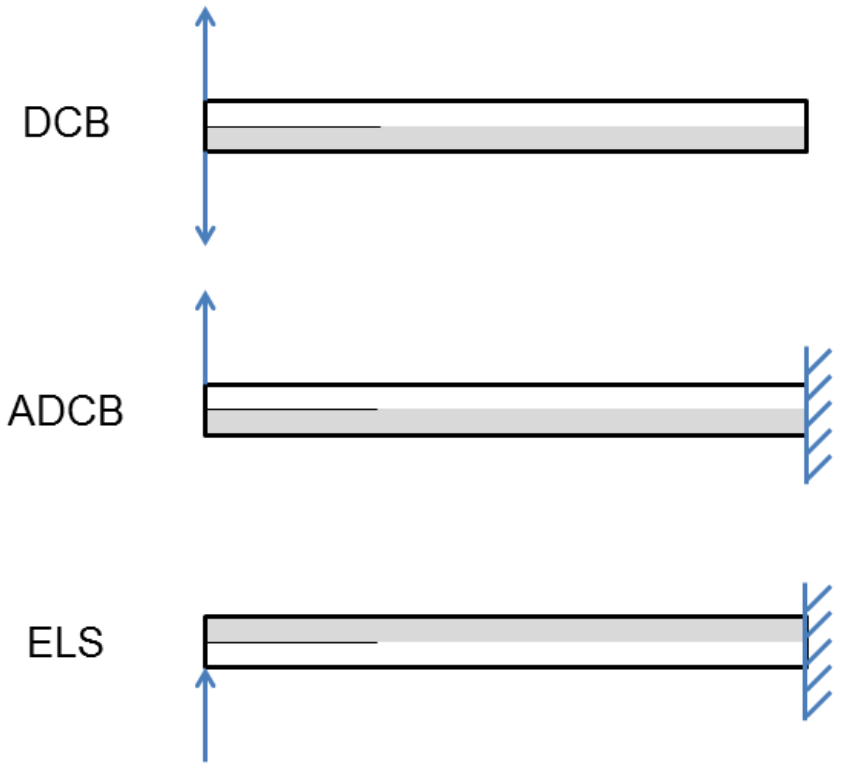

Figure 3.2: Test configurations

4 Experimental investigation

4.1 Specimen description and test setup

The same specimen base geometry and manufacturing method were used for the three delamination test configuration; DCB, ADCB and ELS. The specimen geometry is shown in Figure 4.1. Details of each specimen's dimensions can be found in Appendix A. During the manufacture, several already cured CFRP stripes were placed on a wet layup sheet of glass fabric impregnated by epoxy resin. Then, both components were cured under vacuum. The excess amount of GFRP was cut out after the curing. This manufacturing process was chosen to simulate a technique of manufacturing a wing root section with CFRP flange and GFRP web, i.e. the one shown in Figure 3.1, where epoxy impregnated wet glass fabric is wrapped around already cured unidirectional carbon flange.

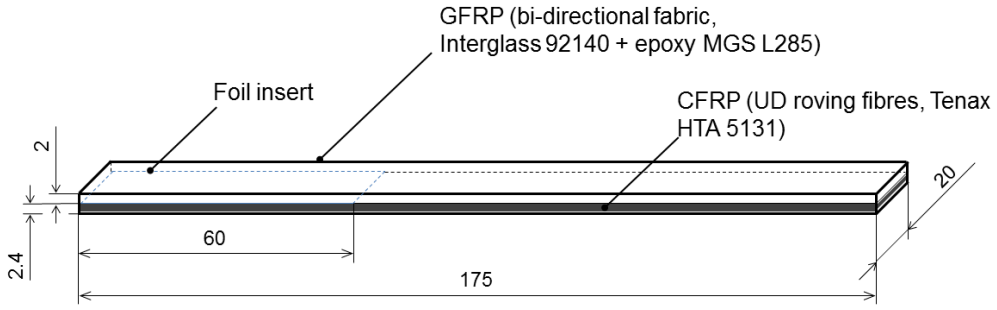

Figure 4.1: Specimen dimensions

Then piano hinges for load application were bonded to the specimens' ends on the side of the foil insert. One hinge was applied to the GFRP side for ADCB and ELS tests. For DCB configuration, hinges were applied both on GFRP and CFRP sides. Because of the bonding area of the hinges, the load application point is moved by approximately 26 mm from the specimen edge. And after considering also the slightly variable alignment of the bond, the resulting length of the starting delamination defect is between 33 and 36 mm.

For DCB test, only universal testing machine with constant displacement load rate is needed. Specimen arms are pulled apart through the hinges that are connected directly to the machine crosshead attachments. ELS test requires a special fixture which allows sliding in horizontal direction. Such fixture was design as shown in Figure 4.2. The base plate can be attached to a frame of universal testing machine; guide and slider allow for the horizontal movement; fixing plates are used for clamping the specimen end by four bolts. Torque wrench is needed to apply a consistent pressure while fixing the specimen in the fixture. This loading jig can be also easily applied to an ADCB test without

any necessary modifications. An example of ADCB test setup is shown in Figure 4.3.

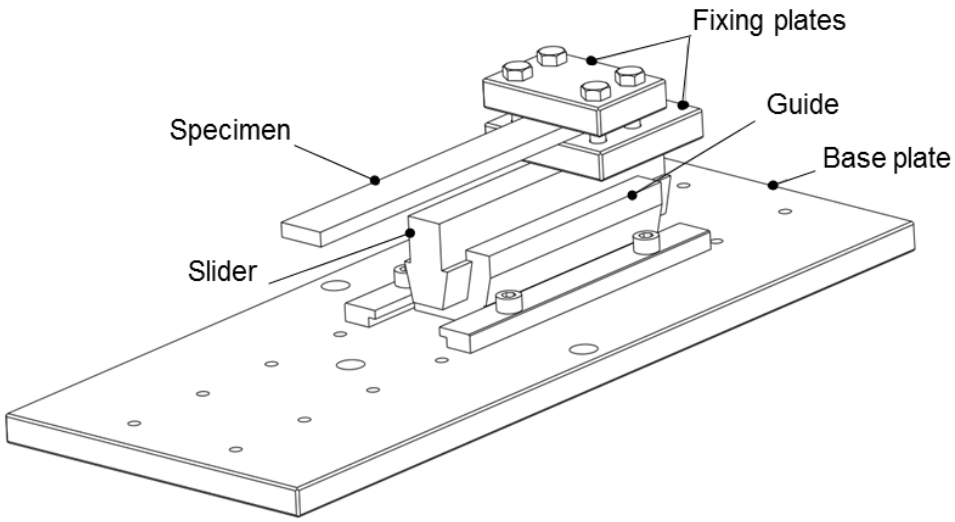

Figure 4.2: ADCB and ELS fixture

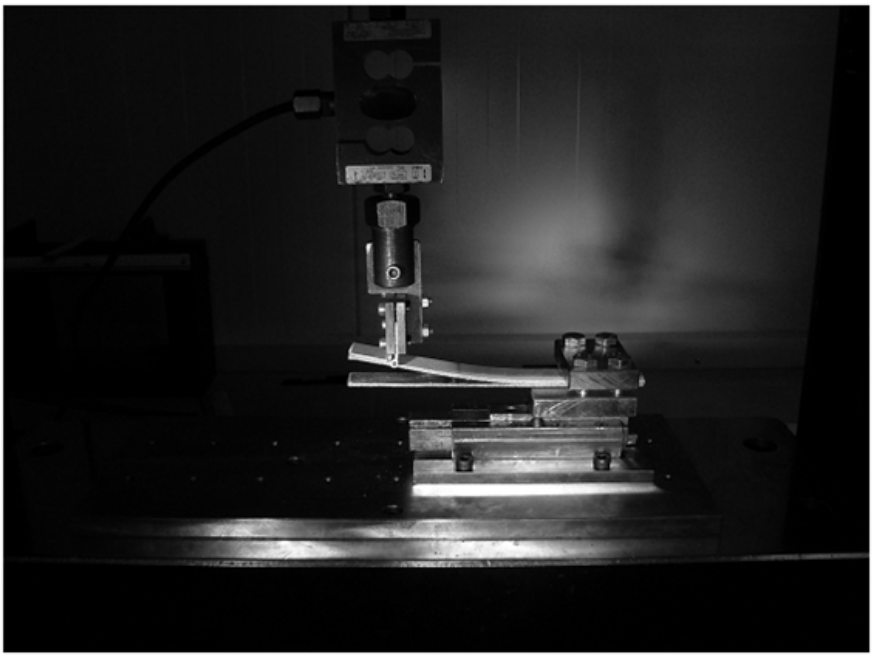

Figure 4.3: ADCB test setup

4.2 Automated crack length measurement

Delamination lengths are usually determined visually with the aid of travelling optical microscope during the test. Major drawback of this method is the dependence on alertness and experience of the operator. Currently, the alternative exact measurement of the delamination length has become a focus of attention [31] and operator independent determination of effective crack length at affordable cost might be a significant improvement of prevailing practise. Non-destructive methods, such as X-ray in situ imaging and acoustic emission [42, 43] has been used, but these methods frequently require expensive equipment and skilled operators and the interpretation of data is not straight forward. One possible approach is to record the test procedure on a high resolution camera and analyse the taken pictures by the means of automated image processing after the test. This method is very similar to the conventional measurement by optical traveling microscope, but takes of the work load from test operator and also eliminates human error. Possible advantage can also be an application not only for quasi-static testing but also for fatigue crack length measurement or high-rate delamination testing.

Several methods of image processing to analyse crack growth in double cantilever beam test for adhesive joints were presented in a recent publication [44]. Although the low resolution camera has been used and illumination was not optimal, even noisy images led to acceptable results.

A new method for automated crack length measurement by image processing has been developed by the author and applied for the DCB and ADCB test of bi-material interface. Despite the very specific application here, the method is general and can be easily applied in mode I and mixed mode testing of single unidirectional composite materials. Image processing for mode II ELS test didn't prove to be practical and no satisfactory results were obtained, because of the lack of clear opening between the specimen arms. However, accurate crack length measurements in ELS test are not so important, because other preferred methods of calculating the energy release rate are available, such as corrected beam theory with effective crack length [33].

4.2.1 Image acquisition

Image processing is used nowadays in many applications, such as biology, astronomy, medical and many others. It is closely related to the field of computer vision, with no clear distinction between these two. Image processing might include many operations, commonly classified as low-, mid- and high level. Low-level processes involve primitive operations such as noise reduction, contrast enhancement, and image sharpening. Mid-level includes tasks as segmentation and classification if individual objects contained in image. Finally high-level pro cessing includes image analysis, performing cognitive functions normally associated with vision. [45]

Image acquisition is the essential step preceding any further processing and analysis. Electromagnetic, X-ray or ultrasonic sensing devices have a wide field of application; however the most used and available are light sensing devices.

Most common digital photography imaging devices (CCD and CMOS sensors) have experienced a rapid development and increase in sensitivity, when for example the CCD pixel has been reduced to a 1/100th of its original size in the last two decades. [46]

CCD camera with a resolution 4096x3072 from system for digital image correlation Aramis 12M, made by GOM mbH, was used for the image acquisition. Digital image correlation (DIC) is a common method in experimental mechanics for measuring surface displacements. A typical DIC system is shown in Figure 4.4.

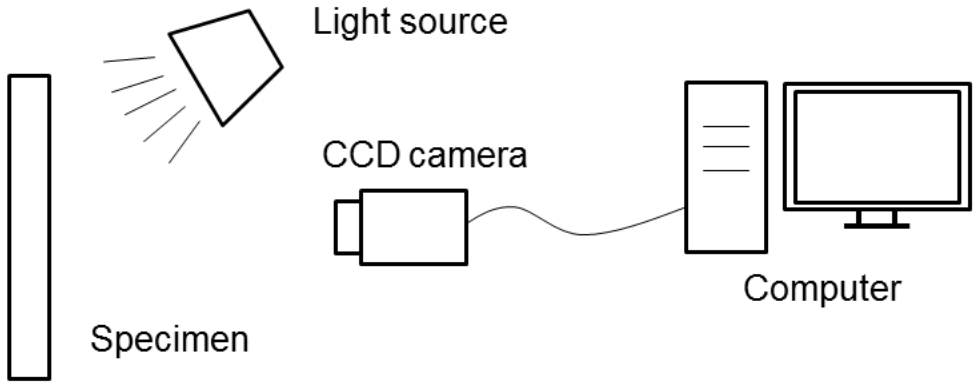

Figure 4.4: DIC system setup

In this method, a sequence of images of a studied object is compared to detect displacements by searching a matched point from one image to another. Here, because it is almost impossible to find the matched point using a single pixel, an area with multiple pixel points (such as 20 $\times$ 20 pixels) is used to perform the matching process. This area, usually called subset, has a unique light intensity (grey level) distribution inside the subset itself. It is assumed that this light intensity distribution does not change during deformation. Figure 4.5 shows the part of the digital images before and after deformation. The displacement of the subset on the image before deformation is found in the image after deformation by searching the area of same light intensity distribution with the subset. Once the location of this subset in the deformed image is found, the displacement of this subset can be determined. [47]

In order to perform this process, the surface of the object must have a feature that allows matching the subset. If no feature is observed on the surface of the object, an artificial random pattern must be applied. Figure 4.6 shows a typical example of the random pattern on the surface of an object produced by spraying paint. [47]

The spray pattern is very important in the typical DIC system, where measuring displacements on the surface is the main goal. On the other hand, when accurate tracking of a crack tip position is the objective, the dark spray pattern can be disadvantageous because there is no clear distinction whether the

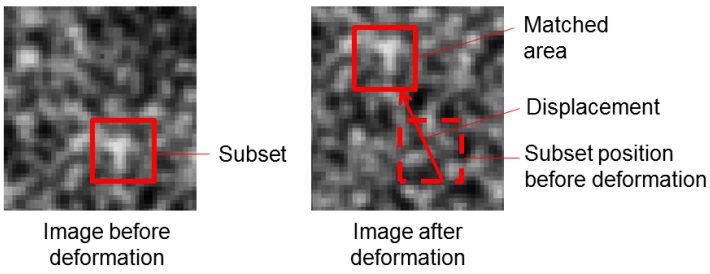

Figure 4.5: Matching patterns in sequence of images

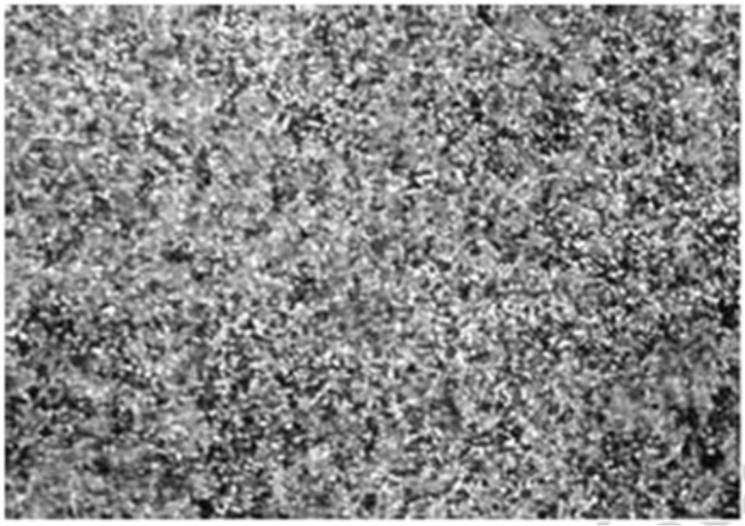

Figure 4.6: Typical image pattern for DIC

dark pixel represents a crack or a spray drop. Clear white contrast paint has proved to be more useful for the purpose of measuring the delamination length. The difference between the specimen with spray pattern and with clear white paint can be seen from Figure 4.7. Better contrast and also image quality is assured by high intensity lighting. Usually, more light sources are required to get consistent light reflection over the observed area with minimum shadows.

4.2.2 Image processing

Python [48] is widely used general purpose programming language, which is distributed as a free and open-source software. There are many community developed libraries and packages that extend the functionality of the standard Python library. The two most commonly used packages for scientific computing; mathematics and engineering are NumPy and SciPy. Image processing and analysis are generally seen as operations on two-dimensional arrays of values. There are however a number of fields where images of higher dimensionality must be analysed. Numpy is suited very well for this type of applications. The scipy.ndimage packages provide a number of general image processing and

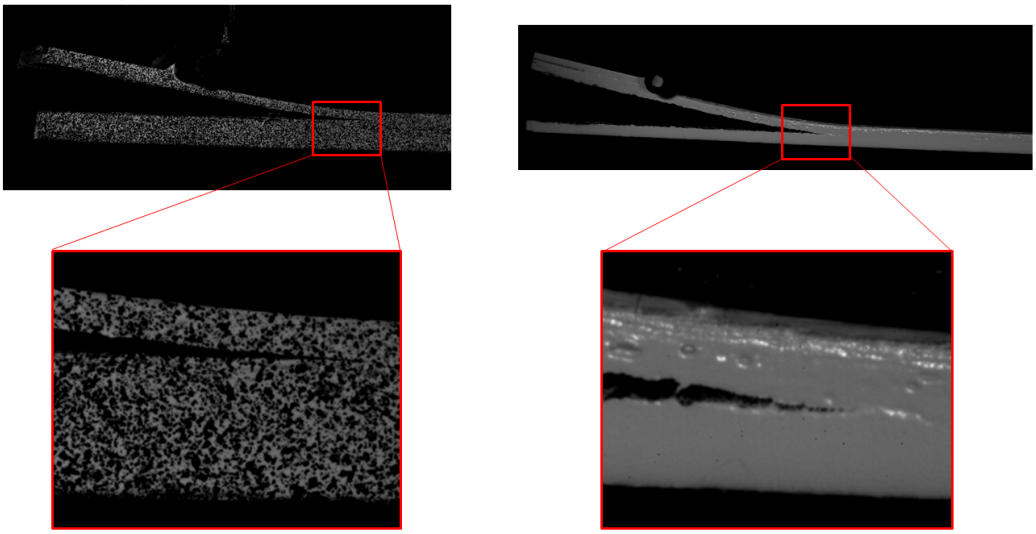

Figure 4.7: Comparison of images with and without random spray pattern

analysis functions that are designed to operate with arrays of arbitrary dimensionality. The packages currently include functions for linear and nonlinear filtering, binary morphology, B-spline interpolation, and object measurements. [49]

In digital grayscale images, each pixel's light intensity is stored as a number ranging between 0, meaning complete black, and a certain maximum value for complete white. Traditionally, when 8 bits per pixel are used the maximum number for complete white is 255. Another digital image representation is binary, when each pixel has only two possible values, i.e. 0 for black and 1 for white. One method of converting a grayscale image into binary image is called thresholding, where each pixel having a lower intensity than a specified limit is replaced by black pixel and each pixel having higher intensity is replaced by white pixel. A simple example of this process is illustrated in Figure 4.8.

Binary thresholding is an effective method for analysing images of the crack propagation, because of the clear distinction between dark background and very light specimen front. However, some of the information in the image is lost during the process and care must be taken when selecting the threshold value. Figure 4.9 shows the effect of different threshold values. In general, lower threshold value leads effectively in shorter cracks being detected and higher threshold values give more accurate representation of the crack geometry. The disadvantage of higher threshold values is that some dark pixels which don't represent the crack geometry are kept in the image and cause a noise, which might lead to false results, when the crack tip searching algorithm is used.

Noise can be effectively removed by morphological operations, such as dilation, erosion, opening and closing. Basic morphological operations are defined by two sets, original image and a structuring element, and Boolean operations between the two. The mathematical details of the operations can be found in [50]. The essential operations are erosion and dilation. Dilation in principle adds pixels to the boundaries of objects in an image, while erosion removes pixel

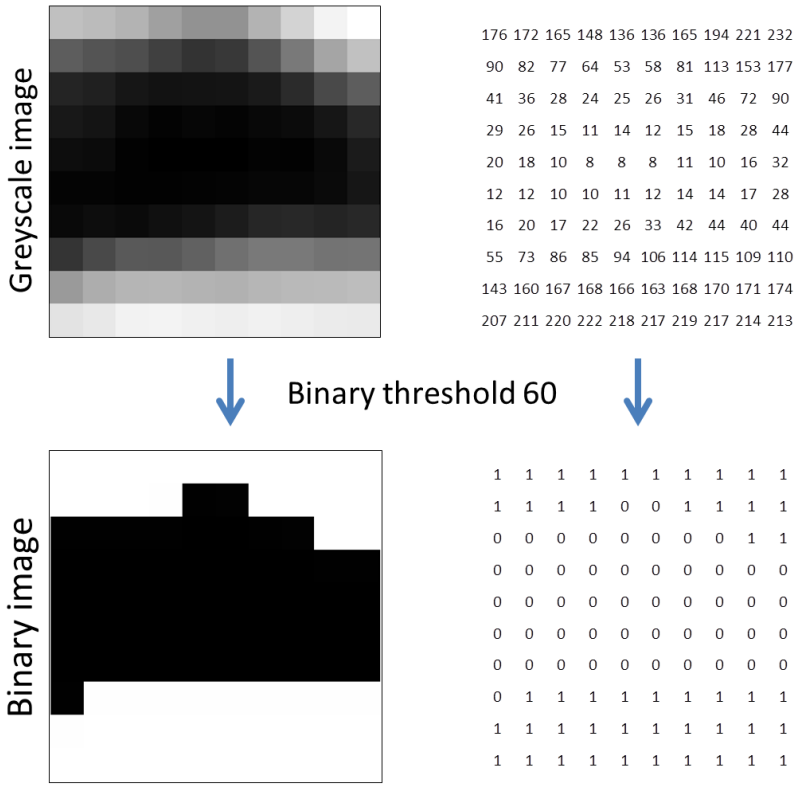

Figure 4.8: Binary thresholding of grayscale image

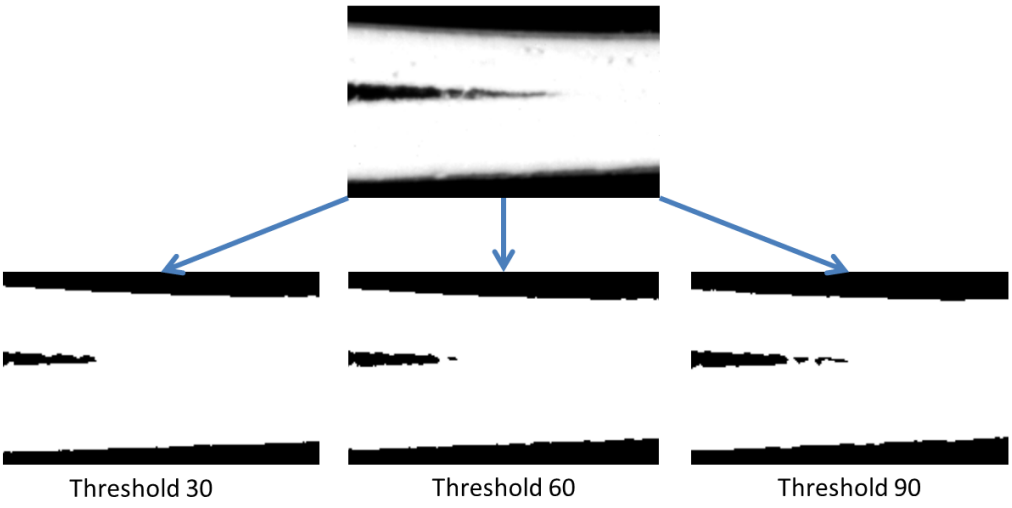

Figure 4.9: Threshold effect

on object boundaries. The number of pixels added or removed from the objects depends on the size and shape of the structuring element used to process the image. Morphological opening is equivalent to erosion followed by dilation with the same structuring element. Morphological closing is the reverse; dilation followed by erosion. Morphological opening is often used to remove noise and

small objects from an image, while preserving size and shape of larger objects. An example of morphological opening used to reduced image noise is shown in Figure 4.10.

Figure 4.10: Noise reduction by morphological opening [51]

4.2.3 Algorithm to find a crack tip

After the recorded grayscale image of a cracked specimen was processed in the way described above, i.e. binary thresholding and noise reduction by mathematical morphology, only black and white pixels remain with a clear geometry describing the crack tip. Finding a crack tip pixel location presented here is based on moving a probe pixel inside the crack, which consists of black pixels, from left to right. Crack tip is found, when there are no more black pixels in the vicinity of the probe.

First step is to position the probe inside the crack opening, on the inside edge of the upper specimen arm. This is process is illustrated in Figure 4.11[1]. The probe is moved from its starting position $[X_{START}, 0]$ in positive Y direction. If the probes crosses more than a specified minimum number of white pixels and find itself on a black pixel, the starting position inside the crack tip $[X_{START}, Y_{START}]$ is returned. This is achieved by following Python function

```
def findCrackStart(current_im, minimum_w=10, x_start=1100):
        image_height = current_im.shape[0]
        count = 0
        for pixel in range(image_height):
                if current_image[pixel,x_start] ==1:
                        count += 1
                        if current_image[pixel+1,x_start] == 0:
                                if count >= minimum_w:
                                        y_start = pixel
                                        break
```

[1]Black and white colours are reversed in this image. In processed images of the delamination test, the background is black and specimen front is white.

```
                        else:
                                count = 0
    return x_start, y_start
```

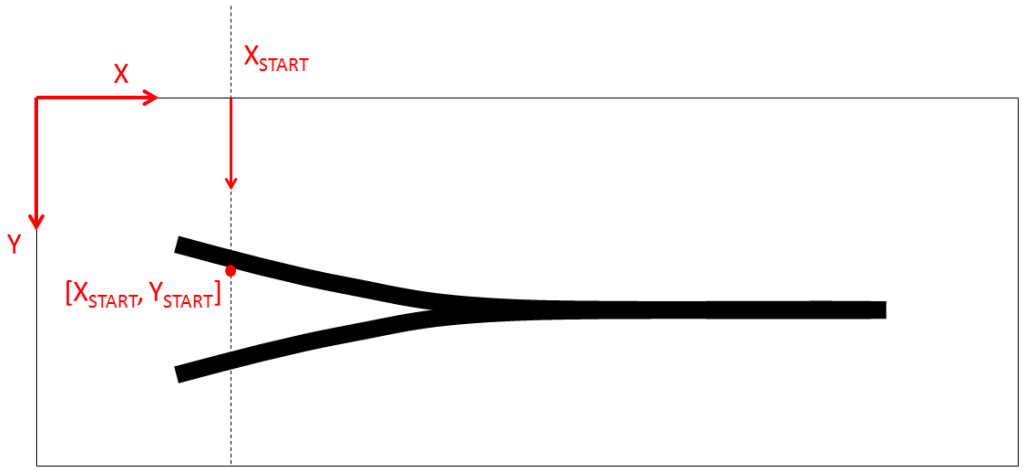

Figure 4.11: Finding the probe starting position

Next, the finding of a crack tip position is achieved by moving the probe within an area specified by a tolerance distance in X and Y directions as shown in Figure 4.12[2]. The probe is moved into a new position if black pixel is found. This tolerance enables the probe to jump over small areas of white pixels, which are usually present around the crack tip due to fibre bridging or crack propagating out of plane. The probe position for reaching the crack tip is described by the following Python function

```
def findCrackTip(current_image,x,y,tolerance_x, tolerance_y):
        tol_Y = tolerance_y
        tol_X = tolerance_x
        while (tol_Y > 0 and tol_Y>0):
                while tol_X > 0:
                        if current_image[y,x+tol_X] == 0:
                                x = x +tol_X
                                tol_X = tolerance_x
                                tol_Y = tolerance_y
                                continue
                        elif current_image[y+tol_Y,x+tol_X] == 0:
                                x = x +tol_X
                                y = y+tol_Y
                                tol_X = tolerance_x
                                tol_Y = tolerance_y
```

[2]Black and white colours are reversed in this image. In processed images of the delamination test, the background is black and specimen front is white.

```
                continue
            elif current_image[y-tol_Y,x+tol_X] == 0:
                x = x +tol_X
                y = y-tol_Y
                tol_X = tolerance_x
                tol_Y = tolerance_y
                continue
            else:
                tol_X = tol_X-1
        tol_X = tolerance_x
        tol_Y = tol_Y -1
return x,y
```

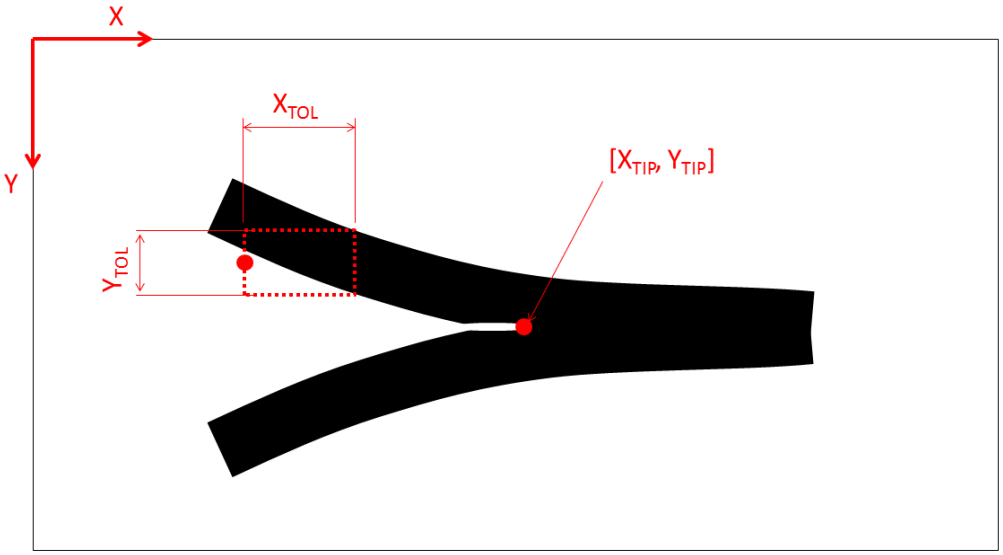

Figure 4.12: Probe step tolerance and tip coordinates

The probe path can be visualised by plotting the X and Y coordinates of the probe position superimposed over the image. Figure 4.13 shows this path and comparison between binary thresholded image and original grayscale image. From this comparison it is apparent that the crack length measurements based on binary black and white images can be shorter then in reality and the level of thresholding and subsequent morphology operations can have effect on the scale of this difference. However, when modified beam theory is used as a test data reduction method, this difference is actually accounted for by a crack length correction factor Δ as described in Section 2.5.2 and Equation (2.66). The corrected crack length compares well with the crack length calculated by a simple beam theory for all measured specimens. Figure 4.14 shows results from mode I specimen DCB#4, the other specimen crack length result are plotted together with their force-displacement curves and crack growth initiation points in Appendix C: VCCT results and Appendix D: DCB results.

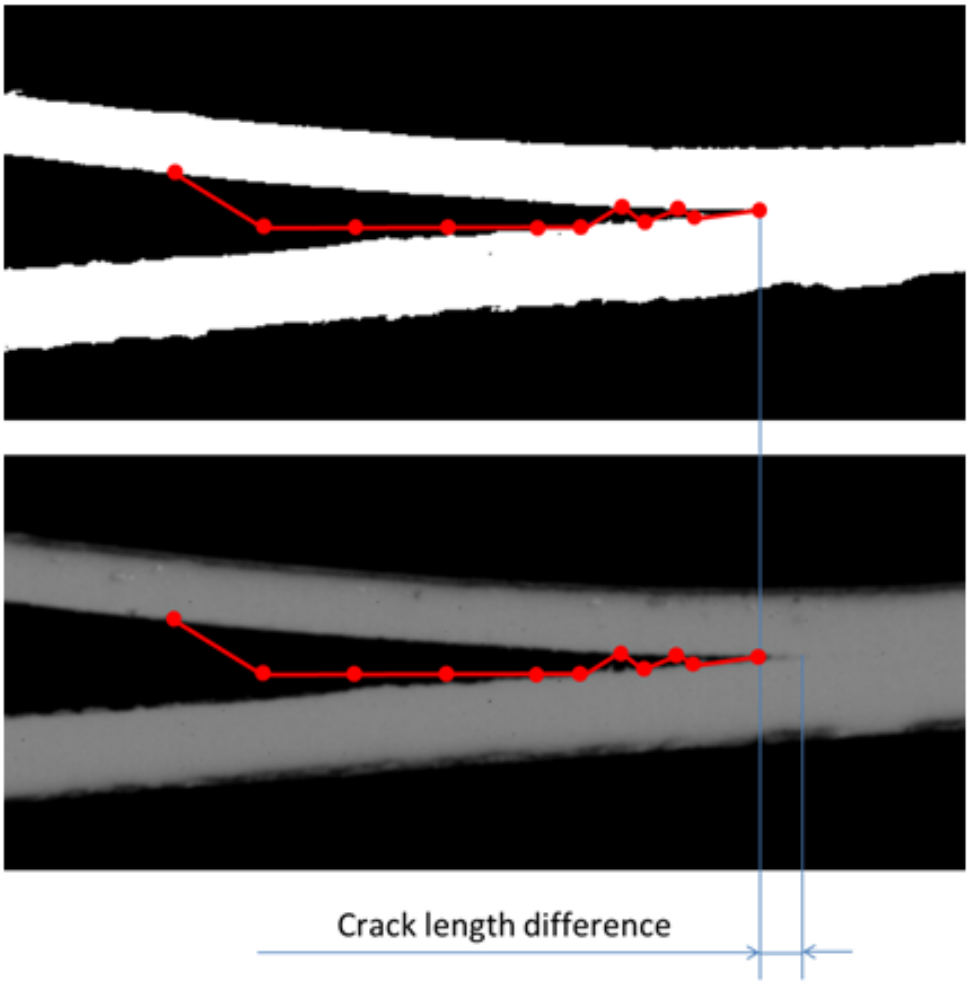

Figure 4.13: Probe path visualisation

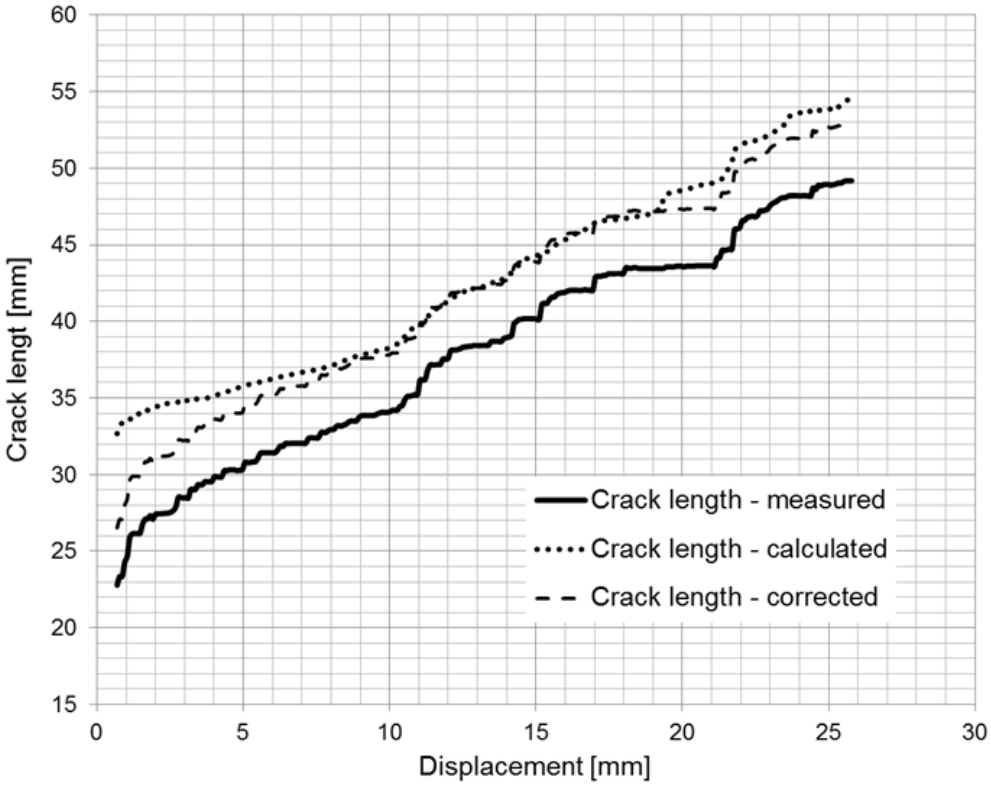

Figure 4.14: Crack length measurements results

5 Analytical investigation

5.1 Beam theory

A general method for calculating the energy release rate G from the local values of bending moments in cracked laminate by Williams [28] as described in Chapter 2.3.3 can be extended to include different moduli in the two sections.

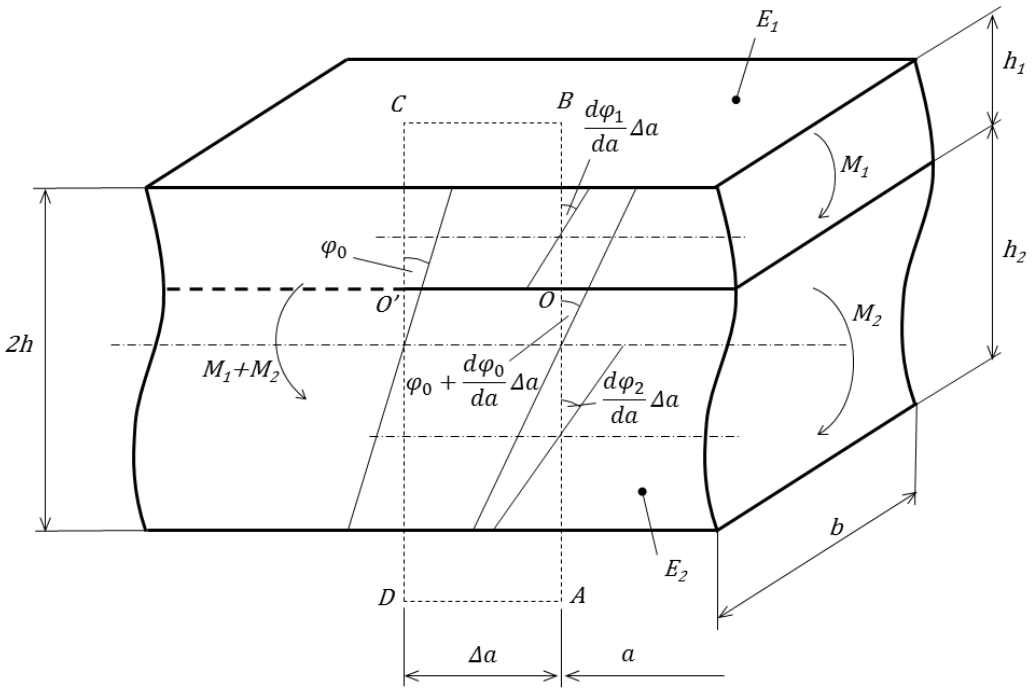

Figure 5.1: Crack tip contour with rotations

Equation for external work (2.36) may be rewritten as

$$\Delta U_E = M_1 \left(\frac{d\varphi_1}{da} - \frac{d\varphi_0}{da} \right) \Delta a + M_2 \left(\frac{d\varphi_2}{da} - \frac{d\varphi_0}{da} \right) \Delta a \tag{5.1}$$

where

$$\frac{d\varphi_1}{da} = \frac{M_1}{E_1 I_1} \tag{5.2}$$

$$\frac{d\varphi_2}{da} = \frac{M_2}{E_2 I_2} \tag{5.3}$$

$$\frac{d\varphi_0}{da} = \frac{M_1 + M_2}{EI} \tag{5.4}$$

E_1 and E_2 are Young's moduli of the two beams, I_1 and I_2 are their second moments of inertia as in equations (2.42) and (2.43). EI is the bending stiffness of the composite beam which can be calculated by parallel axis theorem

$$EI = E_1\left(I_1 + bh_1\left(\frac{h_1}{2} + h_e\right)^2\right) + E_2\left(I_2 + bh_2\left(\frac{h_2}{2} - h_e\right)^2\right) \tag{5.5}$$

where h_e is the distance between the neutral axis and material interface as shown in Figure 5.2, which can be expressed as

$$h_e = \frac{h_2^2 E_2 - h_1^2 E_1}{2\left(E_1 h_1 + E_2 h_2\right)} \tag{5.6}$$

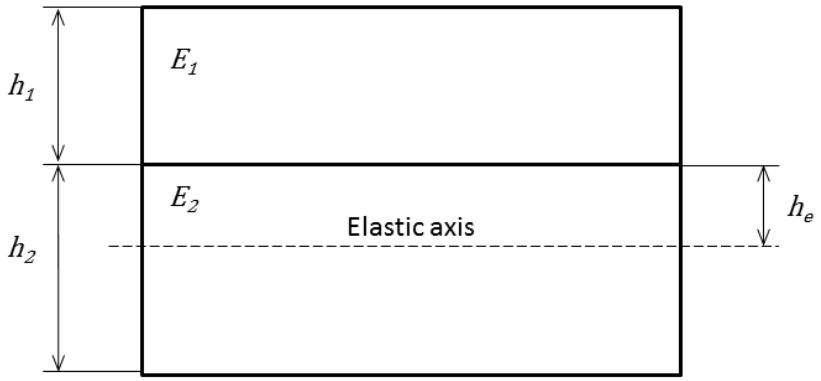

Figure 5.2: Elastic axis position for beam bending stiffness calculation

The equation for the external work (5.1) then becomes

$$\Delta U_E = M_1\left(\frac{M_1}{E_1 I_1} - \frac{M_1 + M_2}{EI}\right)\Delta a + M_2\left(\frac{M_2}{E_2 I_2} - \frac{M_1 + M_2}{EI}\right)\Delta a \tag{5.7}$$

The strain energy change within the contour is

$$\Delta U_S = \frac{1}{2}\frac{M_1^2}{E_1 I_1}\Delta a + \frac{1}{2}\frac{M_2^2}{E_2 I_2}\Delta a - \frac{1}{2}\frac{\left(M_1 + M_2\right)^2}{EI}\Delta a \tag{5.8}$$

After substituting (5.8) and (5.7) into (2.33), total energy release rate for the crack growth is

$$G = \frac{1}{2b}\left(\frac{M_1^2}{E_1 I_1} + \frac{M_2^2}{E_2 I_2} - \frac{\left(M_1 + M_2\right)^2}{EI}\right) \tag{5.9}$$

DCB

For a DCB specimen with an off-centre delamination and materials with different elastic moduli in upper and lower arms, as shown in Figure 5.3, the moments at the delamination front are

$$M_1 = -Pa \tag{5.10}$$

$$M_2 = Pa \tag{5.11}$$

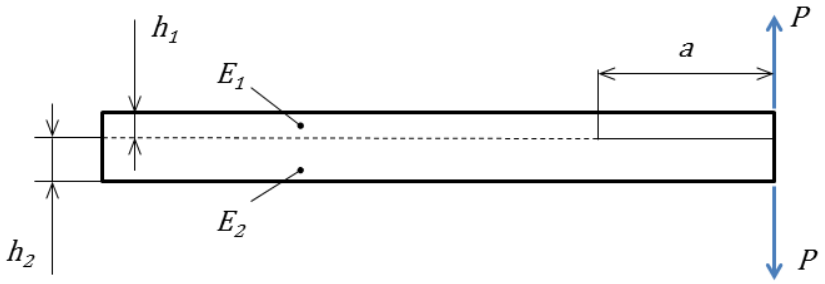

Figure 5.3: DCB specimen

After substituting equations (5.10), (5.11), (5.5),(2.42) and (2.43) into (5.9), the total energy release rate of the DCB specimen is

$$G_C = \frac{6P^2a^2}{b^2}\left(\frac{1}{h_1^3E_1} + \frac{1}{h_2^3E_2}\right) \tag{5.12}$$

To the same results we might get by considering that each arm of the specimen is a single beam fully constrained at the delamination front. Total displacement is then a sum of deflections of the two beams

$$\delta = \delta_1 + \delta_2 = \frac{Pa^3}{3E_1I_1} + \frac{Pa^3}{3E_2I_2} = \frac{4Pa^3}{b}\left(\frac{1}{h_1^3E_1} + \frac{1}{h_2^3E_2}\right) \tag{5.13}$$

Thus, compliance of the DCB specimen is

$$C = \frac{\delta}{P} = \frac{4a^3}{b}\left(\frac{1}{h_1^3E_1} + \frac{1}{h_2^3E_2}\right) \tag{5.14}$$

Differentiating equation (5.14) by the crack length and substituting into (2.59) gives the same definition for total energy release rate as equation (5.12).

In reality, the perfectly clamped condition at delamination front, considered by the simple beam theory is not realistic. Modified beam theory, as described in Chapter 2.5.2, uses the correction factor Δ for the crack length. This can be also applied for the test at bi-material interface, so the modified beam theory expression for energy release rate is

$$G_C = \frac{6P^2(a+\Delta)^2}{b^2}\left(\frac{1}{h_1^3E_1} + \frac{1}{h_2^3E_2}\right) \tag{5.15}$$

The crack length correction factor Δ, can be obtained by the method illustrated in Figure 2.18.

ELS

For an ELS specimen, as shown in Figure 5.4, the total moment, $M = Pa$, will be divided between upper and lower arms in the ratio of their bending stiffness. If we denote the bending stiffness ratio as

$$\psi = \frac{E_2 I_2}{E_1 I_1} = \frac{E_2 h_2^3}{E_1 h_1^3} \tag{5.16}$$

Then the particular moments at the delamination front will be

$$M_1 = \frac{Pa}{1+\psi} \tag{5.17}$$

$$M_2 = \frac{\psi Pa}{1+\psi} \tag{5.18}$$

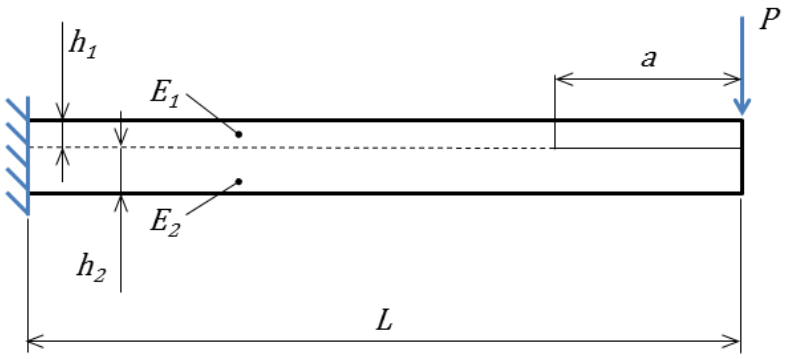

Figure 5.4: ELS specimen

After substituting equations (5.17) and (5.18) in (5.9), the energy release rate for ELS specimen is defined as

$$G_C = \frac{18P^2a^2}{b^2}\left[\frac{h_1h_2(h_1+h_2)^2E_1E_2}{\begin{array}{l}(h_2^3E_2+h_1^3E_1)(h_2^4E_2^2+4h_1h_2^3E_1E_2+\\ \quad +6h_1^2h_2^2E_1E_2+4h_1^3h_2E_1E_2+h_1^4E_1^2)\end{array}}\right] \tag{5.19}$$

ADCB

In and ADCB specimen (5.5), the loading force is acting only on one arm. Therefore, the moments at delamination front are

$$M_1 = -Pa \tag{5.20}$$

$$M_2 = 0 \tag{5.21}$$

And resulting energy release rate is

$$G_C = \frac{6P^2a^2}{b^2}\left[\frac{h_2E_2(3h_1^3E_1 + 6h_1^2h_2E_1 + 4h_1h_2^2E_1 + h_2^3E_2)}{\begin{array}{l}h_1^3E_1(h_2^4E_2^2 + 4h_1h_2^3E_1E_2 + \\ \quad + 6h_1^2h_2^2E_1E_2 + 4h_1^3h_2E_1E_2 + h_1^4E_1^2)\end{array}}\right] \tag{5.22}$$

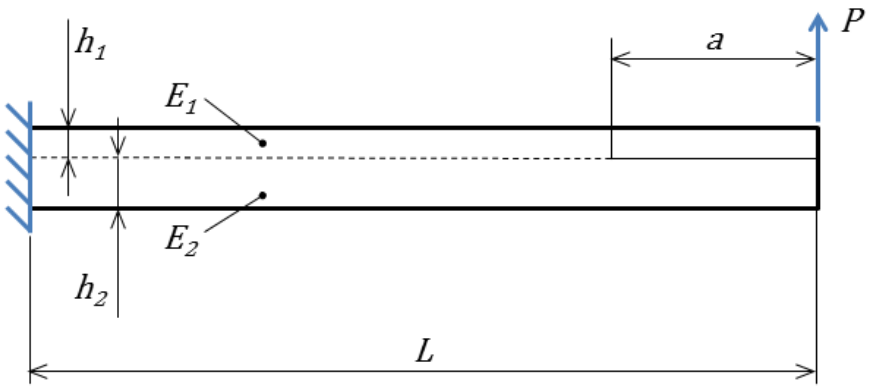

Figure 5.5: ADCB specimen

5.2 Mode partitioning

Beam theory

Contrary to homogeneous, isotropic materials, where cracks tend to propagate in pure mode I locally at the crack tip, mode mixity is a critical parameter for interfacial fractures. The mode mixity (sometimes called the phase angle of fracture) is the relative proportion of traction ahead the crack tip in sliding mode (mode II) and opening mode (mode I) in the fracture. Following the analysis by Williams [28], we can separate the total crack energy release rate into individual modes of fracture if we consider that pure mode II is obtained when the curvature of the two arms is the same

$$\frac{d\varphi_1}{da} = \frac{d\varphi_2}{da} \tag{5.23}$$

Equation (2.50) is then modified to account for different moduli in the two sections

$$\frac{M_{II}}{E_1I_1} = \frac{\psi M_{II}}{E_2I_2} \tag{5.24}$$

where

$$\psi = \frac{E_2I_2}{E_1I_1} \tag{5.25}$$

Equations (2.52) and (2.53) needs to be modified in order to correctly account for the different moduli in the two sections. The simple statement, given previously in [28], that the opening mode only requires moments in opposite senses so we have $-M_I$ on the upper arm and M_I on the lower arm, is only valid for symmetrical DCB specimen. For other configuration, the pure opening mode will be obtained only when the curvature of the two arms will be exactly opposite, i.e. $-M_I$ on the upper arm and ψM_I on the lower arm. Equation (2.52) and (2.53) will then have a form

$$M_1 = M_{II} - M_I \tag{5.26}$$

$$M_2 = \psi M_{II} + \psi M_I \tag{5.27}$$

After substituting (5.26) and (5.27) into (5.9) the energy release rate is

$$\begin{aligned} G = \frac{1}{2b}\Bigg[& \frac{E_1 I_1 EI + E_1^2 I_1^2 + E_2 I_2 EI - 2E_1 E_2 I_1 I_2 + E_2^2 I_2^2}{E_1^2 I_1^2 EI} M_I^2 + \\ & \frac{(E_1 I_1 + E_2 I_2)(E_1 I_1 + E_2 I_2 + EI)}{E_1^2 I_1^2 EI} M_{II}^2 + \\ & \frac{(E_2 I_2 - E_1 I_1)(E_1 I_1 + E_2 I_2 + EI)}{E_1^2 I_1^2 EI} M_I M_{II} \Bigg] \end{aligned} \tag{5.28}$$

and because of the cross term on the third line, the mode I and mode II cannot be separated analytically, in contrast to the results derived in [28].

VCCT

The history and overview of the virtual crack closure technique (VCCT) can be found in [52]. Recently, VCCT was implemented, as a standard analysis tool, into several commercial finite element codes such Abaqus [53], Nastran [54] and Marc [55], and therefore, has become a more frequently used analysis tool [41]. VCCT has successfully been used to obtain both the total strain energy release rate and the mode mixity for cracks in homogeneous materials. For an interface crack, the VCCT has traditionally been used to obtain the total strain energy release rate. Obtaining mode mixity for an interface crack using the VCCT has proven to be more challenging. However, several approaches have been suggested to extract consistent mode mixity values using the VCCT. [56]

In addition to the classical square root singularity at the crack tip, there exists an oscillatory singularity for cracks located at a bi-material interface. Several investigators over the past three decades showed that when numerical methods, such as the finite element method, are used to evaluate the total and individual mode strain energy release rates, the individual modes do not show convergence as the mesh size is refined near the crack tip. [41]

The methods to overcome the oscillatory singularity problem and non-convergence have been reviewed by Krueger et al. [41]. They concluded that practical solutions can be obtained only by few methods: the resin interlayer method, the method that chooses the crack tip element size greater than the

oscillation zone, the crack tip element method that is based on plate theory and the crack surface displacement extrapolation method.

The method based on choice of crack tip element size larger than the oscillatory zone is explored here as a simple approach that can be easily used with current commercially available finite element analysis software. Two sets of models were created in Abaqus/Standard™, where the interface crack problem was represented by the DCB specimen geometry, as shown in Figure 5.6

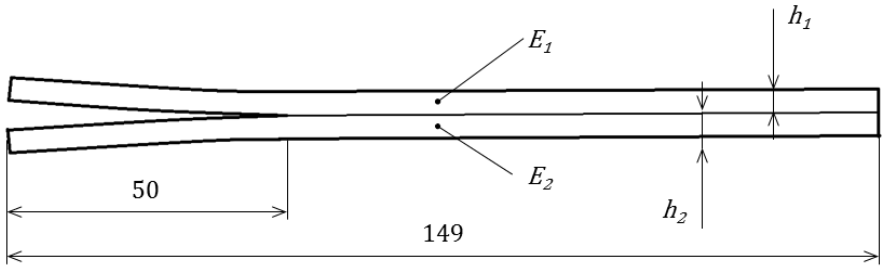

Figure 5.6: Finite element model geometry

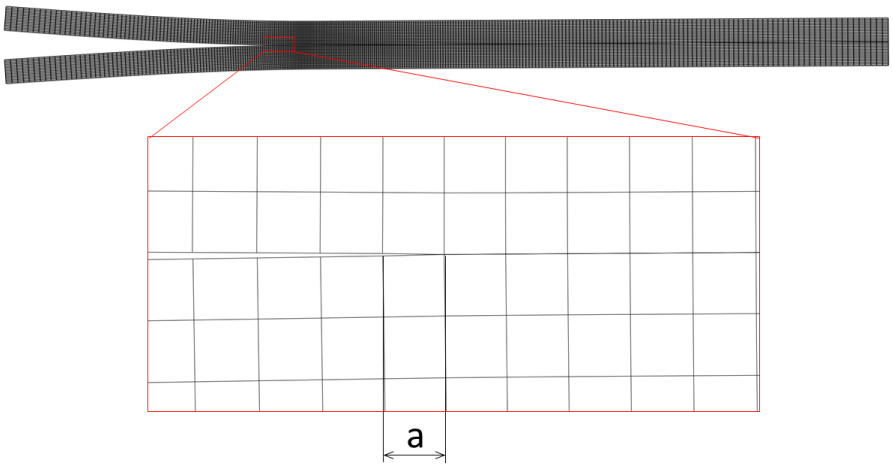

Figure 5.7: Element length at the crack tip

In one set of models, the thickness of both specimen arms was kept constant and difference in bending stiffness was varied by changing the elastic moduli ratio E_1/E_2. In second set of models, the elastic modulus was the same for both arms and the difference in bending stiffness was varied by changing the thickness ratio h_1/h_2. Fixed displacement boundary condition was applied on the lower arm and vertical displacement 5 mm was applied to the upper arm. The parametric study was setup to evaluate the effect of crack tip element edge length, a, as shown in Figure 5.7.

The results from all models are summarized in Appendix C: VCCT results and Figures 5.8 and 5.9. These results confirm the dependence of the mode I and mode II components on the element length near the crack tip. This dependence might be considered small for interfaces where bending stiffness

of the two arms is not very different. In this case, the method of choosing large element length might have some applicability. However, for interfaces where bending stiffness between the two components is larger, the convergence cannot be achieved. In fact, it is misleading to talk about convergence, as the mode mixity at material interfaces is a function of the distance from the crack tip and the energy release rate cannot be partitioned into mode components in principle.

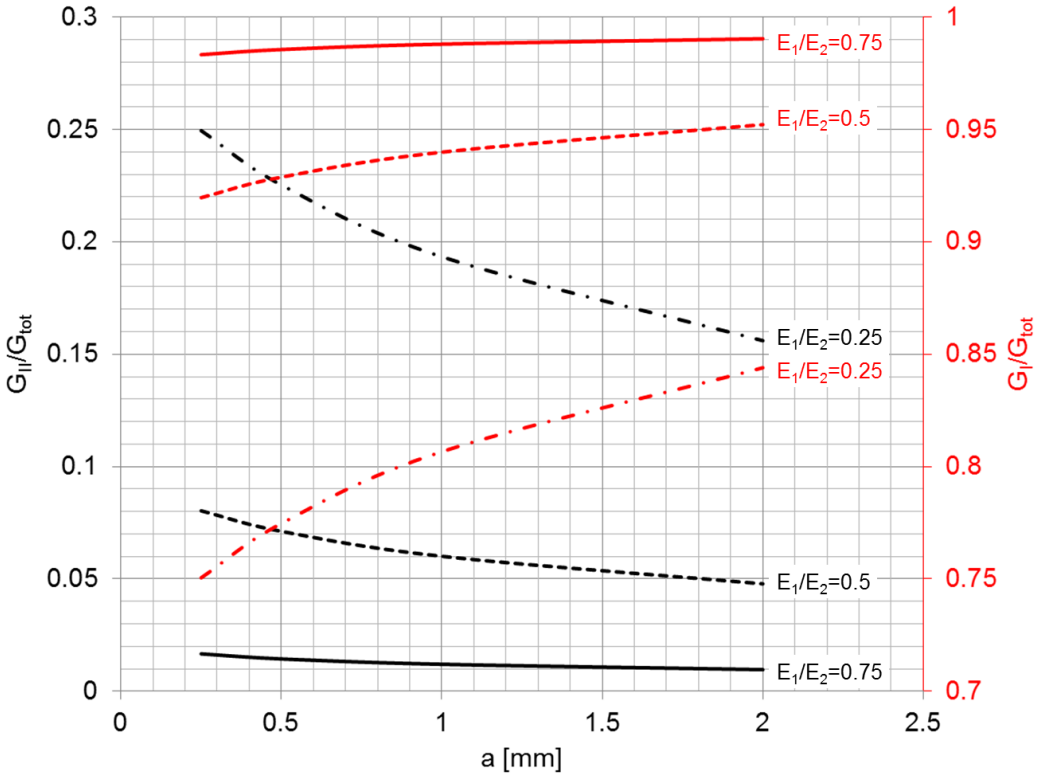

Figure 5.8: Energy release rate components vs. element size (based on different Young's modulus ratio)

These results show that the decomposition of strain energy release rate at the interface of two materials doesn't have any physical meaning, as the results will be dependent on the distance from the crack tip. The larger is the difference in bending stiffness the larger is the oscillatory zone and the methods suggested by many authors as shown in [41] might only be used for limited cases, where the difference in stiffness is not very large.

5.3 Compliance and effective crack length

When using a classical beam, the applied load and the crack length are the main parameters used to calculate strain energy release rate. However, by measuring the displacements, the strain energy release rate can be equivalently calculated

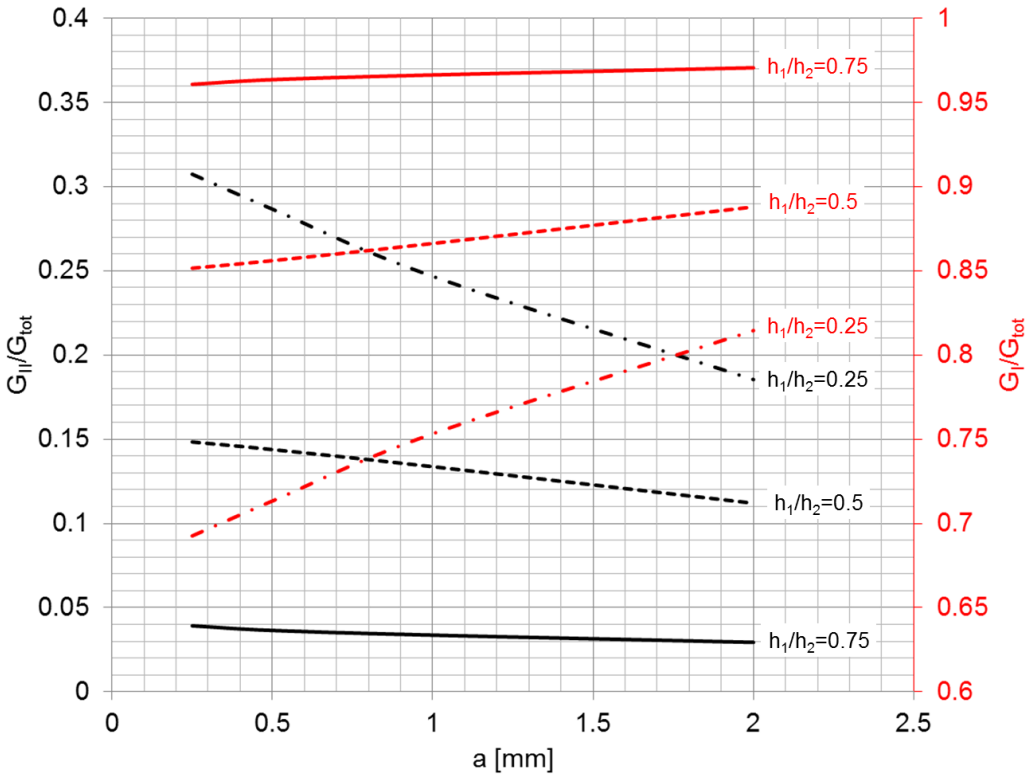

Figure 5.9: Energy release rate components vs. element size (based on different thickness ratio)

from the compliance as suggested by well-known equation

$$G = \frac{P^2}{2b}\frac{dC}{da} \tag{5.29}$$

This also enables to calculate the theoretical value of crack length, a, which then might be used to check on the measured values of crack length, especially when the crack length measurements includes some inherent uncertainties such as operator dependence. From equation (5.29) the compliance might be expressed as

$$C = \int^{a} \frac{2bG}{P^2} da + C_0 \tag{5.30}$$

where C_0 is the compliance with no crack present.

DCB

For DCB specimen, the strain energy release rate is expressed by equation (5.12)

$$G_C = \frac{6P^2a^2}{b^2}\left(\frac{1}{h_1^3E_1} + \frac{1}{h_2^3E_2}\right) \tag{5.31}$$

and the compliance with no crack present is

$$C_0 = 0 \tag{5.32}$$

After substituting equation (5.31) and (5.32) into (5.30), the DCB specimen compliance is

$$C = \frac{\delta}{P} = \frac{4a^3}{b}\left(\frac{1}{h_1^3 E_1} + \frac{1}{h_2^3 E_2}\right) \tag{5.33}$$

and the crack length can be calculated from displacement and applied load as

$$a = \sqrt[3]{\frac{\delta b}{4P\left(\frac{1}{h_1^3 E_1} + \frac{1}{h_2^3 E_2}\right)}} \tag{5.34}$$

ELS

For ELS specimen, the strain energy release rate is expressed by equation (5.19), which might be shortened as

$$G = \frac{18P^2a^2}{b^2}\Omega_{ELS} \tag{5.35}$$

if Ω_{ELS} is defined as

$$\Omega_{ELS} = \frac{h_1 h_2 (h_1 + h_2)^2 E_1 E_2}{\begin{array}{l}(h_2^3 E_2 + h_1^3 E_1)(h_2^4 E_2^2 + 4h_1 h_2^3 E_1 E_2 + \\ \quad + 6h_1^2 h_2^2 E_1 E_2 + 4h_1^3 h_2 E_1 E_2 + h_1^4 E_1^2)\end{array}} \tag{5.36}$$

Compliance with no crack present can be calculated from a simple beam theory equation for deflection of end loaded cantilever beam

$$C_0 = \frac{L^3}{3EI} \tag{5.37}$$

After substituting equation (5.37) and (5.35) into (5.30), the ELS specimen compliance is

$$C = \frac{\delta}{P} = \frac{12a^3\Omega_{ELS}EI + bL^3}{3bEI} \tag{5.38}$$

The crack length can be then calculated as

$$a = -\sqrt[3]{\frac{b\left(PL^3 - 3dEI\right)}{36P\Omega_{ELS}EI}} \tag{5.39}$$

Perfectly clamped boundary condition is assumed in this case. In reality, some amount of beam root deflection and rotation is present. This can be corrected by clamp correction factor, Δ_{clamp}, as described in [33] and in Chapter 2.5.2. The calculated crack length from a corrected beam theory is then

$$a = -\sqrt[3]{\frac{b\left(P(L + \Delta_{clamp})^3 - 3dEI\right)}{36P\Omega_{ELS}EI}} \tag{5.40}$$

ADCB

For an ADCB specimen, the strain energy release rate is expressed by equation (5.22) which might be shortened as

$$G = \frac{6P^2a^2}{b^2}\Omega_{ADCB} \tag{5.41}$$

where

$$\Omega_{ADCB} = \frac{h_2E_2(3h_1^3E_1 + 6h_1^2h_2E_1 + 4h_1h_2^2E_1 + h_2^3E_2)}{h_1^3E_1(h_2^4E_2^2 + 4h_1h_2^3E_1E_2 + \\ + 6h_1^2h_2^2E_1E_2 + 4h_1^3h_2E_1E_2 + h_1^4E_1^2)} \tag{5.42}$$

Compliance with no crack present is the same as in the ELS case

$$C = \frac{\delta}{P} = \frac{12a^3\Omega_{ADCB}EI + bL^3}{3bEI} \tag{5.43}$$

After substituting equations (5.44) and (5.41) into (5.30), the ADCB specimen compliance is

$$C = \frac{\delta}{P} = \frac{12a^3\Omega_{ADCB}EI + bL^3}{3bEI} \tag{5.44}$$

Assuming the same specimen length correction factor as in the ELS specimen, Δ_{clamp}, the crack length can be calculated as

$$a = -\sqrt[3]{\frac{b\left(P(L+\Delta_{clamp})^3 - 3dEI\right)}{12P\Omega_{ADCB}EI}} \tag{5.45}$$

6 Results

In total, seventeen bi-material glass-carbon composite specimens were tested in DCB, ELS and ADCB configurations as described in Chapter 4.1. The dimensions of each specimen is summarized in Appendix A: Specimen dimensions, where h_1 denotes the thickness of GFRP component and h_2 is the thickness of the CFRP component according to Figure 4.1.

6.1 DCB

A typical image of a DCB specimen during the test is shown in Figure 6.1. Here we can see that significant amount of local bending and large displacement is involved even before the initial crack starts to propagate. This is also the reason for nonlinearity in force-displacement curve recorded during the test, as shown in Figure 6.2. The relatively small thickness of GRFP component in combination with its low elastic modulus is the main cause for this nonlinearity. This fact makes the definition of delamination onset very ambiguous and the fracture toughness values obtained by different delamination onset criteria as defined in Figure 2.20 can be as low as 200 J/m^2 (NL definition of onset) or as high as 1600 J/m^2 (5% definition of onset) with a very high scatter between specimens. It is clear the NL definition of the onset is not the real fracture toughness value, because the force-displacement curve nonlinearity is caused by other factors rather than the delamination growth. The visual definition of delamination growth is also difficult and it is still a subject to an operator judgement, despite the fact that the images of the test were recorded and available for detailed inspection after the test. The 5% definition is commonly used in fracture toughness value, although the value of 5% is arbitrary and might not be enough for specimens with high overall compliance and vice versa.

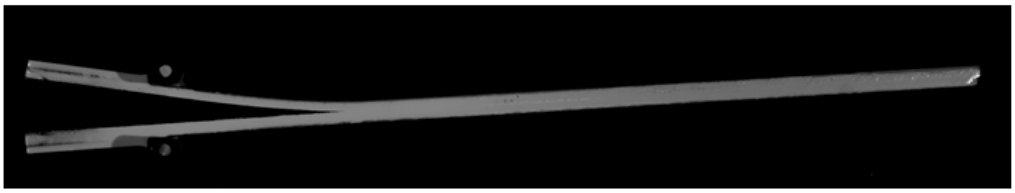

Figure 6.1: DCB specimen opening before crack growth

Finding the NL initiation points is easier when the deviation from linearity is plotted in a separate graph where the displacement is on horizontal axis and the deviation from linearity, i.e. $d_{lin} - d$ in Figure 6.2, is on vertical axis. This graph is shown in Figure 6.3. Here we can also notice that the part of the plot where we are certain that the crack is growing, let's say more than

12 mm displacement for this particular specimen, follows a linear trend. This can be used to define new initiation criteria which have not been considered previously, the "deviation from linearity tangent (DLT)". This new initiation criterion is defined as a point, where a linear fit to the linear part of deviation from linearity plot intersects the horizontal axis.

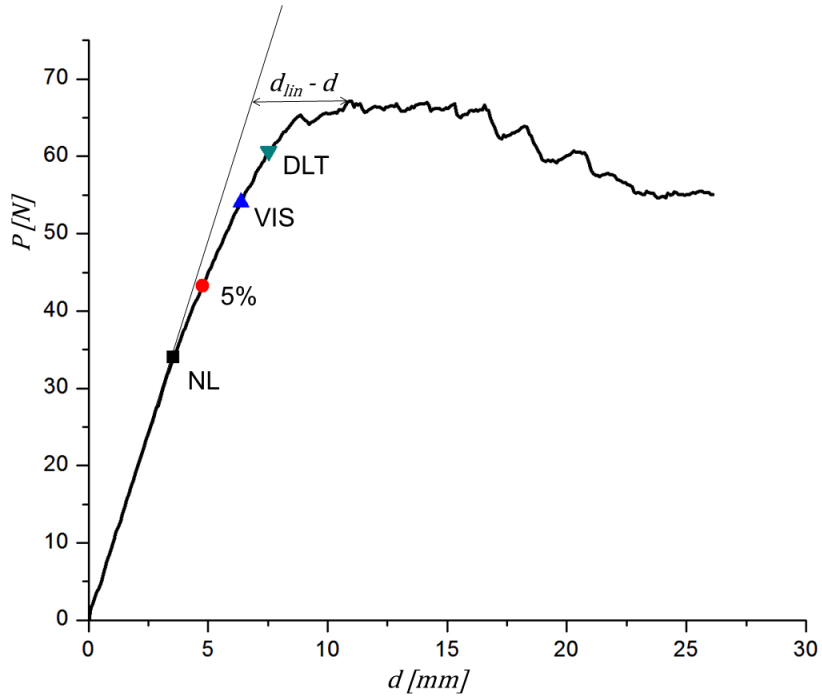

Figure 6.2: Force-displacement graph - delamination onset definition

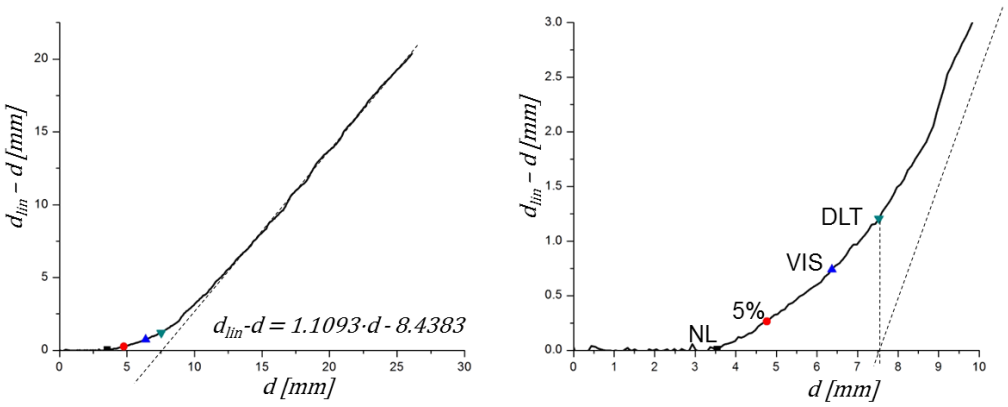

Figure 6.3: Deviation from linearity tangent (DLT) initiation point definition

DLT initiation criterion gives more consistent fracture toughness results with less scatter than both NL and 5% definitions for the 8 specimens tested in DCB configuration. This new initiation criterion has better connection with the actual specimen physical behaviour as it is based on its actual compliance

rather than the arbitrarily chosen value of 5% increase in compliance. It has been developed here for the delamination test for bi-material interface, but the author believes that it can have some utility in general composite material fracture toughness testing, where it can help to reduce the scatter in results that is common with the other definitions of initiation points.

The results of DCB tests are summarized in Table 6.1. Three data reductions methods were used here: simple beam theory (BT), modified beam theory (MBT) and compliance calibration (CC). Equations derived in Chapter 5.1 are used for BT and MBT. CC method uses Equation (2.70), which is not affected by the presence of the two different materials.

	G [J/m²]											
	NL			5%			VIS			DLT		
	BT	MBT	CC	BT	MBT	CC	BT	MBT	CC	BT	MBT	CC
DCB#1	191.3	252.0	289.8	316.6	412.6	446.5	599.3	768.6	743.0	790.9	1008.8	963.0
DCB#2	147.5	171.2	272.5	376.5	431.7	562.8	752.4	855.8	1006.0	1068.3	1209.5	1330.7
DCB#3	363.7	458.6	636.4	845.2	1041.8	1125.3	1273.4	1549.0	1545.7	1066.2	1304.9	1348.4
DCB#4	213.1	270.4	319.6	315.1	397.7	464.2	854.1	1056.7	1093.1	794.5	985.0	1022.5
DCB#5	362.7	395.4	443.1	855.2	930.4	1017.4	754.1	820.7	897.5	1083.3	1177.7	1288.6
DCB#6	441.3	476.7	496.9	1002.1	1080.8	1106.7	822.5	887.2	885.6	1175.1	1265.0	1283.5
DCB#7	743.7	779.3	838.0	1188.2	1244.7	1387.0	901.8	945.0	1027.0	1251.7	1311.2	1473.7
DCB#8	600.0	514.4	769.9	1109.6	956.8	1325.6	1008.8	869.1	1205.9	1222.9	1054.9	1517.2
mean	382.9	414.7	508.3	751.0	812.1	929.4	870.8	969.0	1050.5	1056.6	1164.6	1278.4
std	207.9	191.1	219.4	362.8	342.9	383.2	202.2	249.7	244.6	177.3	132.0	195.6

Table 6.1: DCB fracture toughness results

6.2 ADCB

ADCB specimens showed the same type of nonlinearity as seen previously in DCB specimen and thus the conventional delamination initiation definition (NL, 5%) is not necessarily connected with the crack propagation. An example of force-displacement data, together with a typical specimen opening before the delamination onset is shown in Figure 6.4.

Two variations of beam theory data reduction method, as defined by the Equation (5.22) were used: (a) with a crack length as measured by image processing method, i.e. BT and (b) with a crack length calculated by Equation (5.45), i.e. BT-acalc. Also experimental compliance calibration method (CC) is used to calculate energy release rate initiation values as defined by Equation (2.81). The results are summarized in Table 6.2.

	G [J/m²]											
	NL			VIS			DLT			5%		
	BT	BT-acalc	CC	BT	BT-acalc	CC	BT	BT-acalc	CC	BT	BT-acalc	CC
ADCB#1	384.7	544.1	369.6	801.0	1018.8	769.6	1283.0	1533.6	1232.7	1151.2	1352.9	1106.0
ADCB#2	692.3	705.1	569.2	1142.6	1183.8	939.4	1559.0	1628.5	1281.8	1706.3	1799.4	1402.8
ADCB#3	167.3	419.1	182.3	912.7	1162.5	994.3	1421.3	1618.5	1548.5	1217.6	1400.9	1326.5
ADCB#4	490.7	529.1	476.0	933.0	949.7	904.9	1643.2	1619.3	1593.8	1504.6	1503.5	1459.4
mean	433.8	549.3	399.3	947.3	1078.7	902.1	1476.6	1600.0	1414.2	1394.9	1514.2	1323.7
std	218.7	117.9	166.0	142.5	113.0	95.7	158.2	44.5	183.3	258.1	200.3	155.0

Table 6.2: ADCB fracture toughness results

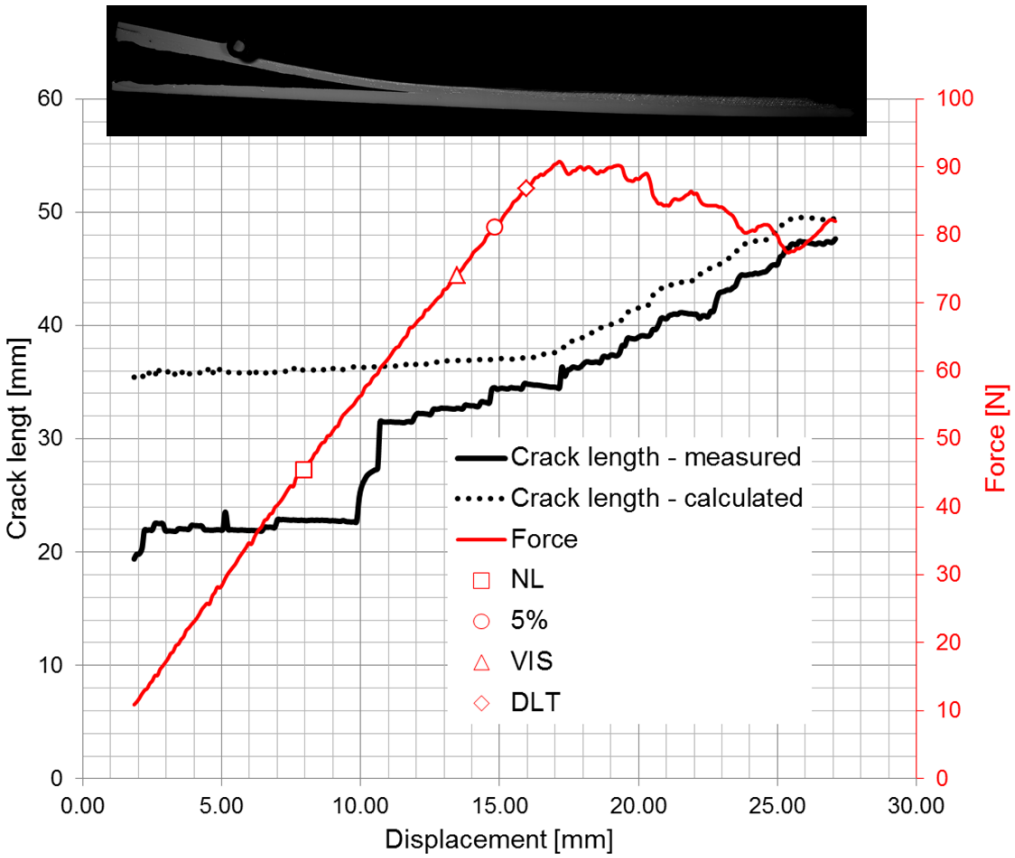

Figure 6.4: ADCB force-displacement data with initiation points and crack length measurements

6.3 ELS

Testing in ELS configuration was accompanied by unstable crack propagation as illustrated in Figure 6.5 with an instantaneous decrease in loading force as shown in Figure 6.6. Because of this fact, no propagation data were recorded and it was not possible to use the experimental compliance calibration method as in DCB and ADCB test configurations, where the crack propagation was stable. Also the image processing for measuring the crack length didn't prove to be sufficiently accurate and without a stable crack propagation also unnecessary. The only method used for the data reduction is therefore the corrected beam theory using effective crack length (CBTE), where the effective crack length is calculated by Equation (5.40) and energy release rate is calculated by Equation (5.19).

There was a very little nonlinear behaviour before the crack started to propagate, and therefore the NL initiation point is very close to the VIS and 5%/MAX initiation points, which coincide for some specimens. Because of the lack of propagation values, the newly proposed DLT initiation definition could not be used.

The clamp correction factor needed for calculating the effective crack length

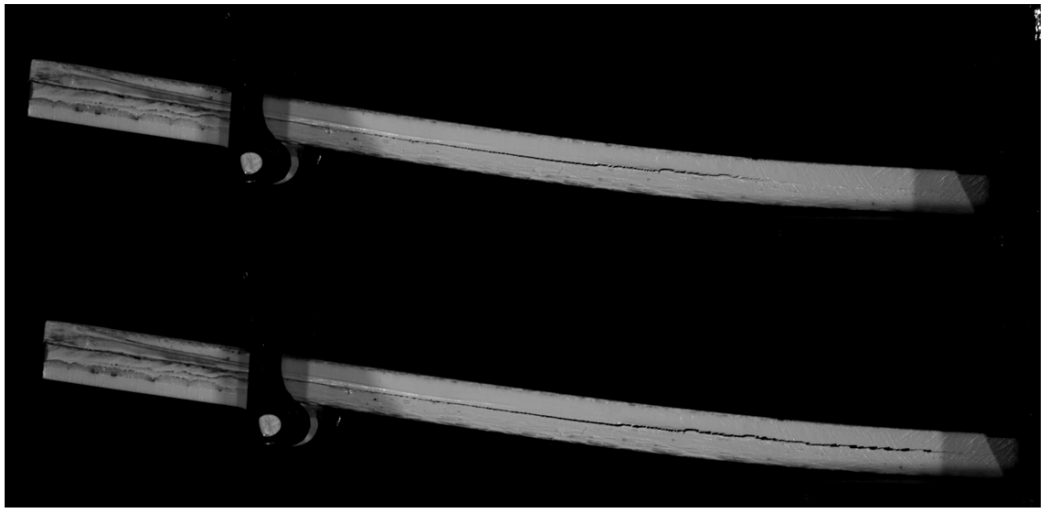

Figure 6.5: ELS specimen unstable crack propagation

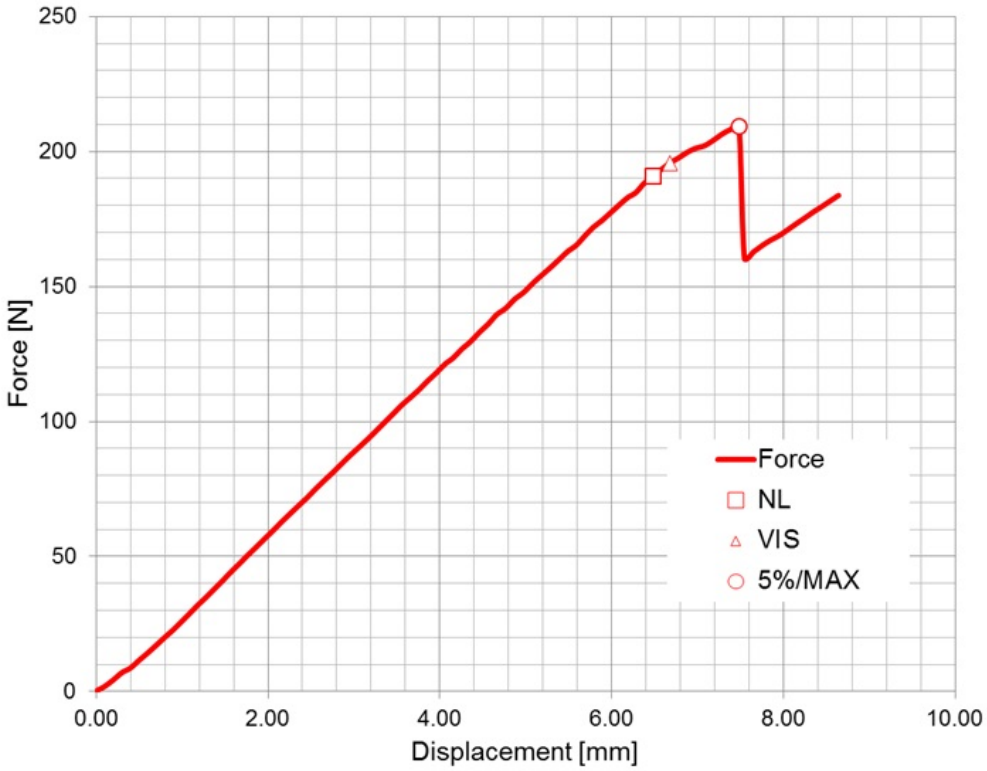

Figure 6.6: ELS Force-Displacement curve

was obtained by the method describe in Chapter 2.5.2 according to [33]. Linear fit to the cube root of compliance vs. the free length of clamped specimen, as

shown in Figure 6.7, gives the correction factor

$$\Delta_{clamp} = \frac{-5.4833 \times 10^{-2}}{3.6338 \times 10^{-3}} = -15.0895mm \tag{6.1}$$

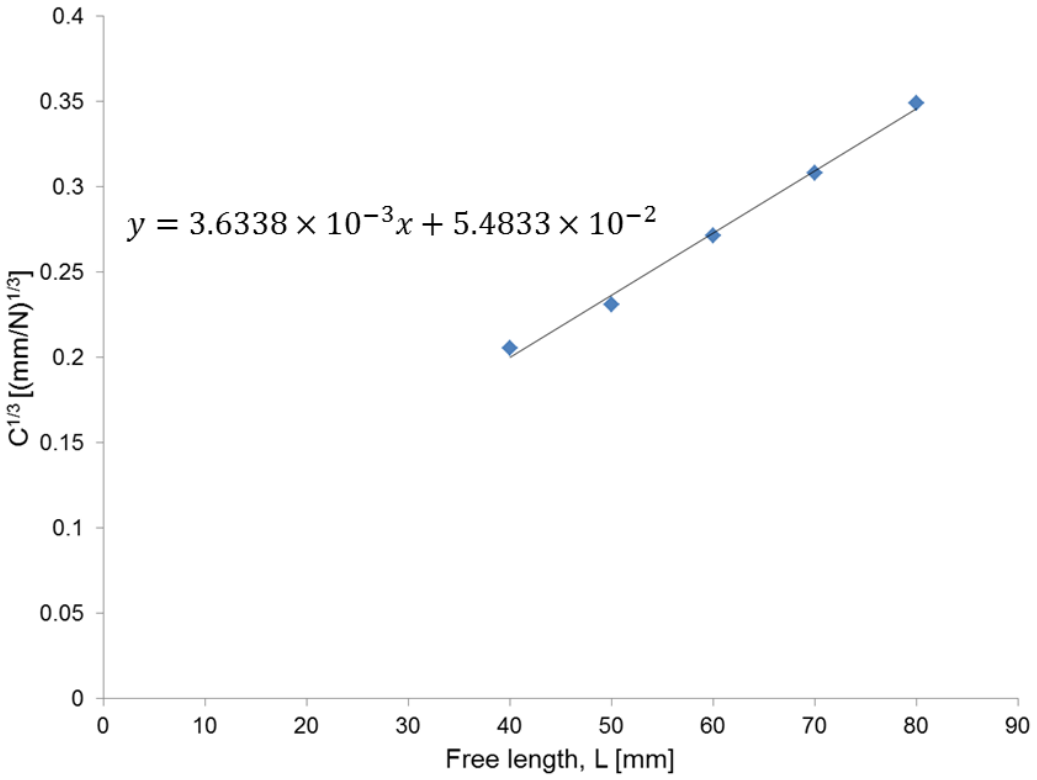

Figure 6.7: ELS clamp correction factor

The energy release rate results for ELS tests are summarized in Table 6.3

	G [J/m²]		
	NL	**VIS**	**5%/MAX**
ELS#1	766.2	808.7	962.8
ELS#2	786.6	989.6	1055.5
ELS#3	588.9	664.9	748.3
ELS#4	776.7	1086.8	1086.8
ELS#5	267.9	967.7	967.7
mean	637.2	903.5	964.2
std	222.0	166.6	132.3

Table 6.3: ELS fracture toughness results

6.4 Summary

Figure 6.8 shows a comparison of fracture toughness results from all three tested configurations. Results obtained by modified beam theory and beam theory with calculated crack length are plotted for DCB and ADCB tests rather than a simple beam theory results, because they are believed to be more accurate. Also result from compliance calibration method are plotted for both, DCB and ADCB for comparison. Only method used to calculate fracture toughness in ELS configuration was the corrected beam theory with effective crack length.

According to expectation, the deviation from non-linearity (NL) initiation point definition yields the lowest fracture toughness results for all tested configurations and data reduction methods. However, these are only included here for completeness, as they do not represent the real fracture toughness because other factors contribute to the non-linear behaviour of the specimen before the crack starts to propagate. This is very significant for DCB and ADCB specimen. In ELS, where local bending of specimen arms before the crack propagation is smaller, the results from deviation from non-linearity are closer to other initiation definitions.

Interesting comparison can be made between the visual onset definition and the 5% increase in compliance definition. Visually determined values are higher for DCB and lower for ADCB. This can be explained by generally higher compliance of ADCB, which is affecting the 5% offset definition results. Also, it is difficult to rely on a judgement and eyesight of a test operator and thus the visual onset values remain only hypothetical.

The new initiation definition, deviation from linearity tangent (DLT), gives the highest fracture toughness results, however with less variability.

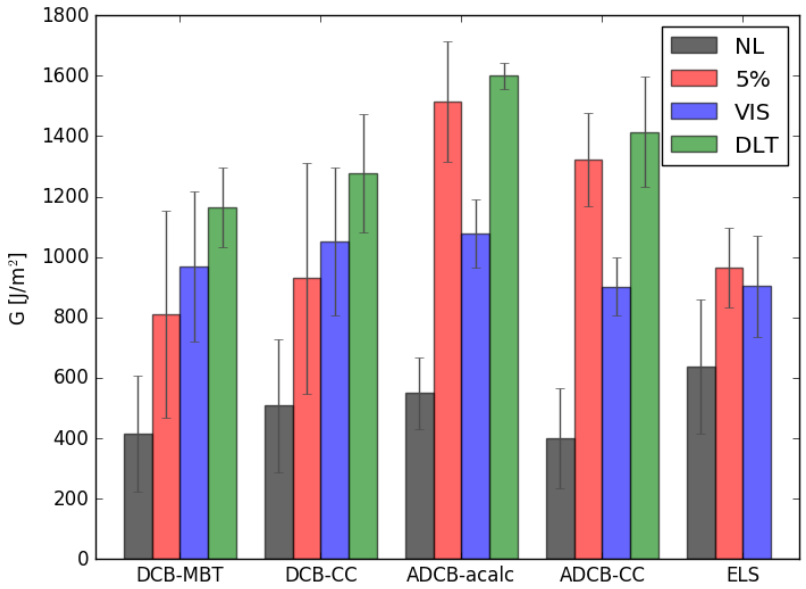

Figure 6.8: Results summary

7 Discussion

Defects in composite structures need to be considered as an important factor that can affect their strength and load-carrying capacity. Economic aspects of composite materials manufacture, quality control and product maintenance require some level of defects to be present, however the safety is the primary concern and the structural integrity needs to be assured throughout the component life. One of the main defects with potential harmful consequences to the structural strength of a product made of composite materials is the delamination. Composite laminates are very prone to this type of defect that usually starts from stress concentration area, such as straight edges, corners or an interface between two components with different elastic properties.

This doctoral thesis focuses on experimental testing methods of delaminations at a bi-material interface. The beam specimens made of combination of glass and carbon composites were tested in several configurations, which are commonly used for testing delamination fracture toughness of composite materials. The analytical equations for test data reduction were modified in order to account for the two different materials in specimen.

One of the issues with the composite delamination testing is the measurement of the crack length. Often, this measurement is done optically with a travelling microscope and the results can be affected by the operator's eyesight and judgement. New method of crack length measurement by digital image processing was developed here and proved to be very accurate with the combination of corrected beam theory data reduction method. This new method can be applied in any test configuration with a clear opening between the specimen arms and not only to a bi-material interface as presented here. This method can reduce the workload of the test operator and it assures consistent results between different specimens within the batch. Python programming language was used for the image processing, because of its simple syntax and easily available open-source libraries for scientific computing. One of the downsides of the current method is the slow speed of image processing. This can be improved by implementing the method in a faster programming language.

Another problem with composite delamination testing is the definition of the delamination onset. The onset criteria used currently are deviation from linearity, visual observation and 5% increase in compliance, but sometimes these criteria can produce significantly different results with a large scatter, especially for specimens with low stiffness and nonlinear behaviour occurrence before the crack starts to propagate. A new initiation point definition was proposed in this thesis; the deviation from linearity tangent. This new initiation point definition is based on the specimen physical behaviour during the crack propagation and yields less scatter than any of the other initiation criteria.

Mode mixity is an essential parameter used in delamination fracture criteria. However, it has been shown here that this parameter has no physical meaning for the bi-material interface, as the mode I and mode II contribution to the

energy release rate will always be a function of the distance from the crack tip. An approximation of the mode mixity can be made for the interfaces where the difference in bending stiffness is small, but the uncertainty about the contribution of each mode grows with the larger mismatch between material properties. The use of the fracture criteria based on the mode mix parameter thus have significant limitation and perhaps the conservative fracture criteria, $G = G_{Ic}$, can be used instead.

8 Conclusion

The aims set in Section 3.2 were met only partially. The analytical investigation presented in Section 5 showed that the fracture toughness at a bi-material interface cannot be divided into mode I and mode II contribution and that the mode mix ratio varies with distance from the crack tip. For this reason, it is impossible to develop a failure criterion based on a mixed mode ratio. Automatic crack length measurement method was successfully developed and validated as described in 4.2.

Bibliography

[1] Hinton M. J., Kaddour A. S., and Soden P. D. *Failure criteria in fibre reinforced polymer composites: the world-wide failure exercise*. Elsevier, 2004.

[2] Raju I. and O'Brien T. Fracture mechanics concepts, stress fields, strain energy release rates, delamination initiation and growth criteria. *Delamination behaviour of composites*, 2008.

[3] Barbero E. J. *Finite Element Analysis of Composite Materials using AbaqusTM*. CRC press, 2013.

[4] Salkind M. Fatigue of composites. In *Composite Materials Testing and Design (2nd Conf). ASTM STP*, volume 497, pages 143–169, 1972.

[5] Baker A. and Kelly D. W. *Composite materials for aircraft structures*. AIAA, 2004.

[6] Talreja R. Assessment of the fundamentals of failure theories for composite materials. *Composites Science and Technology*, 105:190–201, 2014.

[7] Huang Z.-M. and Zhou Y.-X. *Strength of fibrous composites*. Springer Science & Business Media, 2012.

[8] Rankine W. M. On the stability of loose earth. *Philosophical Transactions of the Royal Society of London*, 147:9–27, 1857.

[9] Mises R. v. Mechanik der festen körper im plastisch-deformablen zustand. *Nachrichten von der Gesellschaft der Wissenschaften zu Göttingen, Mathematisch-Physikalische Klasse*, 1913:582–592, 1913.

[10] Hill R. A theory of the yielding and plastic flow of anisotropic metals. In *Proceedings of the Royal Society of London A: Mathematical, Physical and Engineering Sciences*, volume 193, pages 281–297. The Royal Society, 1948.

[11] Azzi V. and Tsai S. Anisotropic strength of composites. *Experimental mechanics*, 5(9):283–288, 1965.

[12] Tsai S. W. and Wu E. M. A general theory of strength for anisotropic materials. *Journal of composite materials*, 5(1):58–80, 1971.

[13] Puck A. *Festigkeitsanalyse von Faser-Matrix-Laminaten: Modelle für die Praxis*. Hanser München, 1996.

[14] VDI 2014 Blatt 3 . Entwicklung von bauteilen aus faser-kunststoff-verbund berechnungen / development of frp components (fibre-reinforced plastics) analysis. VDI 2014 Blatt 3, Verein Deutscher Ingenieure, 2006.

[15] Altenbach H. and Sadowski T. *Failure and Damage Analysis of Advanced Materials*. Springer, 2015.

[16] Hinton M., Kaddour A., and Soden P. A comparison of the predictive capabilities of current failure theories for composite laminates, judged against experimental evidence. *Composites Science and Technology*, 62(12):1725–1797, 2002.

[17] Hinton M., Kaddour A., Pinho S., Vyas G., Robinson P., Huang Z., Zhou Y., Rotem A., Carrere N., Laurin F., and others . Special issue: The second world-wide failure exercise (wwfe-ii): Part b: Evaluation of theories for predicting failure in polymer composite laminates under 3-d states of stress: Comparison with experiments preface, 2013.

[18] Anderson T. *Fracture mechanics: fundamentals and applications*. CRC press, 2005.

[19] Gibson R. F. *Principles of composite material mechanics*. CRC press, 2011.

[20] Griffith A. A. The phenomena of rupture and flow in solids. *Philosophical transactions of the royal society of london. Series A, containing papers of a mathematical or physical character*, pages 163–198, 1921.

[21] Irwin G. Analysis of stresses and strains near the end of a crack traversing a plate. *J. Appl. Mech.*, 1957.

[22] Blanco Villaverde N. and others . *Variable mixed-mode delamination in composite laminates under fatigue conditions: testing & analysis*. Universitat de Girona, 2005.

[23] Krueger R. Fracture mechanics for composites: State of the art and challenges. 2006.

[24] Davies P., Blackman B., and Brunner A. Standard test methods for delamination resistance of composite materials: current status. *Applied Composite Materials*, 5(6):345–364, 1998.

[25] Benzeggagh M. and Kenane M. Measurement of mixed-mode delamination fracture toughness of unidirectional glass/epoxy composites with mixed-mode bending apparatus. *Composites science and technology*, 56(4):439–449, 1996.

[26] Wu E. M. and Reuter Jr R. Crack extension in fiberglass reinforced plastics. Technical report, DTIC Document, 1965.

[27] Shivakumar K., Chen H., Abali F., Le D., and Davis C. A total fatigue life model for mode i delaminated composite laminates. *International Journal of Fatigue*, 28(1):33–42, 2006.

[28] Williams J. On the calculation of energy release rates for cracked laminates. *International Journal of Fracture*, 36(2):101–119, 1988.

[29] ASM Hnadbook . Vol. 19 Fatigue and Fracture. *ASM International*, 1996.

[30] MIL-HDBK-17F . *Composite Materials Handbook - Volume 3. Polymer Matrix Composites Materials Usage, Design, and Analysis*. MIL-HDBK-17, 2002.

[31] Brunner A., Blackman B., and Davies P. A status report on delamination resistance testing of polymer–matrix composites. *Engineering Fracture Mechanics*, 75(9):2779–2794, 2008.

[32] ISO 15024:2001 . Fibre-reinforced plastic composites – determination of mode i interlaminar fracture toughness, gic, for unidirectionally reinforced materials. ISO 15024:2001, International Organization for Standardization, Geneva, Switzerland, 2001.

[33] ISO 15114:2014 . Fibre-reinforced plastic composites – determination of the mode ii fracture resistance for unidirectionally reinforced materials using the calibrated end-loaded split (c-els) test and an effective crack length approach. ISO 15114:2014, International Organization for Standardization, Geneva, Switzerland, 2014.

[34] ASTM D5528-13 . Standard test method for mode i interlaminar fracture toughness of unidirectional fiber-reinforced polymer matrix composites. ASTM D5528-13, ASTM International, West Conshohocken, PA, 2013.

[35] ASTM D6671/D6671M-13e1 . Standard test method for mixed mode i-mode ii interlaminar fracture toughness of unidirectional fiber reinforced polymer matrix composites. ASTM D6671, ASTM International, West Conshohocken, PA, 2013.

[36] ASTM D7905 / D7905M-14 . Standard test method for determination of the mode ii interlaminar fracture toughness of unidirectional fiber-reinforced polymer matrix composites. ASTM D7905, ASTM International, West Conshohocken, PA, 2014.

[37] Kageyama K., Kikuchi M., and Yanagisawa N. Stabilized end notched flexure test-characterization of mode ii interlaminar crack growth. In *Composite Materials: Fatigue and Fracture. Vol. 3*, volume 1, pages 210–225, 1991.

[38] Martin R. and Davidson B. Mode ii fracture toughness evaluation using four point bend, end notched flexure test. *Plastics, Rubber and Composites*, 28(8):401–406, 1999.

[39] Williams J. The fracture mechanics of delamination tests. *Journal of strain analysis for engineering design*, 24(4):207–214, 1989.

[40] Rybicki E. F. and Kanninen M. A finite element calculation of stress intensity factors by a modified crack closure integral. *Engineering Fracture Mechanics*, 9(4):931–938, 1977.

[41] Krueger R., Shivakumar K., and Raju I. S. Fracture mechanics analyses for interface crack problems: a review. In *Proceedings of the 54th AIAA/ASME/ASCE/AHS/ASC structures, structural dynamics, and materials conference*, pages 8–11, 2013.

[42] Brunner A. and Barbezat M. Acoustic emission monitoring of delamination growth in fiber-reinforced polymer-matrix composites. In *Fracture of Nano and Engineering Materials and Structures*, pages 291–292. Springer, 2006.

[43] Bohse J. Acoustic emission examination of polymer-matrix composites. *Journal of Acoustic Emission*, 22:208–223, 2004.

[44] Richter-Trummer V., Marques E., Chaves F., Tavares J., Silva da L., and Castro de P. Analysis of crack growth behavior in a double cantilever beam adhesive fracture test by different digital image processing techniques. *Materialwissenschaft und Werkstofftechnik*, 42(5):452–459, 2011.

[45] Gonzalez R. C. and Woods R. E. Digital image processing 3rd edition, 2007.

[46] Abe H. Device technologies for high quality and smaller pixel in ccd and cmos image sensors. In *Electron Devices Meeting, 2004. IEDM Technical Digest. IEEE International*, pages 989–992. IEEE, 2004.

[47] Yoneyama S. and Murasawa G. Digital image correlation. *Experimental Mechanics. Eolss Publishers*, 2009.

[48] Python software foundation . `https://www.python.org/`, 2001-2015.

[49] The Scipy community . `http://docs.scipy.org/doc/scipy/reference/`, 2008-2014.

[50] Coster M. and Chermant J.-L. Image analysis and mathematical morphology for civil engineering materials. *Cement and Concrete Composites*, 23(2):133–151, 2001.

[51] `http://www.scipy-lectures.org/advanced/image_processing/auto_examples/plot_propagation.html`.

[52] Krueger R. The virtual crack closure technique: History, approach and applications. *NASA, Hampton, USA, ICASE Report*, 2002.

[53] Abaqus/Standard 6.12 User's Manual . Technical report, Dassault Systemes Simulia Corporation, Providence, RI, USA, 2012.

[54] MD Nastran 2008 R1 Documentation . Technical report, MSC.Software Corporation, Santa Ana, CA, USA, 2008.

[55] Marc 2008 R1 User Manual . Technical report, MSC.Software Corporation, Santa Ana, CA, USA, 2008.

[56] Agrawal A. and Karlsson A. M. Obtaining mode mixity for a bimaterial interface crack using the virtual crack closure technique. *International journal of fracture*, 141(1-2):75–98, 2006.

List of acronyms

4ENF	Four point end notched flexure
5%/MAX	5% increase in compliance or maximum load initiation point
ADCB	Asymmetric double cantilever beam
BT	Beam theory
CBTE	Corrected beam theory using effective crack length
CC	Compliance calibration
CCD	Charge-coupled device
CLS	Crack lap shear
CMOS	Complementary metal-oxide semiconductor
CRFP	Carbon fibre reinforced plastic
DCB	Double cantilever beam
DIC	Digital image correlation
DLT	Deviation from linearity tangent initiation point
ECT	Edge crack torsion
ELS	End load split
ENF	End notched flexure
FE	Finite element
GRFP	Glass fibre reinforced plastic
MBT	Modified beam theory
MMB	Mixed mode bending
MMF	Mixed mode flexure
NL	Deviation from linearity initiation point
VCCT	Virtual crack closure technique
VIS	Visual observation inititation point

List of symbols

A	Crack area
a	Crack length or half crack length
b	Specimen width
C	Compliance
δ	Displacement
Δ_{clamp}	Critical energy release rate
E	Young's modulus
EI	Bending stiffness
$\varepsilon_{11}, \varepsilon_{22}, \gamma_{12}$	Strain components in material coordinate system
F	Work done by external forces
F'_{xi}, F'_{yi}	Forces at a crack tip
G	Energy release rate
τ_{max}	Specimen half thickness
I	Second moment of area
K	Stress intensity factor
L	Specimen free length
M	Bending moment
N	Number of cycles
P	External force
ϕ	Angle of rotation
Π	Potential energy
ψ	Bending stiffness ratio
S	Shear strength
$\sigma_1, \sigma_2, \sigma_3$	Principal stress
$\sigma_{11}, \sigma_{22}, \tau_{12}$	Stress components in material coordinate system
σ_{eq}	Equivalent stress
σ_u	Ultimate stress
$\sigma_x, \sigma_y, \tau_{xy}$	Stress components in XY coordinate system
σ_y	Yield strength
τ_{max}	Maximum shear stress
U	Strain energy
u, v	Displacement at nodes
X_C	Compressive strength in longitudinal direction
ξ	Thickness parameter
X_T	Tensile strength in longitudinal direction
Y_C	Compressive strength in transverse direction
Y_T	Tensile strength in transverse direction

List of appendices

Appendix A: Specimen dimensions

Specimen	h_1 [mm]	h_2 [mm]	b [mm]
DCB#1	1.81	2.43	20.15
DCB#2	1.85	2.38	20.11
DCB#3	1.86	2.44	20.22
DCB#4	1.85	2.35	20.19
DCB#5	1.91	2.44	20.22
DCB#6	1.83	2.49	20.03
DCB#7	1.86	2.33	20.12
DCB#8	1.92	2.54	20.32
ADCB#1	1.87	2.44	20.08
ADCB#2	1.76	2.37	20.15
ADCB#3	1.92	2.33	20.17
ADCB#4	1.80	2.32	20.21
ELS#1	2.10	2.46	2.12
ELS#2	2.17	2.38	20.08
ELS#3	2.14	2.39	20.18
ELS#4	2.14	2.41	20.10
ELS#5	2.17	2.41	20.10

Appendix B: Image processing algorithm

```
import numpy as np
import scipy
from scipy import ndimage
import matplotlib.pyplot as plt
import glob
import scipy.ndimage as ndimage
import skimage.filter as skif

def findCrackStart(current_image, minimum_width = 10, x_start = 1100):
        image_height = current_image.shape[0]
        count = 0
        for pixel in range(image_height):
                if current_image[pixel,x_start] ==1:
                        count += 1
                        if current_image[pixel+1,x_start] == 0:
                                if count >= minimum_width:
                                        y_start = pixel
                                        break
                                else:
                                        count = 0
        return x_start, y_start

def findCrackTip(current_image,x,y,tolerance_x, tolerance_y):
        tol_Y = tolerance_y
        tol_X = tolerance_x
        while (tol_Y > 0 and tol_Y>0):
                while tol_X > 0:
                        if current_image[y,x+tol_X] == 0:
                                x = x +tol_X
                                tol_X = tolerance_x
                                tol_Y = tolerance_y
                                continue
                        elif current_image[y+tol_Y,x+tol_X] == 0:
                                x = x +tol_X
                                y = y+tol_Y
                                tol_X = tolerance_x
                                tol_Y = tolerance_y
                                continue
                        elif current_image[y-tol_Y,x+tol_X] == 0:
                                x = x +tol_X
                                y = y-tol_Y
                                tol_X = tolerance_x
```

```
                                tol_Y = tolerance_y
                                continue
                        else:
                                tol_X = tol_X-1
                tol_X = tolerance_x
                tol_Y = tol_Y -1
        return x,y

def imageClearup(image,threshold = 30):
        binary_image = (image > threshold).astype(int)
        binary_image = scipy.ndimage.binary_opening(binary_image)
        return binary_image

image_list = glob.glob('*.tif')
image_list.sort()
write_file =  open('CrackTips.txt', 'w')
write_file.write('%8s %8s %8s\n'%('stage','X','Y'))
for f in range(len(image_list)):
        image = scipy.misc.imread(image_list[f],flatten=True)
        stage = f
        print f
        image = imageClearup(image,30)
        try:
                x, y = findCrackStart(image)
        except:
                print 'Start not found'
                write_file.write('%8s %s8\n'%(stage,'StartNotFound'))
        try:
                x, y = findCrackTip(image,x,y,50,20)
                print 'tip' , x, y
                write_file.write('%8s %8s %8s\n'%(stage,x,y))
        except :
                print 'TipNotFound'
                write_file.write('%8s %s8\n'%(stage,'TipNotFound'))
write_file.close()
```

Appendix C: VCCT results

$h_1 = h_2$	E_1	E_2	E_1/E_2	**a**	G_I	G_{II}
mm	MPa	Mpa	-	mm	kJ/m^2	kJ/m^2
4	75000	100000	0.75	0.25	3.6364	0.0617
4	75000	100000	0.75	0.5	3.6556	0.0535
4	75000	100000	0.75	1	3.6854	0.0449
4	75000	100000	0.75	2	3.7331	0.0363
4	50000	100000	0.5	0.25	2.6641	0.2327
4	50000	100000	0.5	0.5	2.6971	0.2068
4	50000	100000	0.5	1	2.7437	0.1754
4	50000	100000	0.5	2	2.8069	0.1410
4	25000	100000	0.25	0.25	1.3261	0.4408
4	25000	100000	0.25	0.5	1.3716	0.3990
4	25000	100000	0.25	1	1.4349	0.3440
4	25000	100000	0.25	2	1.5143	0.2799

$E_1 = E_2$	h_1	h_2	h_1/h_2	**a**	G_I	G_{II}
MPa	mm	mm	-	mm	kJ/m^2	kJ/m^2
100000	3	4	0.75	0.25	2.5526	0.1042
100000	3	4	0.75	0.5	2.5667	0.0971
100000	3	4	0.75	1	2.5878	0.0901
100000	3	4	0.75	2	2.6269	0.0795
100000	2	4	0.5	0.25	0.8992	0.1567
100000	2	4	0.5	0.5	0.9059	0.1522
100000	2	4	0.5	1	0.9209	0.1421
100000	2	4	0.5	2	0.9537	0.1203
100000	1	4	0.25	0.25	0.1079	0.0479
100000	1	4	0.25	0.5	0.1113	0.0447
100000	1	4	0.25	1	0.1180	0.0387
100000	1	4	0.25	2	0.1290	0.0294

Appendix D: DCB results

DCB#1

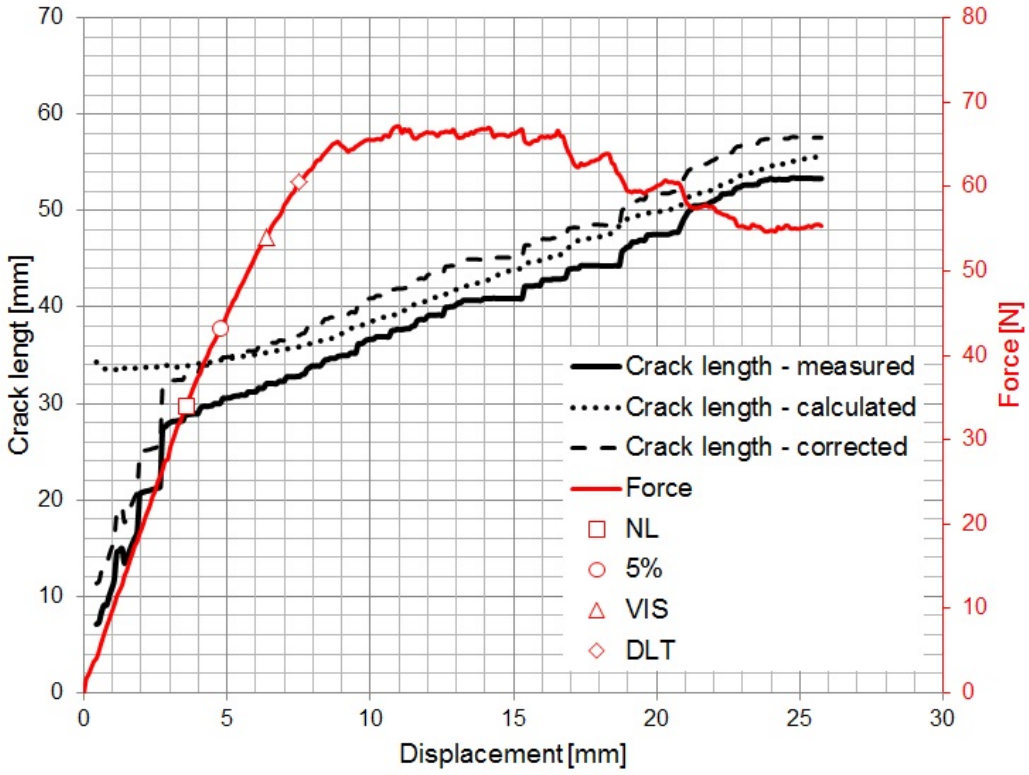

DCB#2

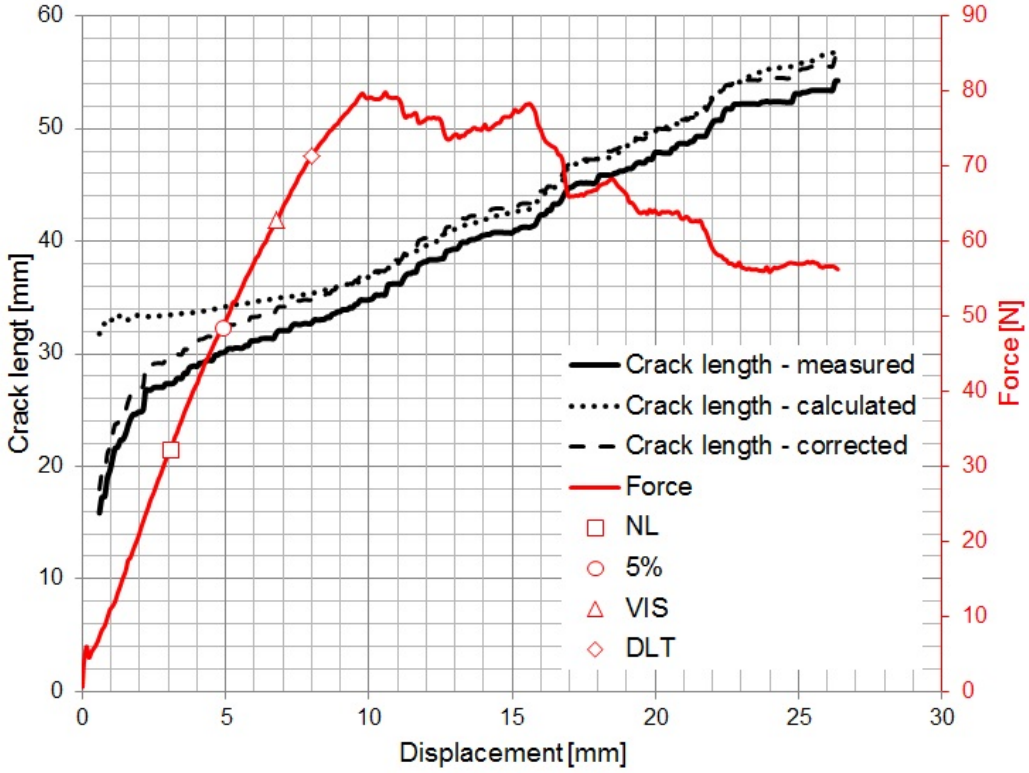
Crack lengt [mm]
Force [N]
Displacement [mm]
Crack length - measured
Crack length - calculated
Crack length - corrected
Force
NL
5%
VIS
DLT
0
10
20
30
40
50
60
0
10
20
30
40
50
60
70
80
90
0
5
10
15
20
25
30

DCB#3

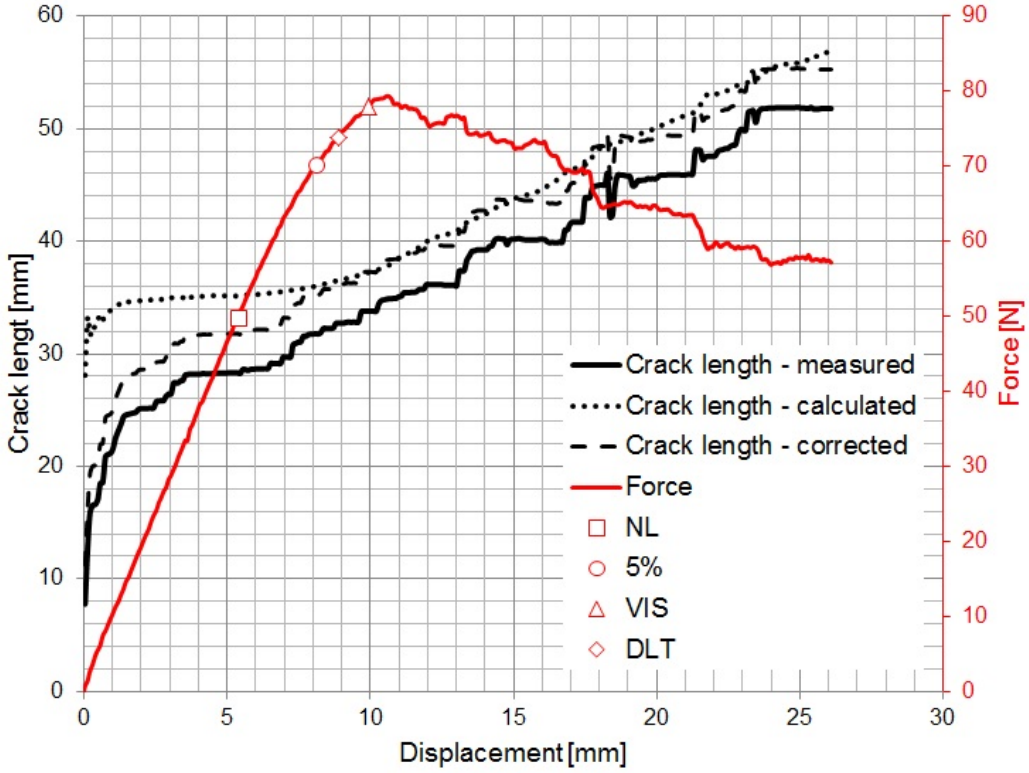
Crack lengt [mm]
Force [N]
Displacement [mm]
Crack length - measured
Crack length - calculated
Crack length - corrected
Force
NL
5%
VIS
DLT
0
10
20
30
40
50
60
0
10
20
30
40
50
60
70
80
90
0
5
10
15
20
25
30

DCB#4

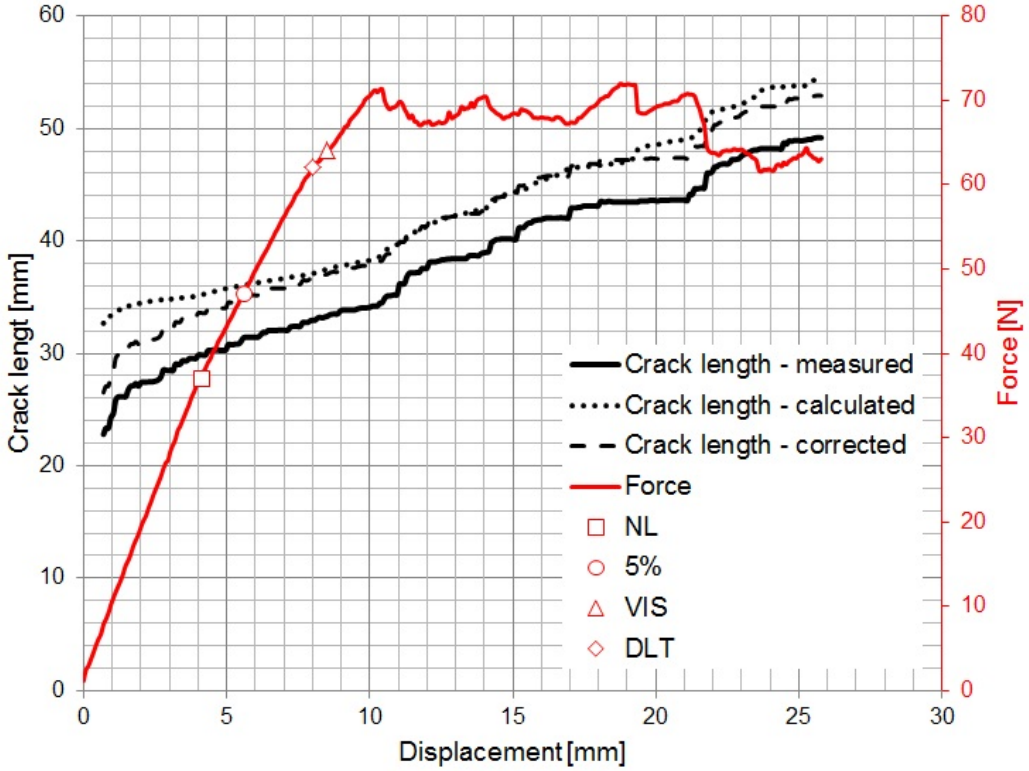
Crack lengt [mm]
Force [N]
Displacement [mm]
Crack length - measured
Crack length - calculated
Crack length - corrected
Force
NL
5%
VIS
DLT
0
10
20
30
40
50
60
70
80
0
5
10
15
20
25
30

DCB#5

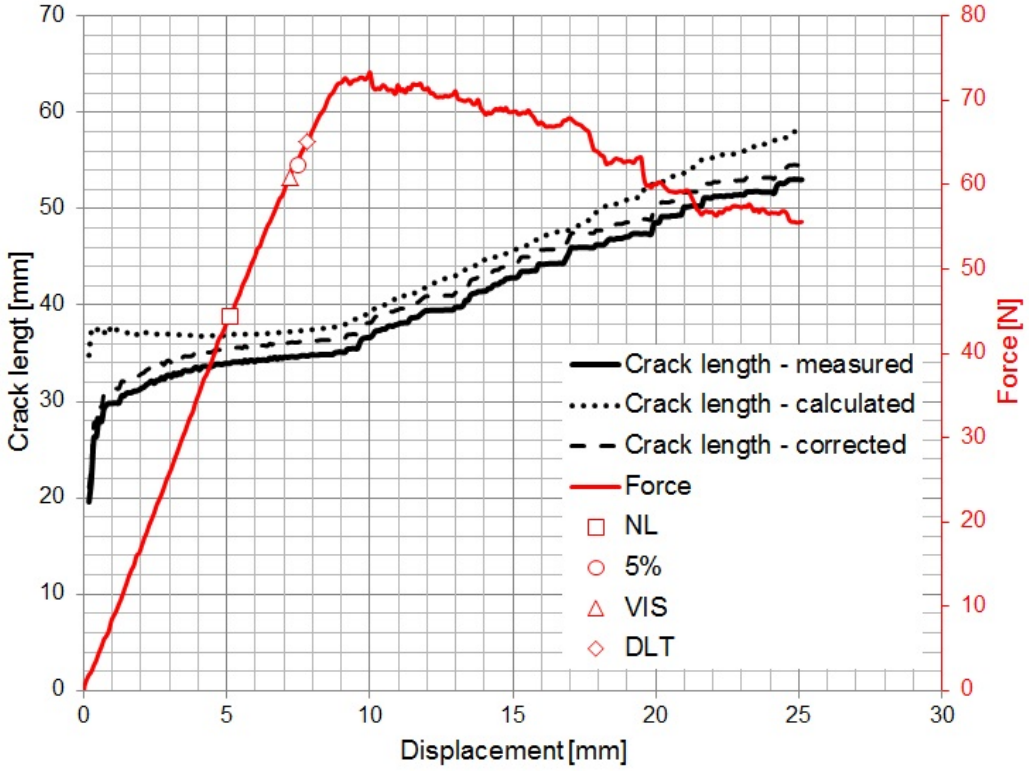
Crack lengt [mm]
Force [N]
Displacement [mm]
Crack length - measured
Crack length - calculated
Crack length - corrected
Force
NL
5%
VIS
DLT
0
10
20
30
40
50
60
70
80
0
5
10
15
20
25
30

DCB#6

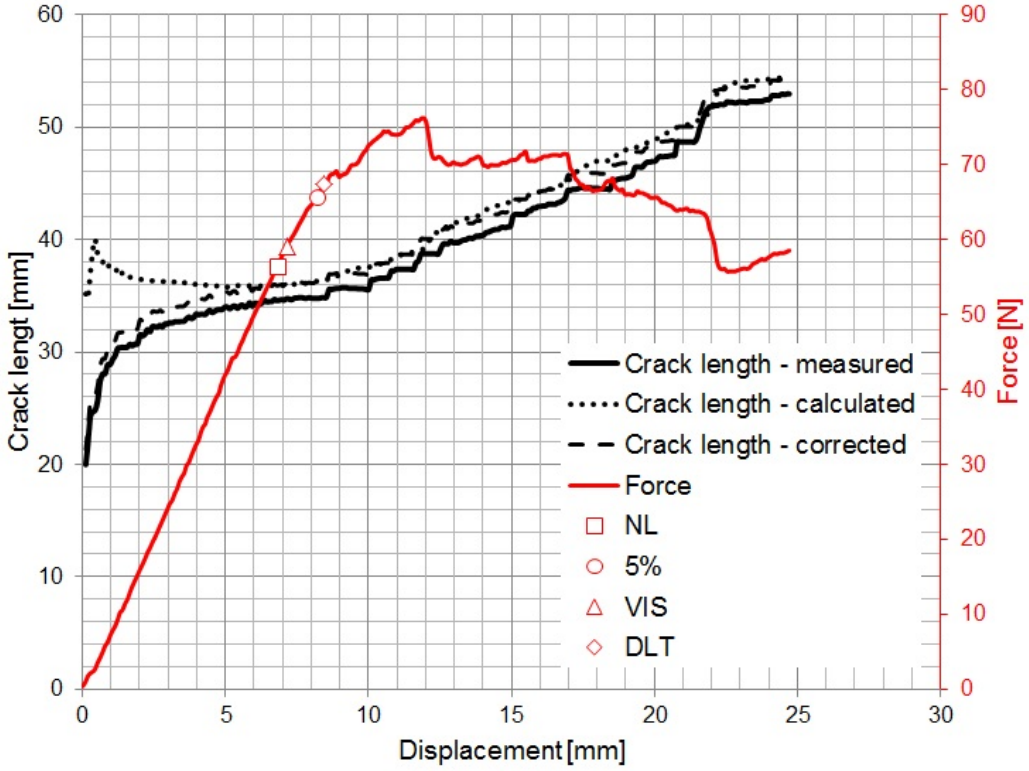
Crack lengt [mm]
Force [N]
Displacement [mm]
Crack length - measured
Crack length - calculated
Crack length - corrected
Force
NL
5%
VIS
DLT
0
10
20
30
40
50
60
0
10
20
30
40
50
60
70
80
90
0
5
10
15
20
25
30

DCB#7

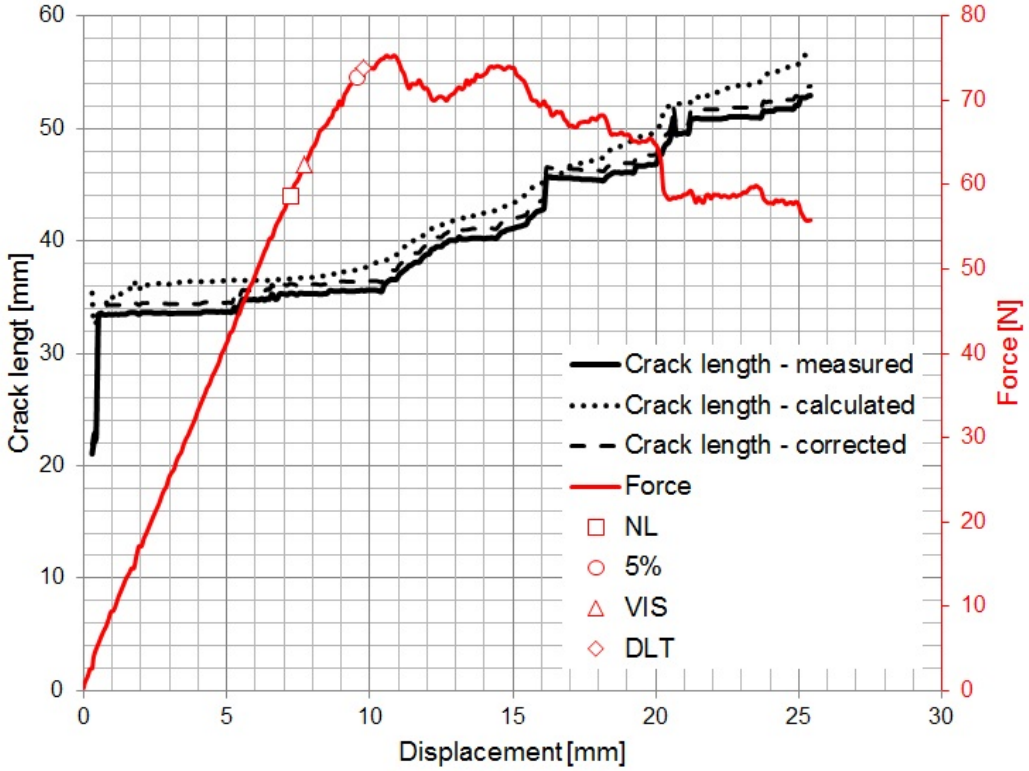
Crack lengt [mm]
Force [N]
Displacement [mm]
Crack length - measured
Crack length - calculated
Crack length - corrected
Force
NL
5%
VIS
DLT
0
10
20
30
40
50
60
70
80
0
5
10
15
20
25
30

DCB#8

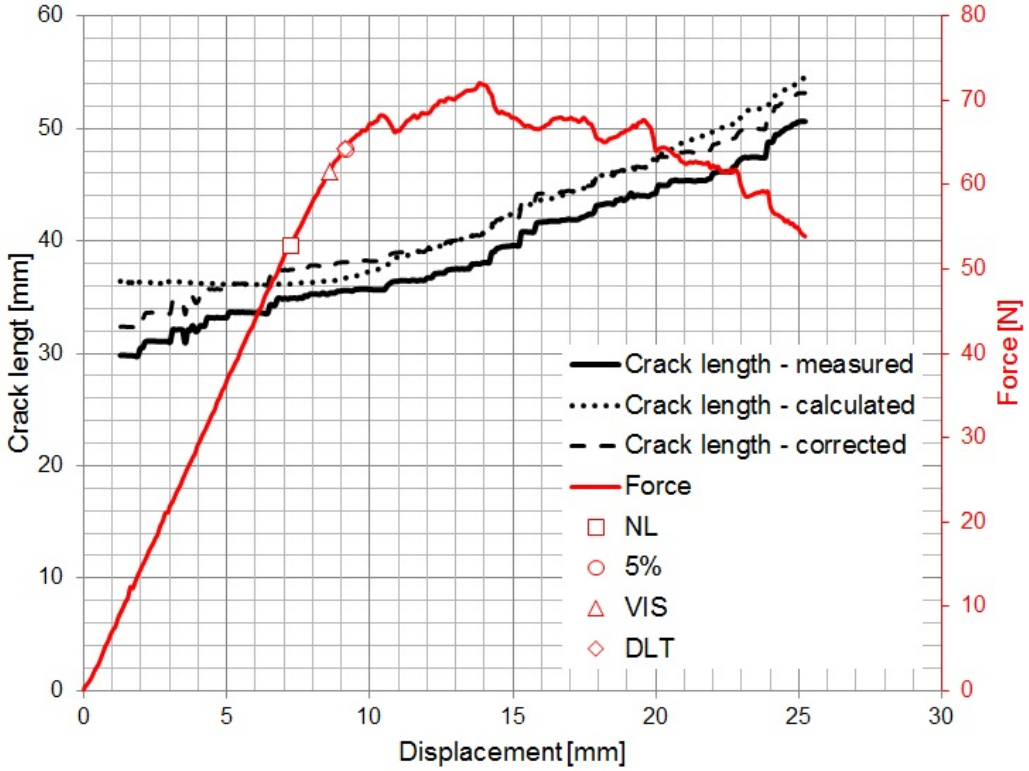
Crack lengt [mm]
Force [N]
Displacement [mm]
Crack length - measured
Crack length - calculated
Crack length - corrected
Force
NL
5%
VIS
DLT
0
10
20
30
40
50
60
70
80
0
5
10
15
20
25
30

Appendix E: ADCB results

ADCB#1

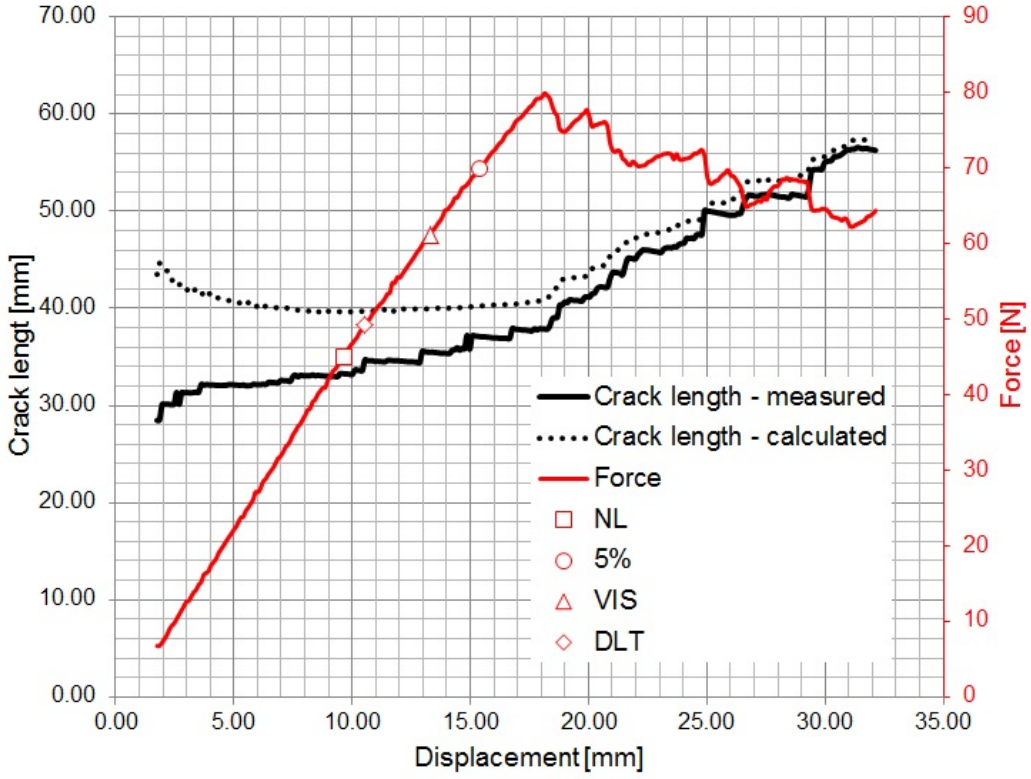

ADCB#2

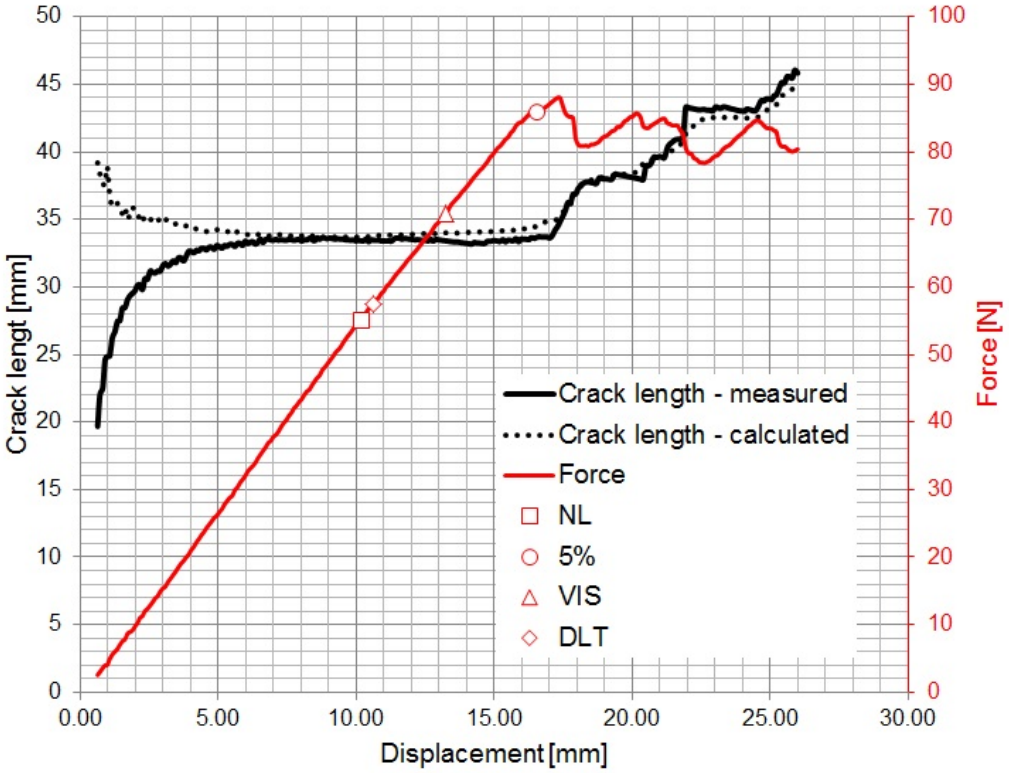
Crack lengt [mm]
Force [N]
Displacement [mm]
Crack length - measured
Crack length - calculated
Force
NL
5%
VIS
DLT
0
5
10
15
20
25
30
35
40
45
50
0.00
5.00
10.00
15.00
20.00
25.00
30.00
0
10
20
30
40
50
60
70
80
90
100

ADCB#3

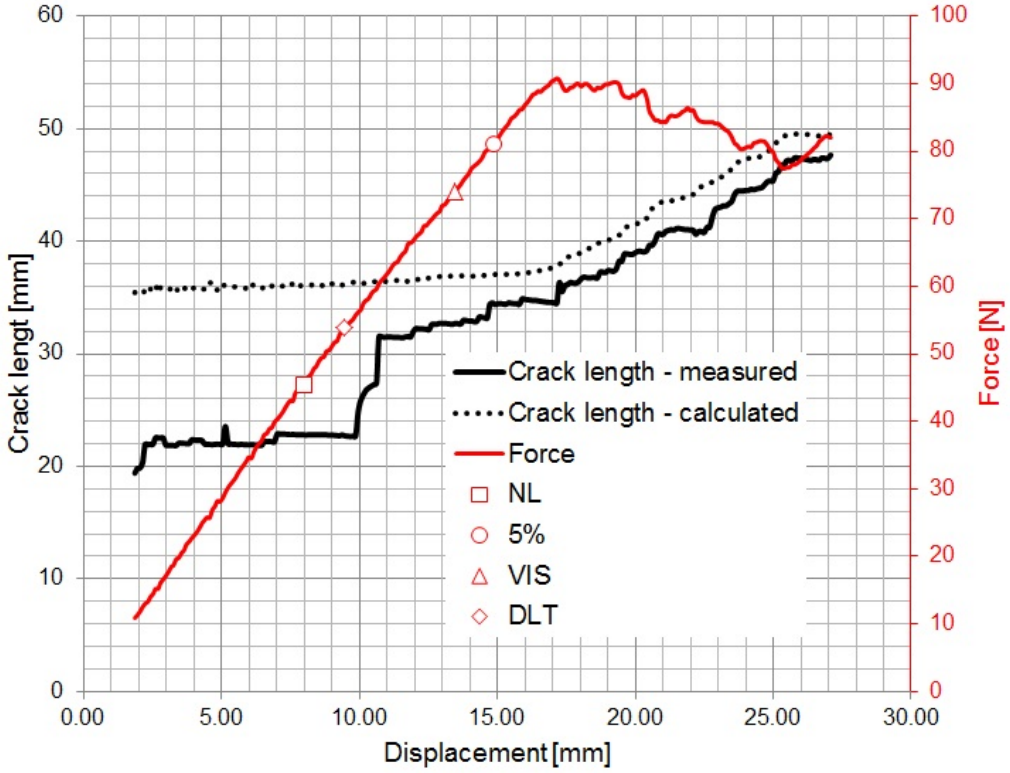
Crack lengt [mm]
Force [N]
Displacement [mm]
Crack length - measured
Crack length - calculated
Force
NL
5%
VIS
DLT
0
10
20
30
40
50
60
0
10
20
30
40
50
60
70
80
90
100
0.00
5.00
10.00
15.00
20.00
25.00
30.00

ADCB#4

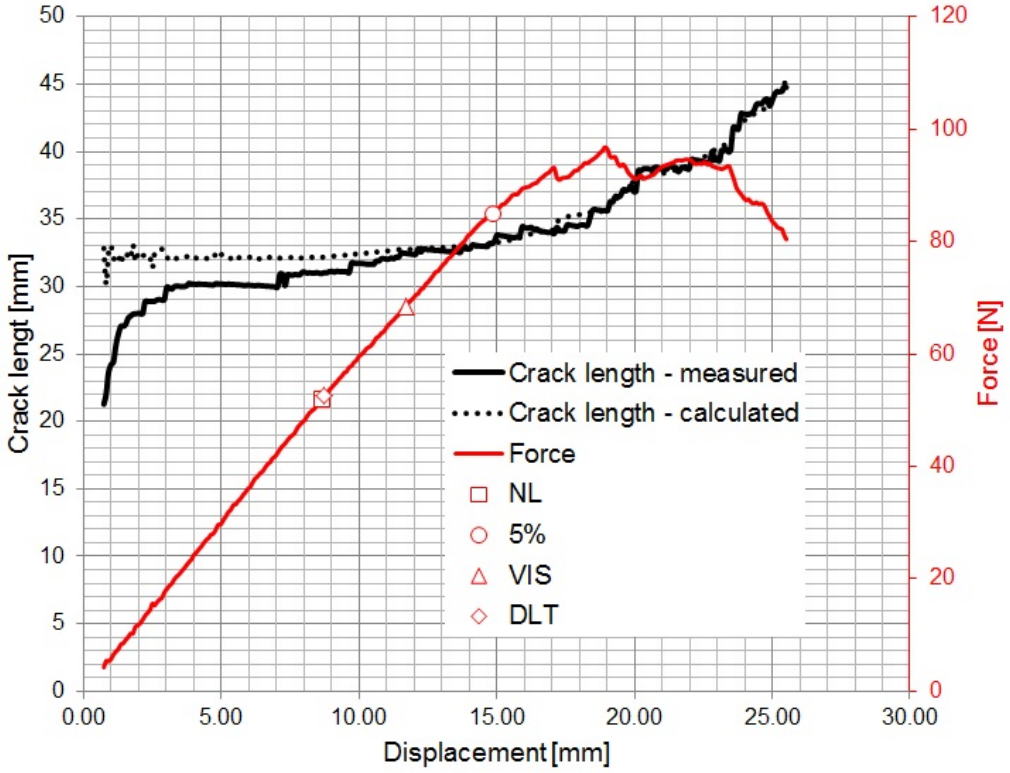
Crack lengt [mm]
Force [N]
Displacement [mm]
Crack length - measured
Crack length - calculated
Force
NL
5%
VIS
DLT
0
5
10
15
20
25
30
35
40
45
50
0.00
5.00
10.00
15.00
20.00
25.00
30.00
0
20
40
60
80
100
120

Appendix F: ELS results

ELS#1

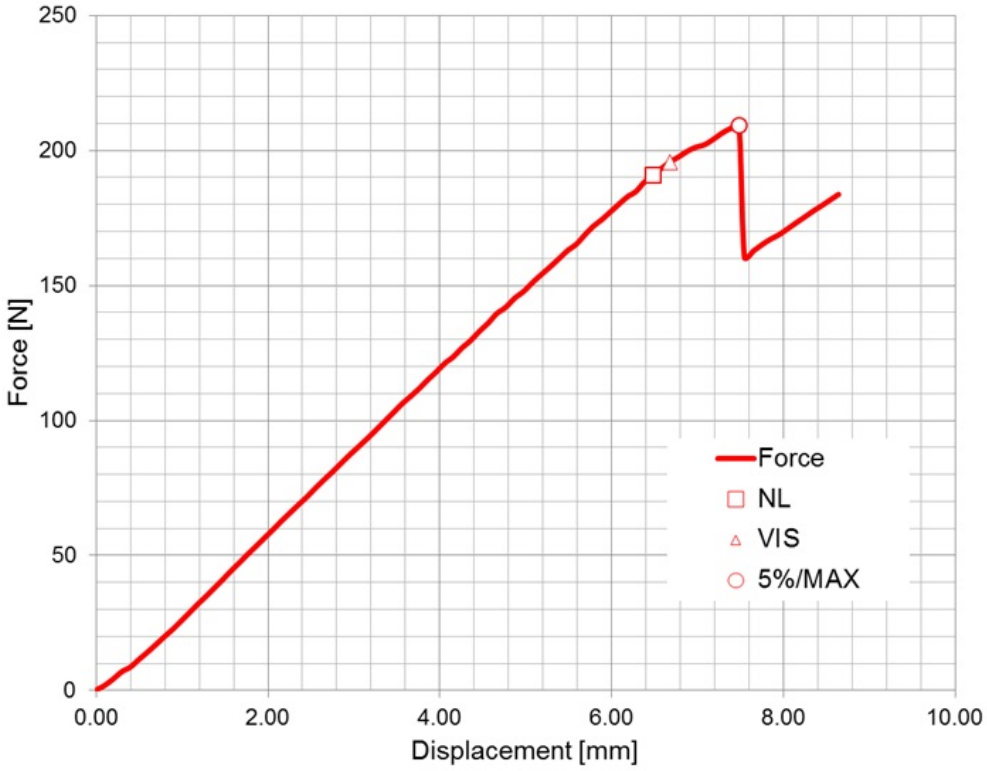

ELS#2

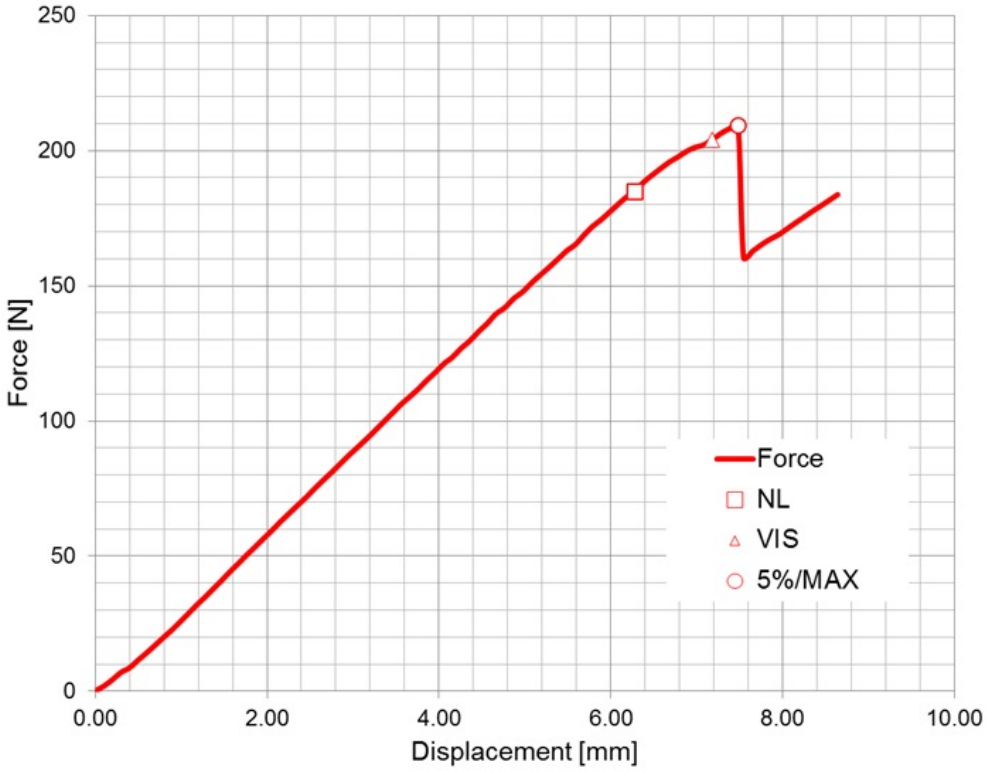
250
200
150
100
50
0
Force [N]
0.00
2.00
4.00
6.00
8.00
10.00
Displacement [mm]
Force
NL
VIS
5%/MAX

ELS#3

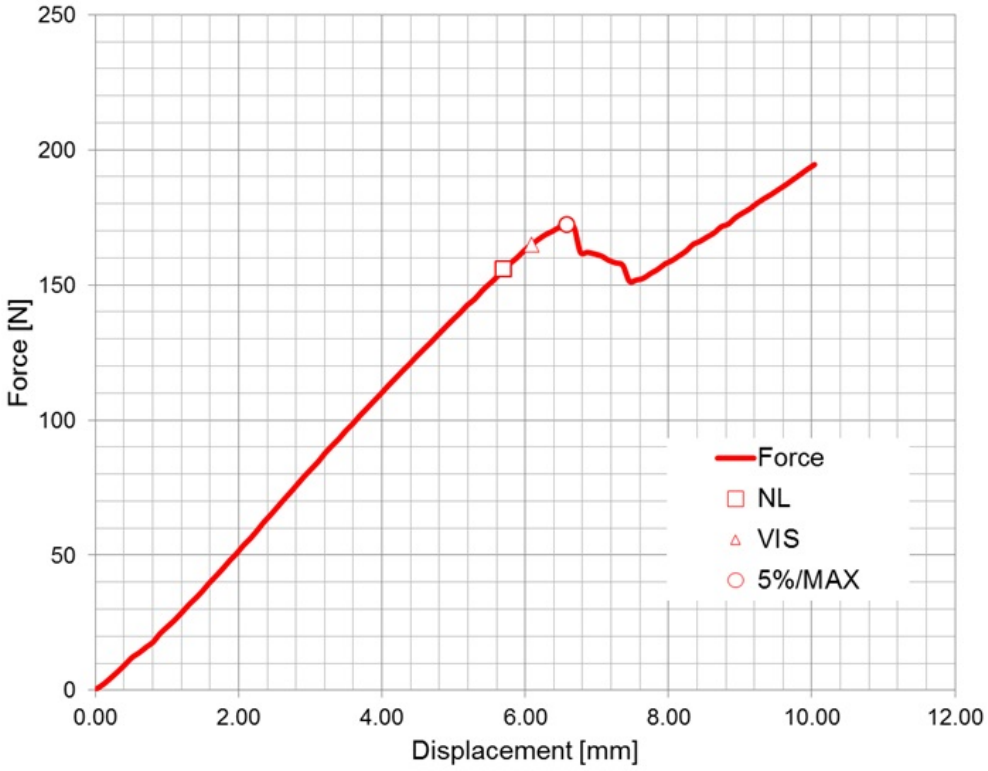
250
200
150
100
50
0
Force [N]
0.00
2.00
4.00
6.00
8.00
10.00
12.00
Displacement [mm]
Force
NL
VIS
5%/MAX

ELS#4

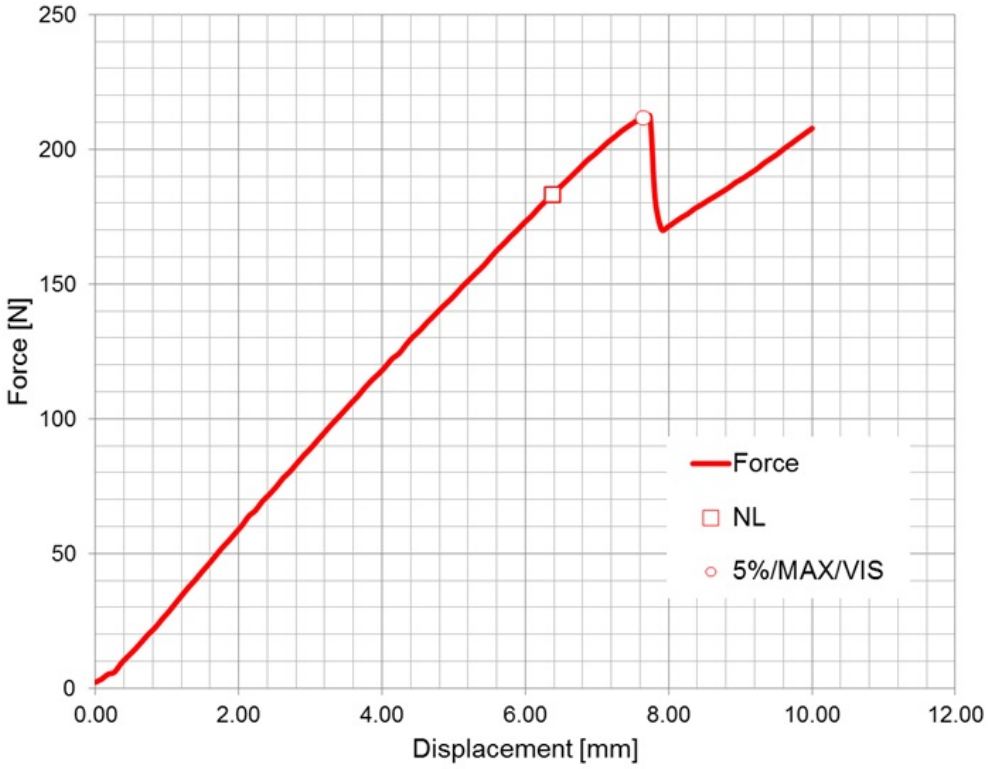
250
200
150
100
50
0
Force [N]
0.00
2.00
4.00
6.00
8.00
10.00
12.00
Displacement [mm]
Force
NL
5%/MAX/VIS

ELS#5

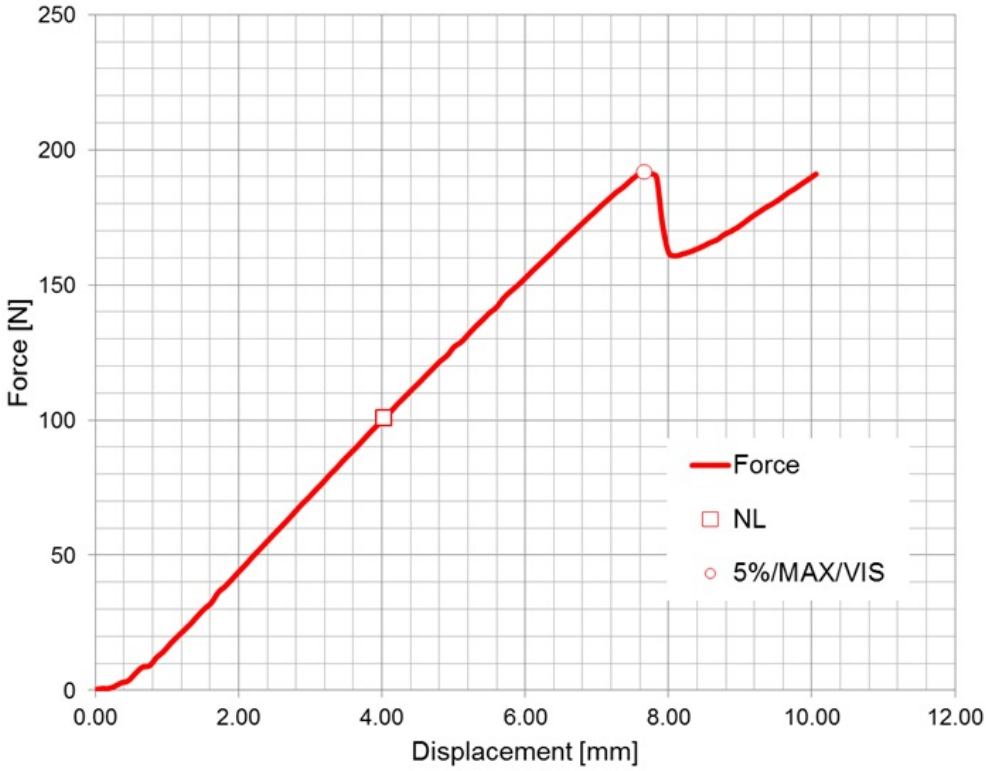
250
200
150
100
50
0
Force [N]
0.00
2.00
4.00
6.00
8.00
10.00
12.00
Displacement [mm]
Force
NL
5%/MAX/VIS